Alma Mater Studiorum – Università di Bologna

DOTTORATO DI RICERCA IN

INGEGNERIA CIVILE, AMBIENTALE E DEI MATERIALI

Ciclo XXVII

Settore Concorsuale di afferenza: 08/B3

Settore Scientifico disciplinare: ICAR/09

COST-EFFECTIVENESS OF ALTERNATIVE RETROFIT OPTIONS TO SUPPORT DECISION MAKING

Presentata da: **Veronica Ligabue**

Coordinatore Dottorato

Prof. Alberto Lamberti

Relatore

Prof. Marco Savoia

Correlatore

Prof. Stefano Pampanin

Esame finale anno 2015

Table of contents

List of figures

1. Introduction

Communicating seismic risk and structural performance is a complex but essential task assigned to the technical community, in order to enable owners of earthquake prone buildings and other stakeholders to consider the implementation of seismic vulnerability reduction interventions and to make informed retrofit decisions.

Seismic performance of existing buildings is generally assessed using the percentage of New Building Standard (% NBS) that the building can achieve, in line with the New Zealand Building Act (2004), NZS 1170.5:2004 and NZSEE (2006) guidelines. It has to be pointed out, however, that relying solely on this performance metric in the definition of existing building performance could be misleading. In fact, the %NBS is not linearly correlated to the seismic risk profile of the building, with an increase of the targeted %NBS resulting in a more than proportional reduction of risk (NZSEE2006 guidelines) as shown in Figure 1(a). Moreover, two buildings achieving the same %NBS could be characterized by a different probability of collapse and almost certainly would sustain different levels of damage under the same seismic event. This is mainly due to the fact that this assessment procedure only addresses the shaking intensity required to reach the Ultimate Limit State (ULS). Neglecting the performance of the structure beyond this point, with no explicit consideration to the post-ULS behaviour and expected collapse mechanism, might lead to significant variation of the actual probability of collapse of two different structures for a given %NBS.

Furthermore, the %NBS is generally obtained, for the sake of simplicity, deterministically and, as such, it does not explicitly account for nor directly reflect the (epistemic) uncertainties related to the structural vulnerabilities. These are, in fact, affected by material variation and/or geometric/mechanical properties which could dramatically alter the relative hierarchy of strength within a structural element or between sub-assembly components and thus change the global mechanism. In addition to the more obvious aleatory uncertainties related to the record-to-record variability, these variabilities can affect older and poorly detailed structures to a greater extent than modern, or newly designed, and well-detailed ones. For this reason,

the assessment can result in unconservative and misleading evaluations of the performance of the building.

On top of this, the common conception, or rather misconception, that the cost of retrofit interventions would increase linearly with the targeted %NBS often discourages stakeholders to consider repair/retrofit options in a post-earthquake emergency phase and the following period of reconstruction and further developments. Conversely, in fact, a cost vs. performance relationship would be expected to follow more a step function, where alternative retrofit techniques could be combined and integrated to reach the next level of performance (e.g. need to intervene on the foundation to introduce an external wall), once the original individual technique or discrete intervention has exhausted its capacity (e.g. FRP wrapping of elements to provide some level of ductility and/or strength). Hence, the cost of the intervention can vary greatly depending on the retrofit scheme adopted and thus it has to be estimated on a case-by-case basis (Figure 1 b and c).

Similarly, when dealing with a non-damaged prevention situation, the legally minimum level of %NBS might be targeted, leading to no-action or to a minimum retrofit intervention.

For these reasons, great caution must be used in evaluating building performance relying only on the %NBS and the relationship between %NBS and other performance measures requires further investigations.

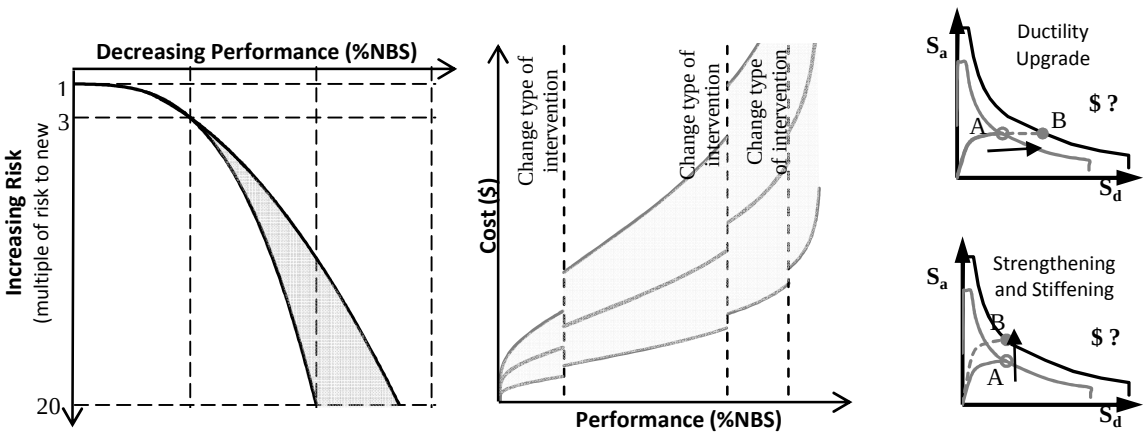

Figure 1: (a) Correlation between performance and risk (reproduced from the NZSEE2006 Guidelines); (b) expected cost of retrofit intervention as a function of performance (adapted from Beetham, 2013); (c) alternative strategies for the achievement of 100%NBS (from Kam and Pampanin, 2009 and Kam, 2010).

In the last few years, in the spirit of Performance-Based Design, a great amount of research efforts were carried out focusing on the evaluation of the consequences for the building

owners and occupants of the occurrence of a seismic event (PEER PBEE methodology – Porter, 2003; Mitrani-Reiser, 2007; Ramirez and Miranda, 2009; ATC-58, 2012; Welch, Sullivan et al., 2014). Among the developed methodologies, the most simplified ones aim at evaluating the direct economic losses due to building repair or replace while the more comprehensive ones (but by far more computationally expensive) also consider indirect consequences, namely the downtime, injuries and casualties, due to either a specified earthquake scenario or expected on a structure within a certain time frame.

In the current contribution, a framework to evaluate the effects in terms of long-term losses, benefits and collapse probability of the targeted retrofit level (expressed as %NBS) is presented in order to explicitly consider these performance measures in the design process (Figure 2). An Earthquake Prone Building (EPB), reflecting the typical features of a pre-1970's New Zealand reinforced concrete frame structure, is selected as a case study. Different retrofit strategies are considered, targeting increasing levels of %NBS, and the actual probability of reaching collapse when considering a suite of ground-motions is evaluated, providing a correlation between %NBS and Risk. A probabilistic time-based loss assessment is then undertaken, adopting the Performance Assessment Calculation Tool (PACT), provided by the ATC-58 (2012) , to investigate the relationship between %NBS and expected direct and indirect losses. As a result, valuable information on the effectiveness of each retrofit option considered can be derived, giving guidance on the actual performance to be expected when an intervention is designed to sustain a selected level of shaking intensity. At the same time some critical aspects related to the deterministic analysis methodology commonly adopted in the evaluation of the building performance are discussed.

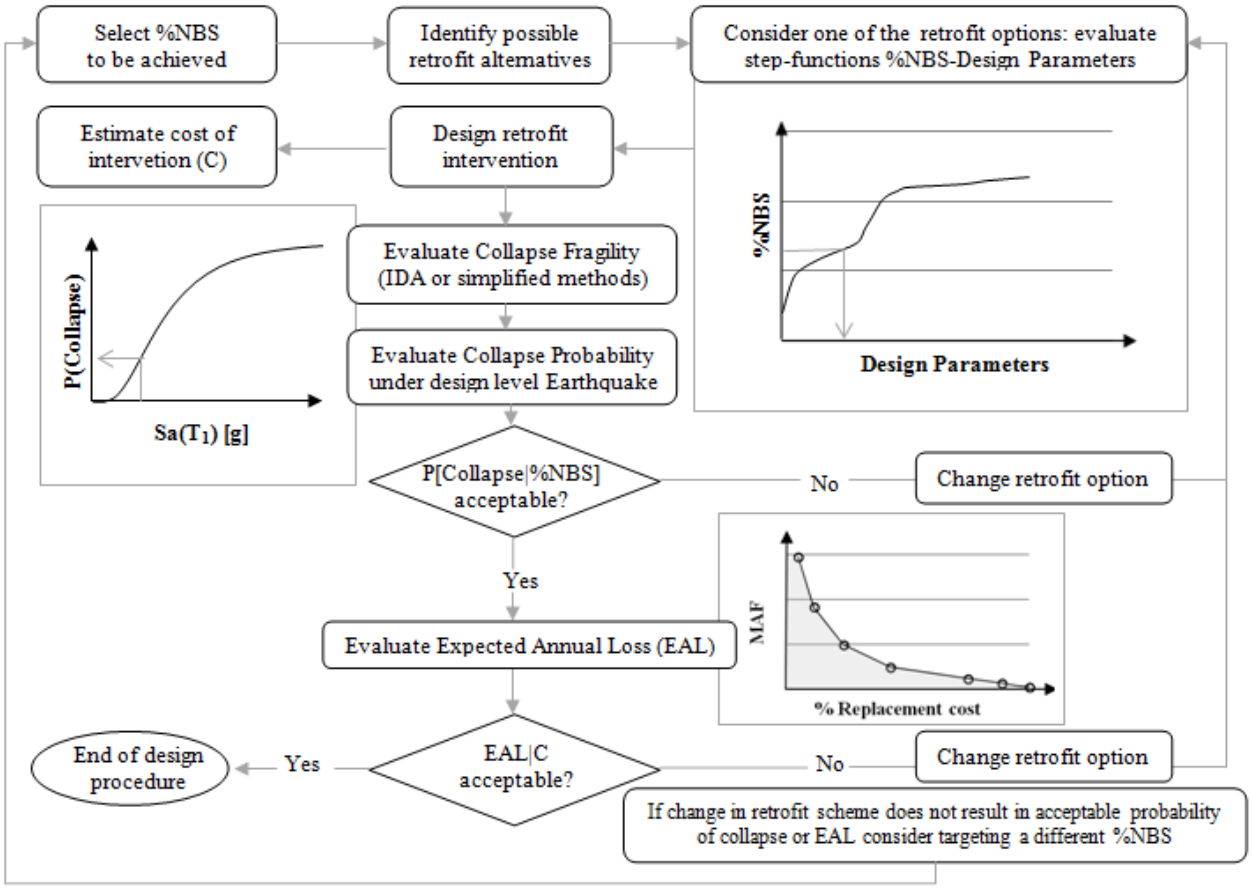

Figure 2: Flow chart of the framework proposed to incorporate collapse probabilities and expected losses in the design process.

Outline of the Dissertation

This dissertation is divided into 9 Chapters, including this introductory **Chapter 1**.

Chapter 2 briefly provides background information on the development of Performance-Based Earthquake Engineering. In **Chapter 3** the typical seismic vulnerabilities of pre-1970's reinforced concrete frames structures in New Zealand are discussed, and a case-study building reflecting these deficiencies is presented. This prototype frame will be adopted in the following for the performance evaluation.

In order to assess the performance of the structure of interest, a procedure to evaluate the hierarchy of strength of non-ductile beam-column joint sub-assemblies is presented in **Chapter 4**. By identifying the critical weaknesses within the system, the sequence of events expected in the joint region can be predicted and hence the probable failure mode can be estimated.

In **Chapter 5** the global seismic performance of the case study building is evaluated by means of non linear static analysis, which provides the %NBS achieved by the building. In the same Chapter, the procedure developed to conceptually design alternative retrofit solutions targeting increasing levels of performance levels (in terms of %NBS) is outlined.

Following the design of the retrofit alternatives, **Chapter 6** presents the results of Incremental Dynamic Analysis (IDA, Vamvatsikos and Cornell, 2002) performed on the original structure as well as on the retrofitted frames to assess their effective probability of reaching/exceeding collapse. In this fashion, some level of uncertainties neglected within the previous approach (such as the record-to-record variability and to some extent the modelling uncertainties) are explicitly considered and the relation between %NBS and Risk is investigated.

In **Chapter 7** direct and indirect losses expected to be induced on the structure by seismic activity within a certain time frame are evaluated in a fully probabilistic manner. The Performance Assessment Calculation Tool (PACT) developed together with the ATC-58 is used in this study as it provides a platform to handle the required (and onerous) calculations. As a result, annualized values of losses, e.g. Expected Annual Loss, EAL, are then evaluated for each retrofit option and for each level of %NBS, providing a correlation between these performance metrics.

Due to the computationally intensive nature of the analyses required to undertake the performance assessment, **Chapter 8** focuses on a simpler loss assessment procedure, which relies on the principles of the displacement based assessment and allows to calculate the Expected Annual Loss for the given structure (Sullivan and Calvi, 2011 and Welch, 2012). By comparison with the results obtained through the more comprehensive loss assessment methodology, strengths and limitations of this simplified method are discussed.

In **Chapter 9** the concluding remarks of this research are presented.

2. Background: Performance-Based Earthquake Engineering

Performance-based earthquake engineering (PBEE) can be described as a framework developed to ensure the achievement of desired structural performance objectives under various levels of earthquake intensity. The principles inspiring PBEE have been developed in the last few decades leading to a shift of focus in the current design approaches. In fact, rather than performing design based on a set of prescriptive requirements, PBEE suggests to select the desired seismic behaviour based on the type of construction and shaking intensity and thus addressing the targeted performance in the design phase directly. By providing guidelines in order to quantitatively define building performance, the engineer and the stakeholders are allowed to make informed decisions reflecting their specific needs and priorities. The following sections will provide a brief overview of the deveopment and codification of PBEE principles. Further and more detailed information on these advancements can be found in Welch (2012).

Vision 2000, FEMA 273/356 and ASCE 41

Among the landmark projects carried out to develop the principles of Performance-based earthquake engineering, *Vision2000: Performance Based Seismic Engineering of Buildings* (SEAOC, 1995), undertaken by the Structural Engineers Association of California (SEAOC) following the 1994 Northridge earthquake, represent a simple but essential advancement in the field of PBEE. This research effort resulted in guidelines for the design of new constructions defining different performance objectives associated with various levels of importance of the structure of interest (from ordinary structures to safety critical facilities) and frequencies of the earthquake considered, as depicted in Figure 3.

The document defines a discrete number of performance levels, namely fully operational, operational, life safety, and near collapse, as well as four intensity levels defined in terms of their return period: frequent (50% in 30 years), occasional (50% in 50 years), rare (10% in 50 years), and very rare (10% in 100 years). As illustrated in Figure 3, the different performance levels are coupled with earthquake intensities based on the building type or

function. In fact, improved performance is required for facilities that have a critical function for the community and higher levels of damage are deemed acceptable for increasing (but less likely) seismic intensities.

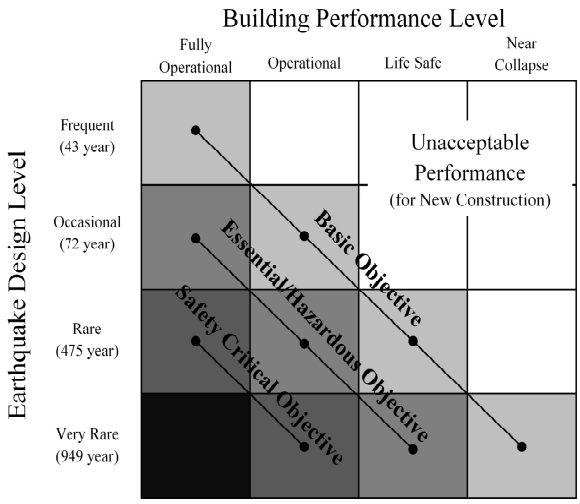

Figure 3: Vision 2000 recommended seismic performance objectives (from SEAOC, 1995)

A further advancement in PBEE has been pursued by the Federal Emergency Management Agency (FEMA) which published in 1997 the *National Earthquake Hazards Reduction Program (NEHRP) Guidelines (and commentary) for the Seismic Rehabilitation of Buildings* (FEMA 273, 1997 and FEMA 274, 1997 respectively). A performance objective framework similar to the one proposed in the Vision-2000 document was developed focusing on rehabilitation of existing structures rather than new constructions, providing the basis of the pre-standard document named FEMA-356 *Prestandard and Commentary for the Seismic Rehabilitation of Buildings* (FEMA 356, 2000).

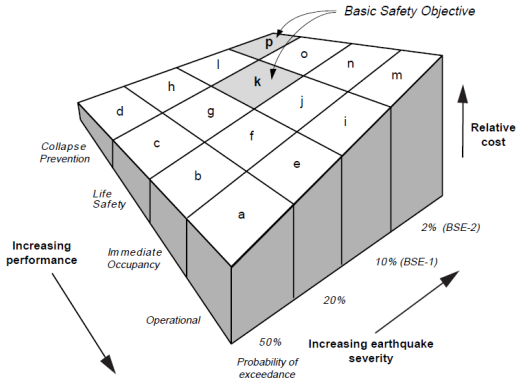

Figure 4: Relationship between seismic performance, earthquake intensity and relative costs of the different rehabilitation objectives (from FEMA-274)

Interestingly, the FEMA-274 commentary document graphically presents an improved version of the performance/intensity matrix by adding a third demension reflecting the cost of the intervantion required to achieve the aforementioned performance objective, as shown in Figure 4. Six years later, the ASCE published a standard named ASCE/SEI 41-06, *Seismic Rehabilitation of Existing Buildings*. The standard specifies provisions for the improvement of seismic performance of structural and/or nonstructural components of a building by addressing the weaknesses identified during the previous seismic assessment phase. Figure 5 shows the performance rehabilitation objectives for existing buildings from ASCE/SEI 41-06.

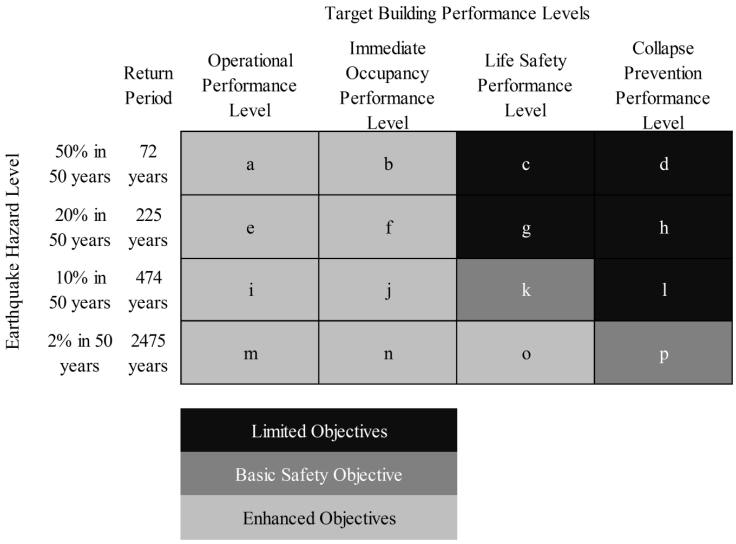

Figure 5: ASCE/SEI 41-06 rehabilitation objectives for existing structures

A Limited Performance objective (or Limited Rehabilitation Objectives, LRO), can be achieved improving the global behaviour of the structure by removing the main critical structural deficiencies such as brittle columns and joint shear failures, and prevention of soft-storey mechanism. As in the case of a partial retrofit strategy, complete structural collapse is prevented minimizing human casualties while accepting extensive damage, both to structural and non-structural components that could be beyond reparability.

Basic Performance (BP) or Basic Safety Objective (BSO) generally corresponds to the achievement objectives close to new building design, in fact, under design level earthquakes (10% in 50 years) and maximum credible earthquakes (MCE – 2% in 50 years), life-safety and collapse prevention must be guaranteed respectively. However, the level of damage and potential economic loss experienced by buildings rehabilitated to the BSO may be greater than those expected in properly designed new buildings.

Finally, Advanced Performance (AP) or Enhanced Rehabilitation Objectives (ERO) could be targeted when a loss of functionality in moderate to strong events is not considered acceptable. This entails that during design of the retrofit intervention, structural and non-structural damage indicators such as floor acceleration and residual deformation should also be directly accounted for.

Multi-Level Performance Objective Matrix

Extending the framework proposed in the previous contributions, Pampanin, Christopoulos et al. (2002) and later Kam, Pampanin et al. (2010) suggested a global performance matrix incorporating performance measures describing both structural and non-structural damage, namely peak inter-storey drift ratio, residual inter-storey drift ratio and peak floor acceleration.

Figure 6 schematically illustrates the concept of accounting for the three performance measures, for a given level of seismic intensity associated with a specified return period, resulting in a three-dimensional performance matrix, enabling to quantify global performance as a combination of structural and non-structural performance levels.

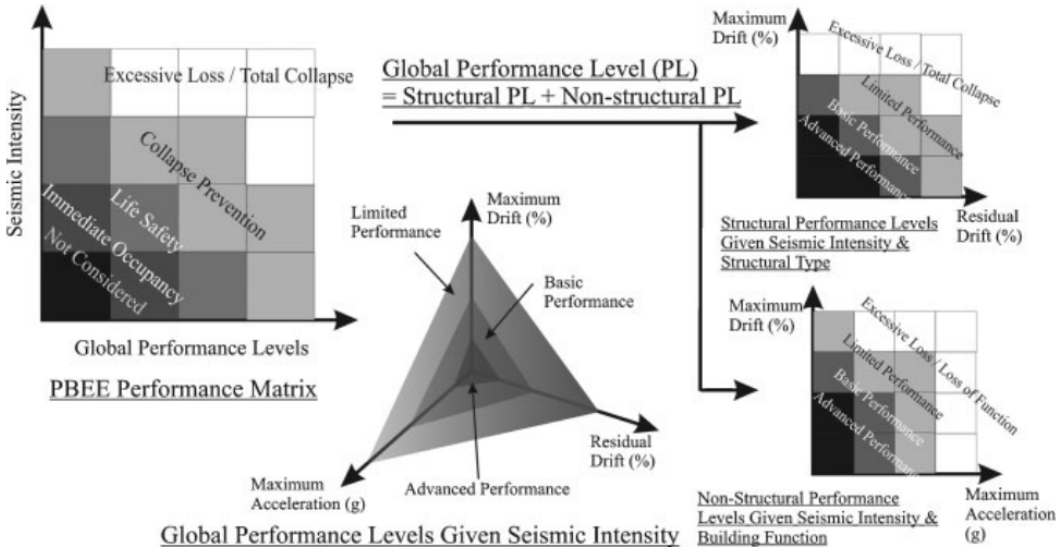

Figure 6: Three-dimensional global building performance matrix (after Kam, Pampanin et al., 2010)

PEER PBEE Methodology

One of the most complete risk assessment frameworks recently proposed is the PEER's Performance-Based Earthquake Engineering methodology (Porter, 2003). The Pacific Earthquake Engineering Research (PEER) Center suggests that besides the proper structural

damage that occurs to a building during an earthquake event, other relevant consequences and thus sources of loss should be taken into account. Economic losses, downtime and number of fatalities could be considered useful seismic performance metrics, upon which various stakeholders could base their decision. Hence, the principal outputs of PEER's approach are system-level performance measures: probabilistic estimates of repair costs, casualties, and loss-of-use duration ("dollars, deaths, and downtime"). The objective of the methodology is to estimate the frequency with which a particular performance metric will exceed various levels for a given design at a given location. These can be used to create probability distributions of the performance measures during any planning period of interest. From the frequency and probability distributions, simple point performance metrics can be extracted that are meaningful to facility stakeholders, such as an upper-bound economic loss during the owner-investor's planning period.

Figure 7 illustrates the PEER methodology. As shown, PEER's PBEE approach involves four stages: hazard analysis, structural analysis, damage analysis, and loss analysis. In the figure, the expression p[X|Y] refers to the probability density of X conditioned on knowledge of Y, and g[X|Y] refers to the occurrence frequency of X given Y.

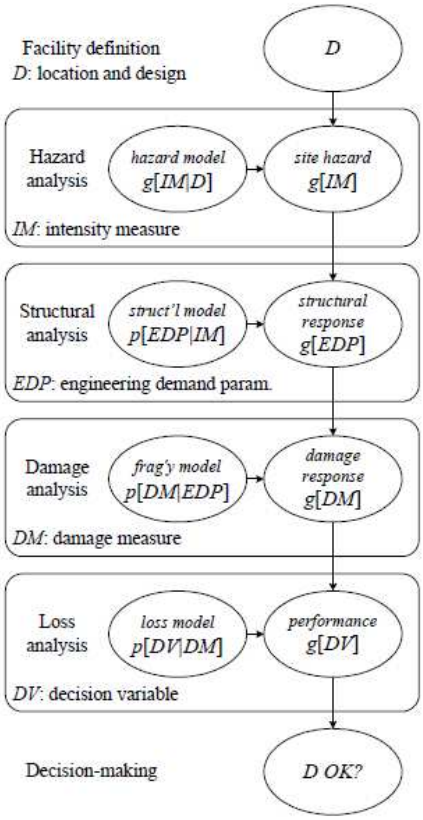

Figure 7: Schematic representation of the PEER PBEE framework (after Porter, 2003)

Each analysis stage results in a probabilistic distribution, hence uncertainties are considered at each level of the framework. At the initial stage of the methodology, the design, D, representing site location as well as structural details, is coupled with a specific site hazard required to identify the values of intensity measure, IM, that will affect the structure of interest together with their probability of occurrence or exceedance within a defined time frame. The information derived from the hazard is adopted to perform the structural analyses required to obtain distributions of Engineering Demand Parameters (EDP's), such as interstorey drift and peak floor accelerations at various shaking intensity levels as well as the collapse capacity of the structure being considered. Hence, in the Damage analysis phase, the EDP's are used to determine damage measures (DM) through the fragility functions, that are distributions modelling the probability of incurring or exceeding particular levels of physical damage, given the parameters of structural response. Finally, in the fourth step of the procedure the DM distributions are used in order to determine decision variables, DV, typically the economic effort required to restore the structure to its original undamaged condition, concluding the performance evaluation. The results of each stage serves as input for the following one, as schematically illustrated in Figure 7.

As the PEER PBEE is an open framework, each stage of the methodology could be adapted to any level of refinement, from empirical or judgmental-based simplified models to the latest and more comprehensive approaches available in literature.

ATC-58: Seismic Performance Assessment of Buildings

In order to assist engineers in undertaking the probabilistic loss assessment procedure proposed by the PEER, the Applied Technology Council (ATC) has recently developed the so-called 'next generation' of PBEE guidelines, providing guidance for the implementation of building specific loss estimation and risk assessment in line with the PEER methodology. However, as this methodology is computationally intensive, ATC-58 (2012) provides a software, the Performance Assessment Calculation Tool (PACT), to collect the data required for the performance assessment and handle the onerous statistical computations. This tool will be adopted within this study to evaluate structural performance in terms of expected annual loss, repairing times and fatalities, which are the performance metrics generally referred to as the three D's.

3. Seismic vulnerability and assessment of reinforced concrete frames

Evolution of seismic regulations in New Zealand

The first known contribution regarding the subject of earthquake resistant design and construction was written by architect C. Reginald Ford, and published in NZ, in 1926. This book describes earthquake damage in past seismic events in New Zealand as well as USA and Japan, providing the first recommendations for designing seismic resistant structures.

While regulatory provisions imposing lateral load design on buildings were introduced in Japan and in the USA already in 1924 and 1933 respectively, a "Draft General Earthquake Building By-law" was presented in New Zealand in 1931, triggered by the occurrence of the catastrophic Hawke's Bay earthquake event in that same year. This Draft became the first standard on the subject in October 1935, when the Standards Association published the NZSS no. 95, New Zealand Standard Model Building By-Law, later revised in 1939. The lateral loading provisions included in the code were minimal, requiring design for a lateral load of 0.08g and 0.10g of building weight for ordinary and public buildings respectively. This lateral force was assumed to be equally distributed along the height of the building and could be enhanced up to 0.15g by the local territorial authority. The Code also required that parts of buildings be tied together, that bracing was to be symmetrical, torsional effects should be taken into account and buildings to be used for public purposes should have frames constructed of reinforced concrete or structural steel. However, the 1935 By-Law was not prescriptive and its adoption depended on the judgement of local authorities.

Following this early legislation, the 1955 revision of the NZS Standard Model Building By-Law (NZS95:1955) introduced an inverted triangular distribution of horizontal load as an alternative loading pattern approximating the first mode deflected shape of the building.

A great advancement was then introduced with the NZS1900:1964 code, in which a seismic zonation for the country was introduced to better represent regional seismicity. Moreover, seismic force was estimated as a function of the building's natural period and the inverted

triangular lateral force distribution was modified to account for higher mode effects. The concept of structural ductility was also introduced. However, no provision for ductile RC detailing or modern capacity design considerations was yet included.
However, in the same period, the concepts of modern seismic RC design and the importance of detailing began to be acknowledged. As an example, the 1971 ACI-318 code contained recommendations for seismic design included some provisions for beam-column joint shear design.

Finally, the 1976 loadings code, "NZS 4203:1976 Code of practice for General Structural Design and Design Loadings for Buildings" incorporated provisions for both capacity design and ultimate strength design forming the basis of the current New Zealand seismic loadings code, NZS 1170.5:2004.

Typical deficiencies of pre-1970s non-ductile RC frames in New Zealand

In this study, a pre-1970's non-ductile reinforced concrete frame building has been taken as the subject of retrofit interventions and loss assessment. As previously briefly reviewed, this kind of building is characterized by typical deficiencies that derive from the lack of technical knowledge (and codification) at the time of their design and construction. In this section, the most relevant design flaws of pre-1970's non ductile RC frames buildings are summarized, while a more comprehensive review can be found in Pampanin, Calvi et al. (2002), Kam (2010), Akguzel (2011), and Beetham (2013) to which the interested reader is referred.

Inadequate seismic and lateral force design requirement

As expected, buildings designed before the definition of modern seismic codes generally exhibit insufficient lateral strength capacity and inadequate lateral stiffness mainly due to the slenderness of their columns. As an example, it has been observed (Brunsdon and Priestley, 1984) that pre 1970's short period buildings could be under-designed by 40% to 60% when compared to the provisions of more recent seismic codes (NZS4203:1976).

Absence of capacity design considerations

Capacity design principles have been included in modern seismic codes to ensure the development of ductile inelastic mechanisms under seismic action. Specific design and detailing requirements are provided in order to avoid brittle failure modes such as shear failures and reinforcing anchorage failures while ensuring the activation of a more desirable

ductile failure mode. In particular, in the case of RC frames, a beam-sway inelastic mechanism should be activated during an earthquake. However, in pre-1970's RC frames, due to the large depths of the beams, they can be characterized by higher capacities when compared to the corresponding columns, increasing the probability of incurring in collapse triggered by the development of a brittle soft-storey mechanism.

Insufficient transverse reinforcement

Transverse reinforcement plays a significant role in modern building design, as it has been acknowledged that it is capable of providing both shear capacity and confinement. Especially in the case of column elements, where high axial loads are expected, transverse reinforcement is also responsible of providing anti-buckling restraint to the longitudinal reinforcing bars. In the case of pre 1970's RC frames the transverse reinforcement is typically inadequate for both columns and beams. In the first case, the columns become susceptible to flexural, shear and axial failures, that could lead to the formation of brittle inelastic mechanisms. On the other hand, inadequate transverse beam reinforcement could result in a lack of confinement that in turn could result in insufficient ductility capacity.

Problems of development lengths, anchorage and splicing

Other typical issues that characterize pre 1970's RC frames are the inadequate reinforcing development lengths and lap splices. In particular, this is mainly due to the following reasons: a) the use of plain round reinforcing bars. These bars usually were terminated with 180° hooks in beam-column joint and had poor bond behaviour. Therefore, bond slip of longitudinal beam and concrete spalling were likely to occur due to concentrated compressive forces at the anchorage. b) The column longitudinal reinforcing was usually lapped at the floor levels. This practice took hold for ease of construction, however it is now well established that these zones are potential locations of moment reversal plastic hinges in the columns. c) Development length and splices were inadequate for the lack of experimental experience and data on the cyclic behaviour of bond between reinforcement and concrete. Only in the mid-1970's the researches and experience on this topic was advanced enough to define specific development lengths for plain-round bars.

Deficiencies in the design and detailing of joints

Two principal inadequacies could be distinguished within the beam column joint region in pre 1970's RC frames, namely the absence of horizontal shear reinforcement and the ineffective

anchorage of beam longitudinal reinforcement into the joint core. These two aspects are critical for various reasons, in fact an adequate reinforcement in the joint panel is essential for the development of a reliable joint shear transfer mechanism beyond joint diagonal cracking, prevents buckling of the longitudinal column reinforcement and provides confinement to the joint core. As for the anchorage detailing of beam longitudinal reinforcing into the joint core, this is crucial to provide an effective transfer of stresses. As an example Figure 8 shows different exterior joint damage mechanisms observed when different schemes of the end anchorages are adopted. In particular, it should be pointed out that, in the 70's, both the bend-away 90° hook and the 180° hook anchorages were considered acceptable anchorage systems.

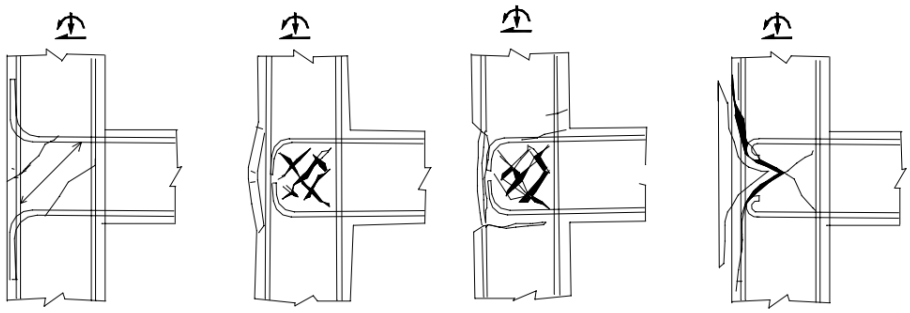

Figure 8: Alternative damage mechanisms for exterior tee-joints (from Pampanin et al. 2002)

Recognizing the relevant effect that beam column joints have on the global response of existing non-ductile frame structures, in the past decades a large body of research and experimental campaigns have been carried out in order to increase the level of understanding of the phenomena involved in the joint region and calibrate appropriate relationships to improve the accuracy of numerical models.

In particular, the influence of many parameters have been investigated, including the amount of longitudinal and transverse reinforcement and their diameters, the level of axial load and the anchorage details. Among them, Beres, White et al. (1992) and Pessiki, Conley et al. (1990) tested 20 interior and 14 exterior full-scale beam-column joints under quasi-static cyclic loading and several as-built parameters. Pull-out anchorage failure of the lower longitudinal bars of the beams was typically observed in the interior joint specimens as a consequence of limited embedded length and loss of bond beyond joint cracking. For exterior joints, however, failure occurred as a consequence of excessive joint diagonal cracking together with lap-splice failure in the column and push-out of the concrete cover. A beneficial effect of an increase in axial load on the column was highlighted by this investigation. In fact, higher axial load delayed critical shear cracking and also provided better confining action to the embedded bars,

delaying their incipient pull-out. A second example is provided by Hakuto, Park et al. (2000), who tested two exterior beam-column joints with two beam anchorage details with very little transverse reinforcement in the members and in the joint core. Due to the different anchorage system, the two specimens provided completely different outcomes. In particular, the one characterized by 90° end-hooks bent into the joint core showed negligible joint and column cracking, while the second, detailed with 90° end-hooks bent away from the joint, failed in shear after the formation of diagonal tension cracking in the joint. As this investigation was performed adopting deformed bars, Liu and Park (2001) repeated Hakuto et al.'s experiments using plain round bar longitudinal reinforcement. It was recognized that the same beam-column joint with plain reinforcement, when compared to the joint with deformed reinforcement, had twice the flexibility and 25% less strength. Moreover, it was observed that increasing the compressive axial load, the non-ductile exterior beam-column joints showed an increase in stiffness and strength.

Of particular interest for this research are the results presented by Pampanin et al. (2002). The authors investigated the behaviour of two exterior, two interior and two knee beam-column joints, all representative of pre-1970's construction practice. Poor detailing and plain round reinforcement were adopted for all the specimens, in particular anchorage is provided by end-hook and the capacity design principles are neglected. The specimens were tested under quasi-static loading. In order to better represent the actual conditions of the stress level in the joint due to the sway of the frame building, the column axial load was varied by means of a hydraulic jack during testing. Brittle failure mechanism was observed for the exterior joints, which led to the expulsion of a concrete-wedge at the outer side of the column. In fact, the authors recognised that this brittle hybrid failure mechanism is triggered by joint shear damage combined with slippage of longitudinal beam bars within the joint region (enhanced by the use of round bars) which resulted in the localized compressive push-out force at the end-hook anchorage responsible for concrete spalling (Figure 8d).

This hybrid failure mode, leading to local failure and loss of bearing-load capacity, was termed by the authors as "shear hinge" mechanism to highlight the fact that in this case the hinge is activated by shear rather than by a flexural behaviour and it is not expected to provide ductility capacities or energy dissipation, as a rapid joint strength degradation after joint diagonal cracking is expected. The same behaviour has also been observed by Kam (2010), who tested 2/3 scale exterior joints with detailing deficiencies and end-hooks anchorages under cyclic loadings to investigate the effect of selective weakening and post-tensioning in typical

pre-70's frame structures. In the as-built specimen, Kam observed progressive joint cracking and reported severe bond degradation in the compressive reinforcement, where the 180° hooks did not provide reliable compressive anchorage leading to the expulsion of the concrete wedge. Localized bond failure was also observed in the tensile reinforcement, in correspondence of a flexural crack at the beam-column interface. However, beyond the unbounded length of the rebar within the crack, tensile stresses could still be developed in the steel as the 180° hook resulted in an effective anchorage in tension. Following the diagonal joint cracking, the ultimate joint strength was then reached due to the loss of compressive strut capacity from the spalling and crushing of the concrete within the joint core. Hence the author suggests that by mitigating these two phenomena, the ductility capacities of the beam-column joint system could be improved.

Figure 9: Development of a shear hinge mechanism with concrete-wedge expulsion (from Kam, 2010)

Based on the results of the experimental investigation carried out by Pampanin et al. (2002) mentioned earlier, and further numerical results, Pampanin, Magenes et al. (2003) proposed the following limit states based on the joint shear distortion for exterior joints with poor detailing.

Limit State	Subassembly Drift (%)	Joint Shear Deformation [rad]
First diagonal cracking	0.65	0.0002
Extensive Damage	1.0	0.005
Critical Damage (repairability issues)	1.5	0.01
Incipient Collapse	2	0.015

Table 1: Limit states for exterior reinforced concrete tee-joints with substandard details based on joint shear deformation (from Pampanin et al., 2003)

These limit states, in particular the values of joint shear deformation corresponding to the critical damage and incipient collapse limit states will be employed within this study to assess structural performance, while the joint distortion corresponding to the cracking limit state will be defined according to the findings of Kam (2010), as the case-study considered here and described in the following section is the one developed by Kam and based on which the tested joint specimens have been realized.

Presentation of the case-study

In order to facilitate the description of the framework, a case study building is considered, consisting of a prototype reinforced concrete frame structure, described in more detail in Kam (2010). This non-ductile six-storey frame was designed to represent a mid-rise office building, reflecting the typical deficiencies of a code conforming pre-1970 multi-storey building. It is symmetrical in plan, with four frames of three bays in each direction. Poor material properties and structural detailing, e.g. lack of joint shear reinforcement in the beam-column joints and plain round beam bars with end-hooks anchorage in the joint region, together with the lack of capacity design principles with beams that are stronger than the columns, represent a possible worst case scenario of older construction practice.

A schematic representation of the considered frame is shown in Figure 10, together with the cross section of both beams and columns.

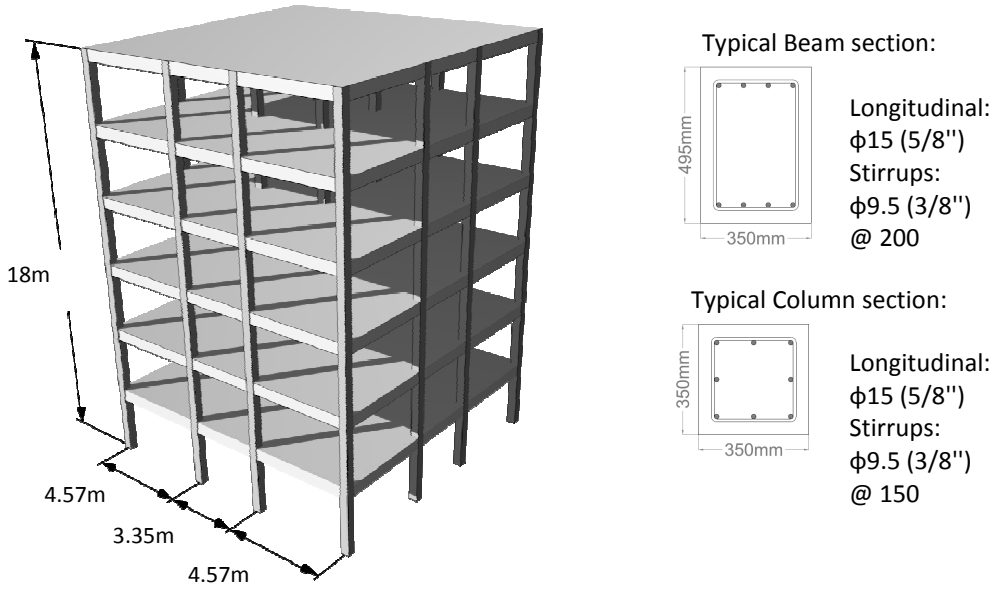

Figure 10: Geometry and structural details for the case study RC frame building (modified after Kam, 2010)

The total gravity loads are summarized in **Table 2**.

	Column Axial Loads (kN)			
	Exterior Frame		Interior Frame	
Level	Exterior Column	Interior Column	Exterior Column	Interior Column
Level 6	33	56	56	98
Level 5	87	139	139	217
Level 4	142	221	221	337
Level 3	197	303	303	457
Level 2	252	385	385	576
Level 1	307	467	467	696

Table 2: Gravity loads for the case study building

Given the relatively short spans characterizing the structure, a perimeter frame is assumed as lateral resisting system. This choice intentionally enhances the seismic vulnerability of the structure, in fact while the tributary width used to determine the seismic mass pertaining to a specific frame is equal to the bay width for space frame structures, this corresponds to half of the total width of the building for perimeter frame structures (refer to Figure 11).

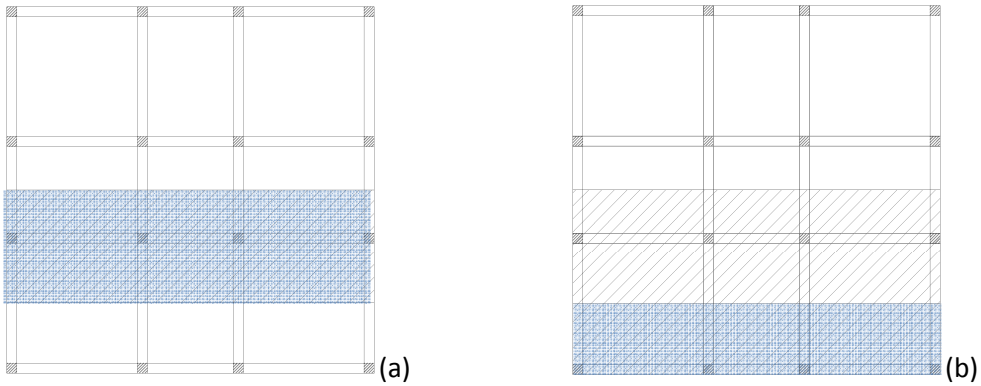

Figure 11: Tributary areas in case of space (a) and perimeter frames (b): the dashed area represents the tributary area computed to evaluate seismic mass, while the blue one is the area adopted to evaluate gravity loads

A concrete compressive strength of 20MPa is assumed for the case study building and a peak compressive strain (ε'_c) and an ultimate unconfined strain (ε_{cu}) of 0.002 and 0.004 respectively are used to define the stress strain relationship. Grade 275 reinforcing is assumed for both longitudinal and transverse reinforcing, the properties of which have been desumed by a study from Andrino and Park (1986), who investigated the properties of New Zealand manufactured deformed reinforcing bars. Despite the fact that the current study considers round bars and not deformed ones, the provided data have been still used to define the reinforcing properties

for the case study structure. Non-linear concrete and steel stress-strain relationships are described through Mander model and King model respectively.

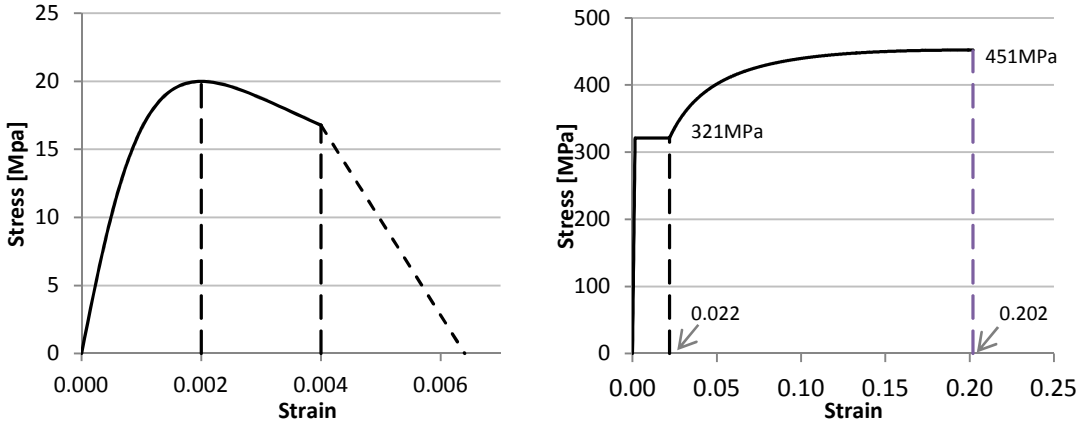

Figure 12: Material properties for the case study RC frame building: (a) concrete stress-strain relationship and (b) reinforcing steel stress-strain relationship.

4. Hierarchy of Strengths Assessment

Introduction

In order to assess the performance of the structure of interest, the hierarchy of strength of the beam-column joint sub-assembly is evaluated. By identifying the critical weakness within the system, the plastic mechanism and hence the likely failure mode can be estimated.

Following the methodology suggested by Pampanin (2006), the relative capacities of beams, columns and beam-column joints can be compared in terms of a so-called "Equivalent" Column Moment, M_c, for the limit state of interest. In fact, while assessing structural performance, different limit states can be defined for each structural element of the beam-column joints. For the purposes of this study, the assessment is performed targeting life-safety and collapse prevention, hence focusing on critical strength and ductility/displacement ultimate limit states.

Once the capacities of the structural elements are evaluated, they can be represented in an Equivalent Column Moment-Axial Load interaction diagram, or performance domain, and compared with the level of demand (expressed in terms of variation of axial load due to the frame lateral swaying under seismic action) associated to the considered limit state, predicting the sequence of events expected within the joint region, as shown in Figure 13, taken from the reference paper.

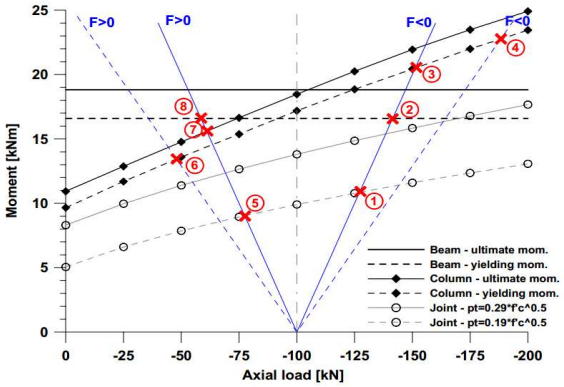

Specimen T1 (as-built)			
Type of lateral force	N°	Event	Lateral force [kN]
Open joint F<0	1	Joint cracking and deterioration starting $p_t = 0.19\sqrt{f'_c}$	-10.94
	2	Beam yielding	-16.59
	3	Upper column yielding	-20.50
	4	Lower column yielding	-22.75
Close joint F>0	5	Joint failure	9.37
	6	Lower column yielding	13.50
	7	Upper column yielding	14.50
	8	Beam yielding	16.59

Figure 13: Hierarchy of strength of the beam-column joint sub-assembly and identification of the predicted sequence of events (from Pampanin, 2006).

The equivalent column moments for beam flexural capacity, M_b, beam shear capacity, V_b, and beam-column joint horizontal shear capacity V_{jh}, termed $M_{c,bf}$, $M_{c,bs}$ *and* $M_{c,j}$ respectively, can be derived from equilibrium and geometrical considerations for exterior and interior joints, as will be outlined in the following sections.

Equivalent column moments for exterior joints

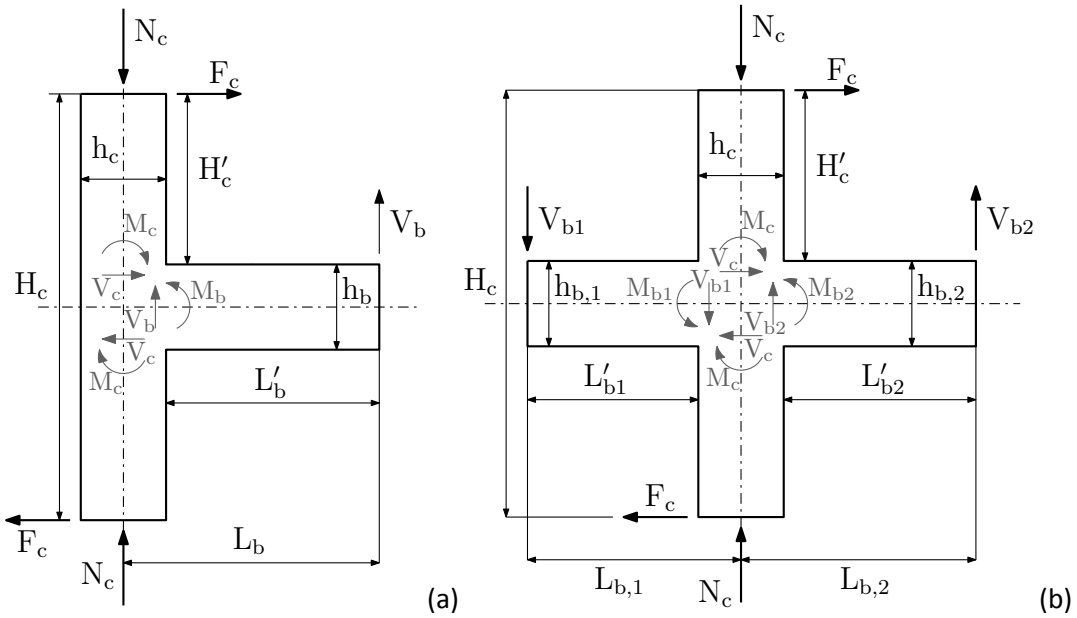

Figure 14: Schematic representation of geometry and nomenclature for exterior (a) and interior joints (b).

With reference to Figure 14(a) the equivalent column moment $M_{c;bf}$ for the beam flexural capacity at the beam-column interface can be calculated as follows:

$$F_c \cdot H_c = V_b \cdot L_b \tag{4.1}$$

$$M_b = V_b \cdot L'_b \tag{4.2}$$

Combining these first two equations:

$$M_b = F_c \cdot H_c \cdot \frac{L'_b}{L_b} \text{ where } F_c = \frac{M_c}{H'_c} \tag{4.3}$$

$$M_b = M_c \cdot \frac{H_c}{H'_c} \cdot \frac{L'_b}{L_b} \tag{4.4}$$

resulting in a beam moment which is approximately twice the column moment, as it can be expected for exterior joints.

The column moment due to beam flexure $M_{c,bf}$ is then given by:

$$M_{c,bf} = M_b \cdot \frac{H'_c}{H_c} \cdot \frac{L_b}{L'_b} \tag{4.5}$$

Similarly, the equivalent column moment due to a given beam shear, $M_{c,bs}$, can be calculated as follows:

$$V_b \cdot L'_b = F_c \cdot H_c \cdot \frac{L'_b}{L_b} \tag{4.6}$$

$$V_b = M_c \cdot \frac{H_c}{H'_c} \cdot \frac{1}{L_b} \tag{4.7}$$

Rearranging the previous equation, the equivalent column moment can be obtained:

$$M_{c,bs} = V_b \cdot L_b \cdot \frac{H'_c}{H_c} \tag{4.8}$$

Finally, the equivalent column moment for a given horizontal joint shear, $M_{c,j}$, can be calculated based on horizontal equilibrium:

$$V_{jh} = C_c + C_s - V_c \tag{4.9}$$

where C_c and C_s are the resultants of the compressive stresses in the concrete and steel respectively, while T_s is the force associated to the reinforcing steel in tension. Assuming that $C_c + C_s = T_s$, the previous equation can be reduced to:

$$V_{jh} = T_s - V_c \quad \text{where} \quad T_s = \frac{M_b}{d} \quad \text{and} \quad V_c = \frac{M_c}{H'_c} \tag{4.10}$$

$$V_{jh} = \frac{M_b}{d} - \frac{M_c}{H'_c} \tag{4.11}$$

where d is the internal lever arm of the moment couple in the beam critical section

By substituting equation (4.4) into equation (4.11), the following equation for the equivalent column moment for a given horizontal exterior joint shear can be obtained:

$$M_{c,j} = \frac{V_{jh} \cdot H'_c}{\frac{H_c}{d} \cdot \frac{L'_b}{L_b} - 1} \tag{4.12}$$

where *d* is the internal lever arm of the moment couple in the beam critical section.

Equivalent column moments for interior joints

Similar considerations lead to the evaluation of the equivalent column moments for the interior joint (refer to Figure 14(b)). In particular, from global equilibrium:

$$F_c H_c = V_{b1} L_{b1} + V_{b2} L_{b2} \tag{4.13}$$

Substituting $F_c = M_c / H'_c$, $V_{b1} = M_b / L'_{b1}$ and $V_{b2} = M_b / L'_{b2}$ into the previous equation and assuming $M_b = M_{b1} = M_{b2}$, the equivalent column moment corresponding to a given beam moment can be obtained:

$$M_{c,bf} = M_b \cdot \frac{H'_c}{H_c} \cdot \left(\frac{L_{b1}}{L'_{b1}} + \frac{L_{b2}}{L'_{b2}} \right) \tag{4.14}$$

Substituting $F_c = M_c / H'_c$ into equation (4.13) gives the equation for the equivalent column moment for a given beam shear.

$$M_{c,bs} = V_b \cdot \frac{H'_c}{H_c} \cdot \left(L_{b1} + L_{b2} \right) \tag{4.15}$$

The equivalent column moment for a given horizontal joint shear at an interior joint can be determined through the following equations based on horizontal equilibrium:

$$V_{jh} = 2T_s - V_c \tag{4.16}$$

$$V_{jh} = \frac{2M_b}{d} - \frac{M_c}{H'_c} \tag{4.17}$$

Substituting M_b from equation (4.14) in equation (4.17) gives:

$$V_{jh} = \frac{2 \cdot M_c \cdot H_c}{d \cdot H'_c} \frac{1}{\left(L_{b1}/L'_{b1} + L_{b2}/L'_{b2} \right)} - \frac{M_c}{H'_c} \tag{4.18}$$

Hence, the following expression for the equivalent column moment for a given horizontal joint shear capacity can be deducted:

$$M_{c,j} = \frac{V_{jh} \cdot H'_c}{\frac{2 \cdot H_c}{d \cdot \alpha} - 1} \quad \text{where} \quad \alpha = \left(\frac{L_{b1}}{L'_{b1}} + \frac{L_{b2}}{L'_{b2}} \right) \tag{4.19}$$

Evaluation of elements capacities:

Beam and Column Flexural Strength Evaluation

Beam and columns flexural capacities have been evaluated based on their geometrical characteristics and material properties through sectional analysis. CUMBIA (Montejo and Kowalsky, 2007), was adopted in order to perform the moment-curvature analysis.

Column Lap Splice

Under reversal cyclic loading, longitudinal column reinforcement could be subjected to tension forces. For this reason, the stresses that can be developed in the longitudinal column bars at the lap splices have to be assessed.

The maximum stress developed in the reinforcing bars without sufficient development lengths is determined according to the ACI-318 as follows:

$$f_s = 1.25 \left(\frac{l_{d,prov}}{l_d} \right)^{2/3} f_y \tag{4.20}$$

where $l_{d,prov}$ is the provided development length and l_d is the required development length.

The required development length in tension have been calculated in accordance with NZS 3101:Part 1:2006 and was taken as twice the value specified in the standard to allow for the use of plain round bars:

$$l_{db} = 2 \cdot \frac{0.5 \alpha_a f_y}{\sqrt{f'_c}} d_b \tag{4.21}$$

where α_a=1.3 for beam top reinforcement with at least 300mm concrete underneath the bars and 1.0 for all other cases.

The required development length was found to be in good agreement with the same parameter obtained following the ACI-318, which is given by:

$$l_d = \frac{9}{10}\frac{f_y}{\lambda\sqrt{f_c'}}\frac{\Psi_t\Psi_e\Psi_s}{\left(\frac{c+K_{tr}}{d_b}\right)}d_b \tag{4.22}$$

where the transverse reinforcement index, K_{tr}, is a function of the area of confining stirrup with yield strength f_{yt}, the number of bars and the spacing of transverse reinforcement; c is the smaller of the distance from the center of the bars to concrete surface and one-half of the center-to-center spacing of the bars; λ is to account for lightweight aggregate. Ψt , Ψe, Ψs are modification factors accounting for reinforcement location, coating type and size respectively. For most pre-1970s existing RC frames, these factors (λ, Ψt, Ψe, and Ψs) can be taken to be 1.

Beam and Column Shear Strength Evaluation

For the purposes of this study, the shear strength capacity of the beam and columns are evaluated using the model proposed by Sezen and Moehle (2004) for lightly-reinforced columns and included in the ASCE-41:

$$V_n = k_\Delta\left(V_c + V_s\right) \tag{4.23}$$

$$k_\Delta = \begin{cases} 1.0 & \mu_\Delta \le 2 \\ 1.0 - 0.075\left(\mu_\Delta - 2_s\right) & 2 < \mu_\Delta \le 6 \\ 0.7 & \mu_\Delta > 6 \end{cases} \tag{4.24}$$

$$V_c = \left(\frac{0.5\sqrt{f_c'}}{a/d}\sqrt{1+\frac{P}{0.5\sqrt{f_c'}A_g}}\right)0.8A_g \tag{4.25}$$

$$V_s = \frac{A_{st}\,f_{yh}\,d}{s} \tag{4.26}$$

where μ_Δ is the displacement ductility, P is the axial compressive load, a is the distance from maximum moment section to point of inflection (typically 0.4-0.6H_c for columns), d is the effective depth of the section, A_g is the gross area of the section and A_{st}, f_{yh} and s are the reinforcement area, yield strength and spacing of the transverse reinforcement respectively.

Joint shear strength assessment: Principal stresses approach

The Joint shear capacity has been assessed adopting an approach based on principal joint stresses. For a beam-column joint without shear reinforcement the horizontal joint shear stress inducing diagonal cracking, v_{jh}, is governed by the behaviour of unconfined concrete

under bi-directional stresses. Given a limit for the principal compressive and tensile stresses of the concrete (p_c and p_t) the maximum horizontal shear stress prior cracking (v_{jh}) is given by:

$$p'_c, p'_t = \frac{f_v + f_h}{2} \pm \sqrt{\left(\frac{f_v - f_h}{2}\right)^2 + v_{jh}^{\ 2}} \tag{4.27}$$

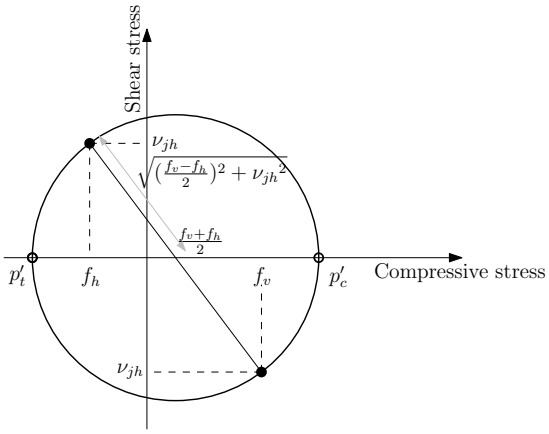

Figure 15: Representation of vertical and horizontal stresses as well as principal stresses through Mohr's circle.

The maximum joint shear stress sustained prior to cracking can thus be obtained rearranging the previous equation and noticing that the average horizontal stress (f_h) is typically equal to zero, as no pre-stressing is assumed, while the average vertical stress (f_v) is given by P/A_g.

$$v_{jh} = \sqrt{p'^{\,2}_t - p'_t \cdot (f_v + f_h) + f_v \cdot f_h} \tag{4.28}$$

The principal compression stress, p'_c, is assumed equal to $0.3\, f'_c$ following the suggestion by Priestley et al. (1996) in order to prevent a diagonal compression strut failure.

As for the considered principal tensile stresses, these are typically expressed as a function of the square root of concrete compression strength, $\sqrt{f'_c}$. According to the findings of experimental and numerical investigations on exterior beam-column joints with end hooks and smooth bars carried out by Pampanin, Calvi et al. (2002) and Calvi, Magenes et al. (2002) the principal tensile stress corresponding to first cracking can by defined as $0.2\sqrt{f'_c}$. Given the configuration of the anchorage of the beam longitudinal reinforcement into the panel zone, this should also be considered as an upper bound of tensile stress, as no alternative shear transfer mechanism can be activated beyond joint cracking. Conversely, for interior joints, cracking is suggested to initiate at higher levels of principle stress, namely $0.29\sqrt{f'_c}$,

followed by a hardening behaviour until $0.42\sqrt{f'_c}$, thanks to the compression strut that can still be developed. The behaviour of the joints beyond the maximum achievable tensile stress will be discussed in more details in the following chapter.

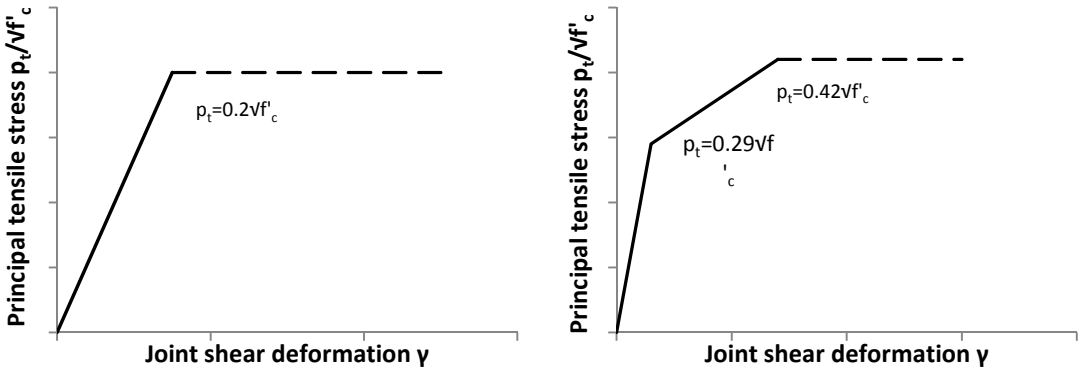

Figure 16: Behaviour of exterior (a) and interior (b) beam-column joint shear hinge model after Calvi et al. (2002)

Evaluation of seismic demand

As already mentioned, seismic demand is acknowledged in the hierarchy assessment by introducing the variation of axial load due to the horizontal loading on the considered frame. This varying axial demand on columns can greatly affect the capacities of the structural elements within a beam-column joint sub-assembly. As a consequence, the relative strengths and thus the sequence of events leading to failure might be modified.

The variable axial load have been imposed and quantified as a function of the lateral load applied to the columns (Kam, 2010), as illustrated in the equation below, where the constant α is a geometric function of the frame and $V_{c,ext}$ is the lateral force applied at the top of one of the exterior columns:

$$N = N_g + \Delta N_e = N_g + \alpha \cdot V_{c,ext} \tag{4.29}$$

The variation in the axial load at the exterior beam-column joints due to seismic excitation can be estimated through geometry and equilibrium considerations based on the following hypothesis:

- the variation of axial loads due to seismic excitation affects only the exterior columns;
- the total lateral force F is acting at 2/3 of the total building height, H_n;
- the point of contra-flexure of the columns is located at $0.6h_c$;

- failure is governed by the inelastic mechanism of the exterior beam-column joints, hence the column shear and moments are assumed to be equal at the interior and exterior columns.

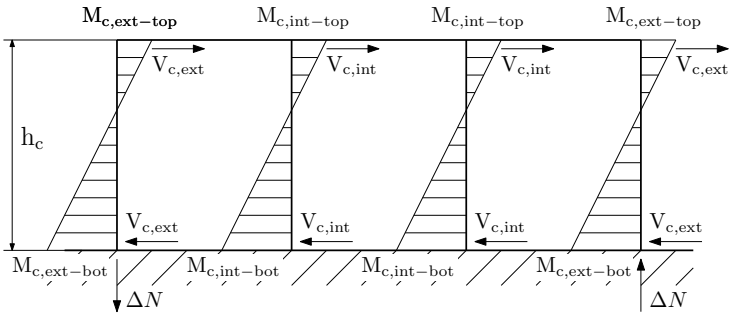

Figure 17: Schematic representation of the actions considered in the estimation of the variation of axial loads in the exterior columns.

With reference to Figure 17, the following equations apply:

$$M_{c,ext-top} = \frac{2}{3} M_{c,ext-bot} \tag{4.30}$$

$$V_{c,ext} = \frac{M_{c,ext-top} + M_{c,ext-bot}}{h_c} = \frac{5}{2}\frac{M_{c,ext-top}}{h_c} \tag{4.31}$$

$$V_{c,int} = \frac{M_{c,int-top} + M_{c,int-bot}}{h_c} = \frac{5}{2}\frac{M_{c,int-top}}{h_c} \tag{4.32}$$

$$F = \sum V_c = 2 \cdot V_{c,ext} + 2 \cdot V_{c,\mathrm{int}} = 5\frac{M_{c,ext-top}}{h_c} + 5\frac{M_{c,int-top}}{h_c} \tag{4.33}$$

Assuming $M_{c,ext\text{-}top}$=$M_{c,int\text{-}top}$:

$$F = 10\frac{M_{c,ext-top}}{h_c} \tag{4.34}$$

The ratio of the total lateral force F to the lateral force at the exterior column $V_{c,ext}$ can be derived:

$$\frac{F}{V_{c,ext}} = \frac{10\dfrac{M_{c,ext-top}}{h_c}}{\dfrac{5}{2}\dfrac{M_{c,ext-top}}{h_c}} = 4 \tag{4.35}$$

Moreover, from equilibrium:

$$\frac{2}{3} F \cdot H_n = \Delta N \cdot B + \sum M_c \tag{4.36}$$

$$\frac{2}{3} F \cdot H_n = \Delta N \cdot B + F \cdot 0.6 h_c \tag{4.37}$$

Therefore for an exterior column the variation in the axial load is governed by the following relationship:

$$\Delta N = \alpha \cdot V_{c,ext} = \frac{F \cdot \left(\frac{2}{3} H_n - 0.6 h_c \right)}{B} \tag{4.38}$$

$$\Delta N = \frac{F \cdot \left(\frac{2}{3} H_n - 0.6 h_c \right)}{B} \cdot \frac{V_{c,ext}}{V_{c,ext}} = \alpha \cdot V_{c,ext} \tag{4.39}$$

where

$$\alpha = \frac{F}{V_{c,ext}} \cdot \frac{\left(\frac{2}{3} H_n - 0.6 h_c \right)}{B} \tag{4.40}$$

Performance Domains for the beam-column joints of the case-study building

The Performance Domains for exterior and interior joint sub-assemblies are presented in Figure 18 and Figure 19 respectively with reference to an exterior frame.

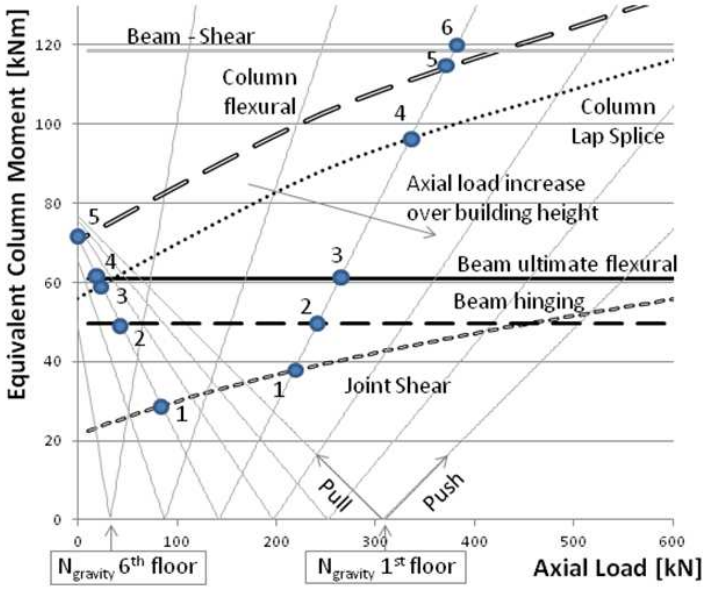

Figure 18: Hierarchy of strength for the exterior joints in the M_c-N performance domain (the numbered dots, for example, represent the sequence of events expected within the elements of the exterior joint region at the fourth floor).

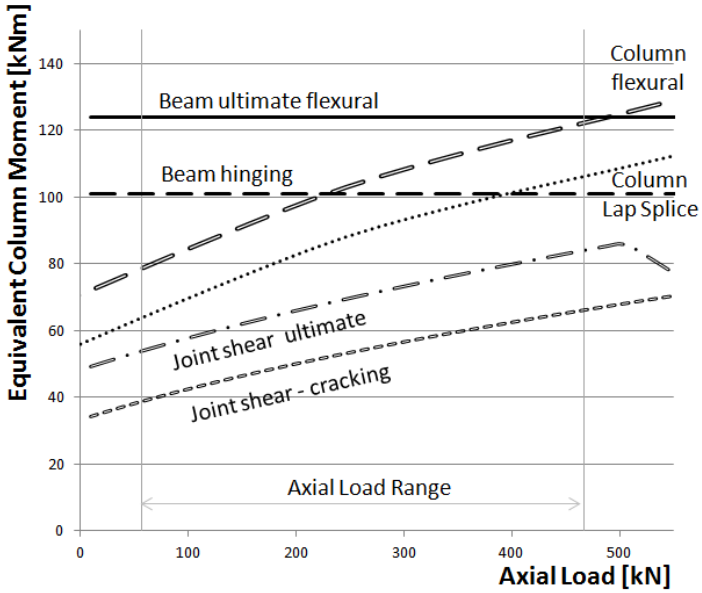

Figure 19: Hierarchy of strength for the exterior joints in the M_c-N performance domain.

It can be observed that for exterior beam-column joints, joint cracking can be expected to develop before any other mechanism due to the combined effects of inefficient strut mechanism and concentrated compressive force associated to bond deterioration of the reinforcement in compression and bar slip at the end-hook anchorage. However it can be observed that thanks to the positive effect of the axial load increase, some beam hinging might also occur at the ground level in the push-direction. This observation is consistent with a comment found in Priestley (1997), which stated: "*Joint cracking will first develop under positive beam moments, since axial force on the column is reduced for this direction of response. In a multistory building, the axial force variations in exterior, and in particular, in corner columns can be very high, and as a consequence, cracking under negative moment will be delayed, and may not occur at all.*".

The assessment of the interior joints show that shear cracking should be expected over the full range of axial loads, followed by the achievement of the joints' ultimate capacities.

The expected poor bond behaviour within the beam-column joint region due to plain round bars is almost unavoidable but could be mitigated if joint cracking is prevented by means of a retrofit intervention. However, several authors acknowledged that beam bar slip could result in a reduction of moment capacity leading to a modification of the local hierarchy of strength within the beam-column joint sub-assembly. In fact, since gravity load design typically results in a weak-column strong-beam system, the effects of bar slip in beams framing in the interior joints could result in a safer weak-beam/strong-column failure mode, limiting the joints' shear demand and their damage. Furthermore, considering the confinement deriving from the framing beams, the load-bearing capacity can be generally maintained in interior joints, as the axial load demand can be sustained by alternative load paths of concrete compression struts and by column longitudinal reinforcement. As a result, life safety and collapse-prevention could be achieved adopting a retrofit strategy involving only the exterior joints, which are expected to govern the seismic performance of the building.

5. Assessment of seismic performance of the existing structure and design of retrofit alternatives through finite element modelling

Introduction

In order to accurately predict the seismic response of reinforced concrete structures, different modelling approaches have been proposed and developed in the last decades, reflecting the improvements in understanding the phenomena governing structural behaviour under seismic excitation coupled with the increasing available computational resources.

The finite element models for the non-linear analysis of RC frames belong to two fundamental categories: lumped-plasticity and distributed-plasticity models. A third category, the three-dimensional continuum finite element modelling could be also identified, but due to the highest level of discretization and complexity, it is typically employed to model smaller portions of the building and not the whole structure (e.g. beam column joint sub-assembly).

Lumped-plasticity models (Giberson, 1967) require that the portion of the elements where plastic deformations are expected is defined "a priori", identifying the location, usually at both ends of beam and column elements, and length of the expected plastic hinges, which is the only portion of the element where inelastic deformations can occur. This is a simplification of the actual behaviour, as inelastic deformations are expected to spread gradually into the member as a function of loading history. The plastic hinge must be defined by a moment-curvature relationship, usually obtained from a sectional analysis conducted beforehand and described by a bi-linear law.

On the other hand, the distributed-plasticity models replace the non-linear concentrated plastic hinge zone with a smeared (distributed) non-linear zone at the location of the plastic hinges, allowing to model the spread of the inelastic deformation along the elements. When the element is subdivided into longitudinal fibers, these models are termed Fiber Models. In such an approach, the cross-sections of the frame elements is subdivided in fibres, each of them characterized by an appropriate stress-strain relation representing either concrete or longitudinal steel reinforcement (or even other materials), depending on the location of the

fiber within the section. Hence, conversely to what happens in the lumped-plasticity models, the force-deformation relationship of the cross-section is not specified directly by the user, but it is obtained by the integration of all the fibres across the thickness of the section.

The diffusion of the lumped-plasticity modelling is due to the relatively lower computational cost, however this approach requires the adoption of an appropriate moment-rotation hysteresis rule, the parameters of which must be defined with care and possibly calibrated against experimental results. Moreover, the Flexural-Axial interaction behaviour must be accounted for introducing rules expressly implemented for this purpose.

On the contrary, fiber models do not require a sectional analysis to be performed in advance and the aforementioned hysteresis loops and interaction diagrams do not need to be defined, as the interaction between flexural actions in orthogonal directions and axial force are directly computed, as well as the member post-peak behaviour. However, the main shortcoming of this modelling technique is represented by the phenomenon of strain localisation (Bazant, Pan et al. (1987); Taucer, Spacone et al. (1991) among others) that can lead to results that are dependent on the level of discretization of the element cross-section.

Only recently, more advanced finite elements have been proposed, combining the advantages of lumped and distributed-plasticity models, using only one monitoring section in each end inelastic zone of the structural member, but able to model the spread of the inelastic deformation under strain hardening response (Lee and Filippou, 2009).

For the purposes of this study the finite element software Ruaumoko (Carr, 2007), based on lumped-plasticity, have been adopted to model the prototype frame.

It was already pointed out that the global response under seismic loading of existing pre-70's RC frame structures is strongly influenced by the behaviour of its beam-column joints. These in turn depend on many different parameters including the joint shear capacity, confinement of joint core, level of axial forces, reinforcing details and material properties. Many approaches aiming at modelling beam-column joints are available in literature, targeting different levels of discretization and accuracy. Among the approaches that could be adopted within a lumped plasticity model, the simplest level is to model joint region adopting a macro-model with lumped plasticity spring. An example of this typology of models has been adopted by several researches (El-Metwally and Chen (1988) and Alath and Kunnath (1995) among others) and consists in a zero-length rotational spring element connecting beam to column elements and thus represents the shear distortion of the beam-column joint. Increasing the level of

refinement, different inelastic mechanisms of beam-column joints such as the anchorage failure, joint core shear failure and bond-slipping can be discretized and modelled using multiple non-linear springs macro-models. An example of this kind of models is provided by Lowes, Mitra et al. (2003), which proposed a model based on eight bar-slip components that are intended to simulate stiffness and strength loss associated with bond strength deterioration for beam and column longitudinal reinforcement embedded in the joint core, one shear-panel component that is intended to simulate strength and stiffness loss associated with shear failure of the joint core and four interface-shear components that simulate loss of shear-transfer capacity at the joint-beam and joint-column perimeter under severe loading of the joint (Figure 20b).

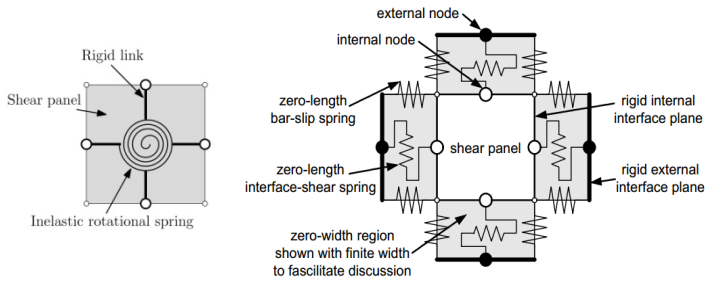

Figure 20: Single non-linear spring and multiple non-linear springs macro-models.

As already anticipated, when lumped-plasticity macro-models are adopted, the definition of an appropriate hysteretic rule is required, representing the expected behaviour under cyclic loading. Various hysteresis loops have been developed and are available in literature for RC beam-column joints. However only a smaller number of them are deemed adequate to represent the response of non-ductile RC beam-column joints. As an example, the Wayne-Stewart hysteresis, the SINA hysteresis and the Pampanin hysteresis rules are capable of model pinching and stiffness degradation typical of the pre-1970's beam-column joints with plain round bars and non-ductile detailing and have been implemented in the software Ruaumoko.

Due to their simplicity, macro-models constituted by a single non-linear rotational spring allow to model the joint region in a computationally-efficient manner. For this reason, Pampanin et al. (2003) proposed a simple joint shear rotational spring model, governing the relative rotation of beams and columns. The behaviour of the spring is governed by a moment-rotation relationship, where the moment values are derived from the principle stresses approach, once an appropriate empirical principle tensile stress versus shear-deformation relation has been

assumed. This modelling approach has been adopted in this study, and will be described in greater detail in the following sections.

In this Chapter, the model developed to represent the case-study building will be presented. Through non-linear static analysis the structure's performance will be assessed in terms of achieved %NBS. Then the procedure developed to conceptually design alternative retrofit solutions will be outlined.

Structural model of the existing RC frame structure

As mentioned earlier, the AB structure as well as the retrofitted alternatives are modelled using Ruaumoko (Carr, 2007), which relies on lumped-plasticity models, while the sectional analyses have been performed with CUMBIA (Montejo and Kowalsky, 2007).

Given the regular layout of the structure, a 2D model is deemed accurate. Newmark constant average acceleration with analysis time steps of either 0.001 seconds or one tenth of the excitation data interval has been adopted, together with Rayleigh damping based on the initial stiffness matrix.

Beams and columns are modelled using Giberson one-component beam members and concrete beam-column members respectively, where this latter element allows for Moment-Axial load interaction. The adopted hysteresis loops (represented in

Figure **21**) are "Fat modified Takeda" for the former and "Thin modified Takeda" for the latter to represent the energy dissipation expected for members subjected to high axial loads.

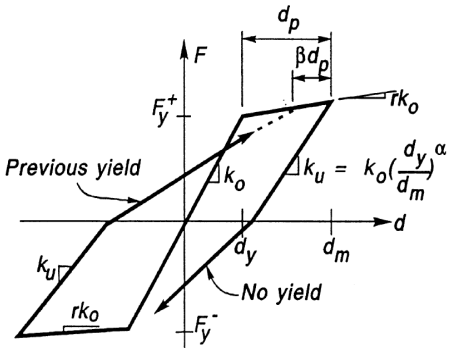

Figure 21: Illustration of modified Takeda hysteresis rule adopted for columns and beams (Carr, 2007).

The beam cracked section modulus is assumed as the secant stiffness at the 75% of the yield moment, while the column cracked section modulus is taken as $0.6I_g$, in which I_g is the gross section modulus following the recommendations of Paulay and Priestley (1992).

Both types of elements present rigid-ends at each edge, representing the portion of the elements comprised within the panel zone. The beam-column joint is modelled introducing rotational springs in each beam-column node whose moment-rotation characteristics have been derived from the principal tensile stress approach, as proposed by Pampanin et al. (2003). In particular, the equivalent joint spring moments are evaluated based on equilibrium considerations adopting the equations reported in Chapter 4 by defining the levels of principal tensile (or compression) stress in the joint region characterizing the levels of damage of interest (e.g. first cracking). The principal tensile stresses considered for the exterior and interior joints respectively are summarized in the figure below (reported for clarity from the previous chapter).

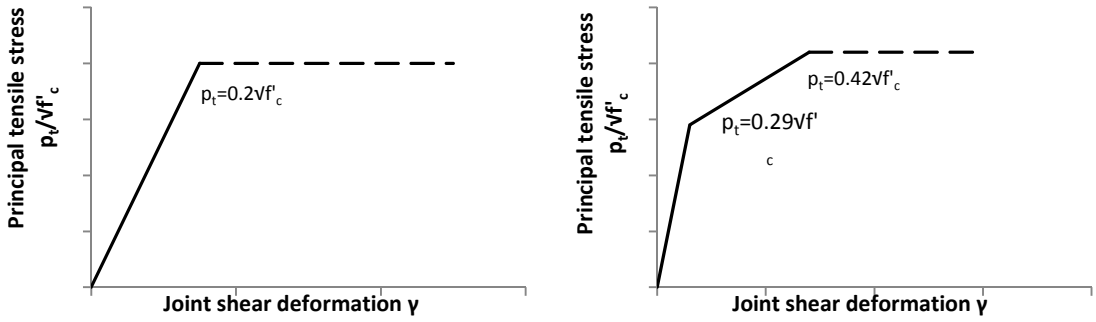

Figure 22: Behaviour of exterior (a) and interior (b) beam-column joint shear hinge model after Calvi et al. (2002)

The values of joint spring rotation are assumed based on the finding of an experimental campaign on exterior beam-column joints sub-assemblies carried out by Kam (2010). The tested specimens are representative of the joints of the same prototype building modelled within this study. Hence, according to the aforementioned investigation, a joint shear distortion at cracking of 0.15% can be assumed. Shear distortion at the same damage level for interior joint is obtained assuming equal rotational stiffness for both typologies of joints.

The SINA hysteresis rule is adopted for these elements as it can capture both pinching and degrading behaviour. In particular, the slope of the degrading branch, which is governed by gradual reduction of the effective joint principal tension stress, have been evaluated in

accordance with the relationship suggested by Priestley (1997), reported in the following graph.

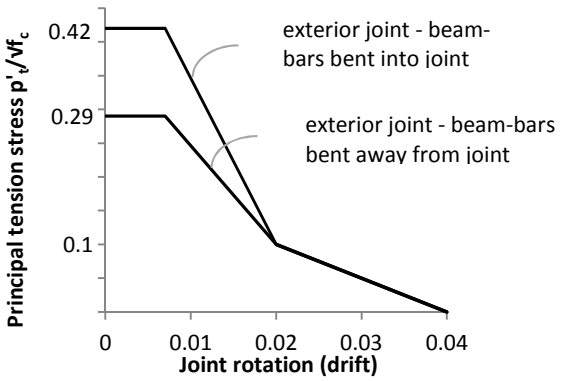

Figure 23: Strength degradation model for exterior joints (Priestley, 1997)

It is worth noticing that the peak principal tension stress allowed for the exterior joints with longitudinal reinforcement bars bent into the joint region according to Priestley has the same value of principal stress adopted by Calvi, Magenes et al. (2002) for the interior joints. This choice implicitly reflects the belief that the behaviour of interior joints can be considered similar to that of those exterior joints characterized by proper detailing allowing for the development of an efficient compression strut mechanism. For this reason, the strength degradation model suggested by Priestley has been adopted to evaluate the behaviour of the interior joints after the achievement of the maximum tensile strength. The slope of this latter degrading branch has been assumed equal for both interior and exterior joints.

Figure 24 illustrates the modelling assumptions for an exterior and an interior joint together with the hysteresis loop adopted.

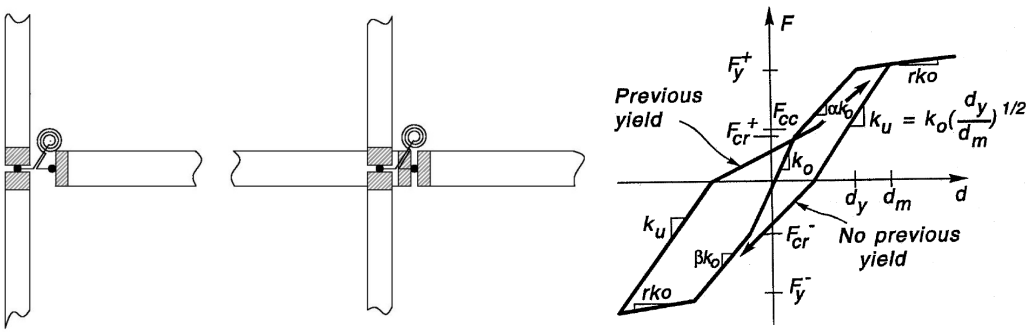

Figure 24: Beam, column and joint elements used in the modelling and representation of the SINA hysteresis rule associated with the joint element.

Moreover, the columns are assumed fixed at the base and P-Delta effects are included in the analyses.

At this stage, strength degradation in the beams and column elements have been omitted in order to limit the numerical complexity that could lead to convergence issues. However, the model could be refined introducing a backbone curve to be combined with the hysteretic response of beam and column members. The parameters of this curve could be evaluated using empirical equations proposed by Haselton, Liel et al. (2008), based on calibration to tests of reinforced concrete columns, as suggested by the PEER/ATC-72-1 (2012) report.

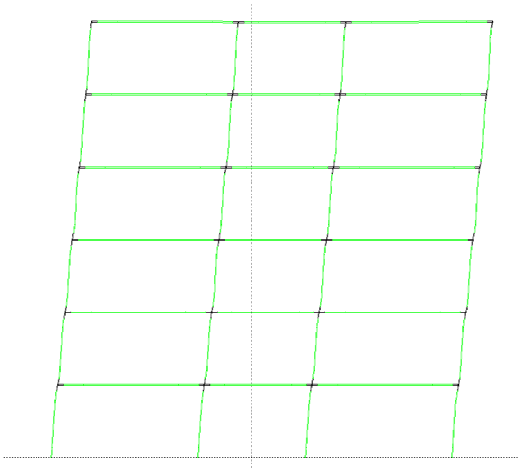

Figure 25: Image from the graphic interface of Ruaumoko2D (Carr, 2007) running a dynamic analysis.

Two considerations should be made about the aforementioned modelling assumptions:

- It has been shown in the previous chapters that the joint shear capacity is expected to vary with the level of axial load demand on the beam-column joint sub-assembly. For this reason, the modelling of the joint shear capacity would require a flexural-axial interacting element. However, this type of element is currently implemented in Ruaumoko only to model columns. Hence, the improved joint behaviour under higher compressive stresses (in the push-direction) can not be represented adequately so far, and the joints capacities can only reflect the contribution of static axial load.
- Constant Rayleigh damping (based on initial stiffness matrix) is used instead of the tangent stiffness Rayleigh damping, where the damping matrix is updated at each time step during the analysis together with the stiffness matrix. This simplifying assumption is introduced in order to limit the numerical complexity of the model, as it was

observed that selecting the latter damping model could lead to numerical instability issues.

- Moreover, it has been recognised that the choice of the damping matrix affects in a quite significant way the post-yield branch of the Base shear-displacement curve obtained through pushover analyses. This aspect is not usually considered since in this kind of analyses the loads are increased slowly and thus the contribution of the velocity term is neglected. However, the software adopted can acknowledge this contribution even in quasi-static loading. In fact, once yielding occurs, the localized deformations can reach relatively high local deformation velocities (Carr, 2007).
- The current model represents the bare RC frame, without consideration for the infill panels. However, masonry infills can typically be found in existing pre-1970's RC frames. Experience from past earthquake events have demonstrated that these non-structural elements can significantly affect structural behaviour in different ways depending on their characteristics and layout, in fact they could either improve the response by stiffening and strengthening the structure or trigger a soft-storey mechanism due to stiffness irregularities.

The dynamic characteristics of the as-built frame model are given in Figure 26.

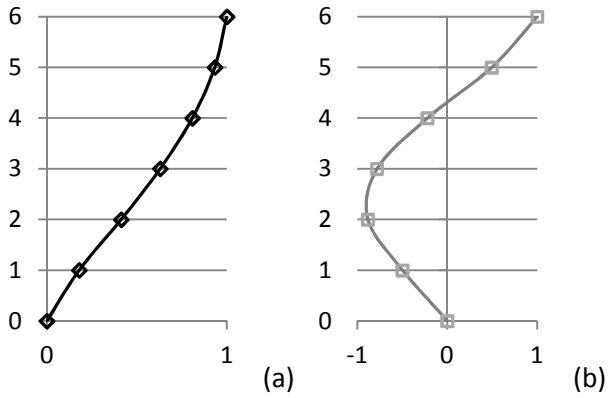

Period		Mass Participation	
1st mode	2nd mode	1st mode	2nd mode
1.838s	0.5982s	83%	94%

Figure 26: Dynamic characteristics of the as-built model and representation of the first (a) and second (b) modal shapes.

Being a pre-1970's RC frame building, the structure is expected to be relatively heavy and it is characterized by slender columns. As a consequence, the fundamental period results quite long with respect to newer code-conforming structures. By comparison, Figure 27 shows the structural periods of other non-ductile RC frame buildings characterized by different number of storeys and designs described by Liel and Deierlein (2008).

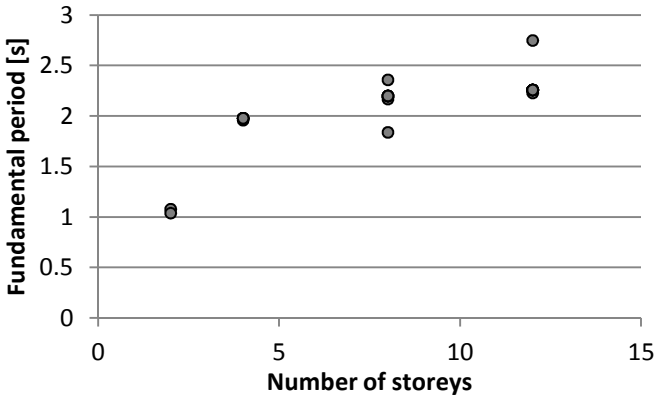

Figure 27: Structural periods of various non-ductile RC frame buildings characterized by different number of storeys and designs (Liel and Deierlein, 2008).

Assessment of the seismic performance of the existing structure

The seismic performance of the existing building is assessed through the Percentage of New Building Standard, which identifies the seismic action that the building can sustain without exceeding a predefined limit state. The addressed performance level is life safety.

In order to do so, the structural model is subjected to a non-linear static analysis in which the profile of the horizontal forces are selected to be proportional to the first modal shape, given the high percentage of mass participating at that mode. During the analysis, global parameters (such as the IDR) and local member deformations are monitored in order to stop the simulation whenever the level of demand in one of the elements is exceeded. In particular, the maximum value of IDR is set to 2.5%, as recommended by the NZS1170 and as reported in the DBD Model Code (Sullivan, Priestley et al., 2012). Moreover, a maximum allowable rotation value of 1% is selected for the exterior joints according to the already introduced limit states defined by Pampanin et al. (2003), value that is judgmentally doubled for the interior joints to account for their expected less vulnerable behaviour.

Once that the Force-Deformation relationship has been established, the performance assessment is carried out according to the Capacity-Spectrum Method (CSM) described by the ATC-40 (1996).

According to the CSM, the structural response must be represented in acceleration-displacement response spectrum (ADRS) format, by converting the multi-degree of freedom system in an equivalent non-linear SDOF structure and the result is termed capacity curve of the structure. The capacity curve can then be plotted against the ground motion, as the seismic demand can be also represented in ADRS format.

The method relies on the basic assumption of equivalent linearization methods, which states that the maximum displacement of a non-linear SDOF system can be estimated from the maximum displacement of a linear elastic SDOF system characterized by an appropriate period and damping coefficient, referred to as equivalent period and equivalent damping ratio, respectively. The Capacity-Spectrum Method assumes that the equivalent damping of the system is proportional to the area enclosed by the capacity curve while the equivalent period is taken as the secant period (radial line emanating from the origin) intersecting the capacity curve at its maximum displacement and are both function of the displacement ductility capacity of the structure.

The ATC-40 (1996) gives guidance for the evaluation of the equivalent damping ratio based on the hysteretic behaviour and ductility capacity.

Hence, the seismic action, reduced by an appropriate coefficient accounting for the effective damping of the structure reaching the selected limit state, is scaled to match the ultimate point of the capacity curve (i.e., performance point). This reduced spectrum represents the seismic action required to achieve/exceed the assessed limit state and can be adopted to estimate the value of %NBS that the structure can sustain.

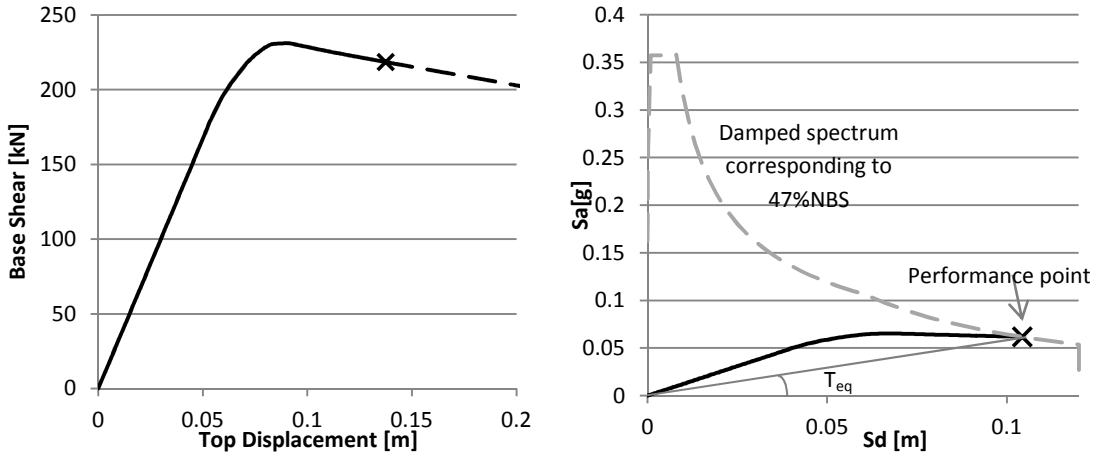

Figure 28: Pushover curve and representation of Capacity curve and seismic demand in ADRS format

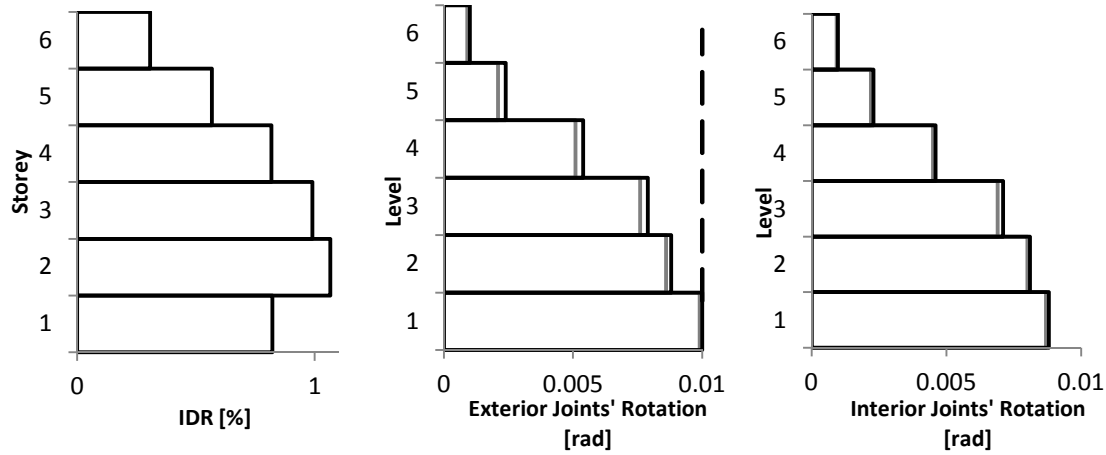

Figure 29: Interstorey drift ratios and joint rotations at life safety limit state for the As-Built structure

Figure 29 shows the interstorey drifts and joints rotations for the existing structure once the life safety limit state has been achieved, confirming that the seismic performance of the building is governed by the inelastic mechanism of the exterior beam-column joints.

Conceptual design of retrofit alternatives

Pushover analyses are also adopted to design possible retrofit interventions for the case study structure. In order to improve the seismic performance of the building, four retrofit strategies are considered, primarily addressing the vulnerability of the exterior joints.

At first the joint shear capacities are increased simulating a local intervention on the external joints with Fiber Reinforced Polymers (FRP), enabling the formation of a more desiderable ductile failure mechanism induced by beam flexure.

Then, the same objective is pursued by decreasing the beam moment capacities, indicating a Selective Weakening (SW) of the beams relating to the exterior joints.

A Full Selective Weakening (FullSW) is considered, leading to a reduction of the beam section at the interface with the column and an improvement of the joint performance due to the addition of post-tensioned tendons, which have a beneficial confining effect on the exterior joints.

Finally, stiffness and strength are modified by intervening on the size of the columns, simulating concrete jacketing (CJ). It should be pointed out that with this latter strategy the joint shear resistance is implicitly increased as it is dependent on the dimensions of the column cross-section.

It should be pointed out that strictly speaking, retrofit strategies and techniques are different concepts. However, for the sake of simplicity, strategies and techniques (FRP, SW, FullSW and CJ) will be herein coupled.

For each of the considered strategies, increasing levels of performance (expressed in terms of %NBS and evaluated through pushover analyses) are achieved by iteratively altering the characteristics of the structural elements involved in the intervention, as shown in the flow chart in Figure 30.

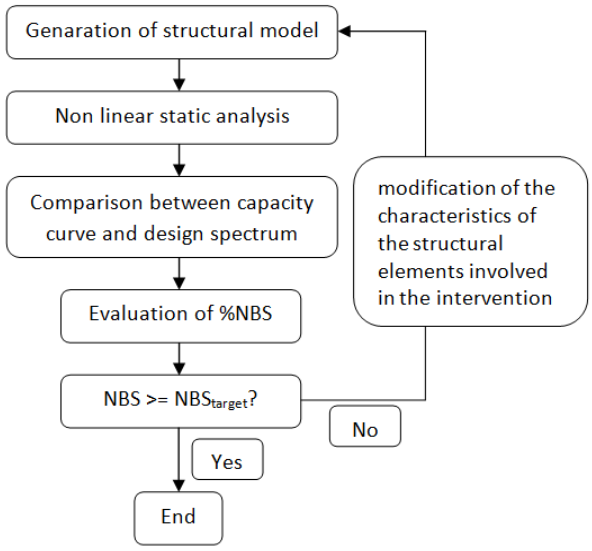

Figure 30: Flowchart of the design process of retrofit alternatives achieving different levels of %NBS

The iterative procedure is used to develop the curves presented in Figure 31.

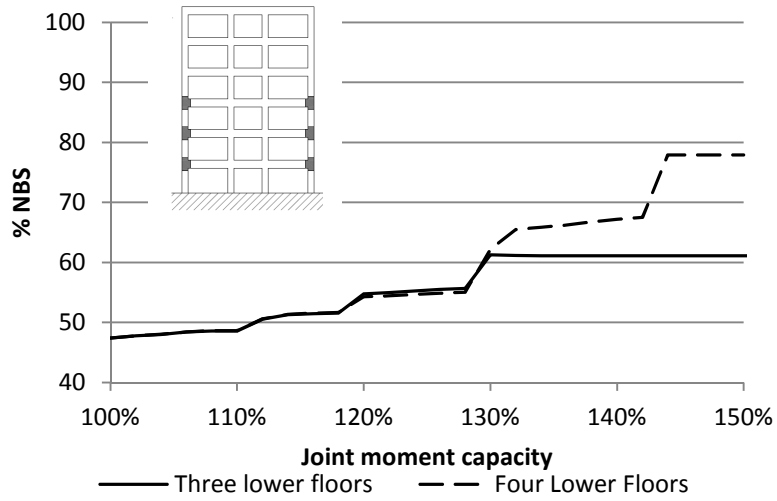

(a)

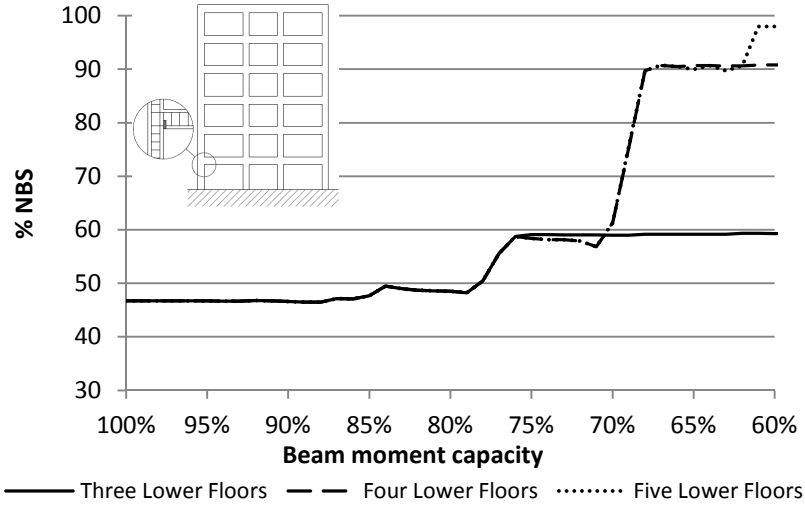

(b)

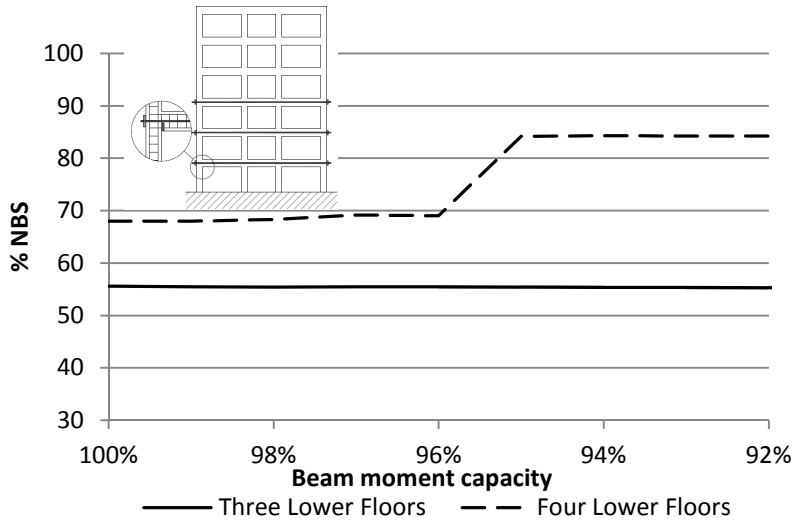

(c)

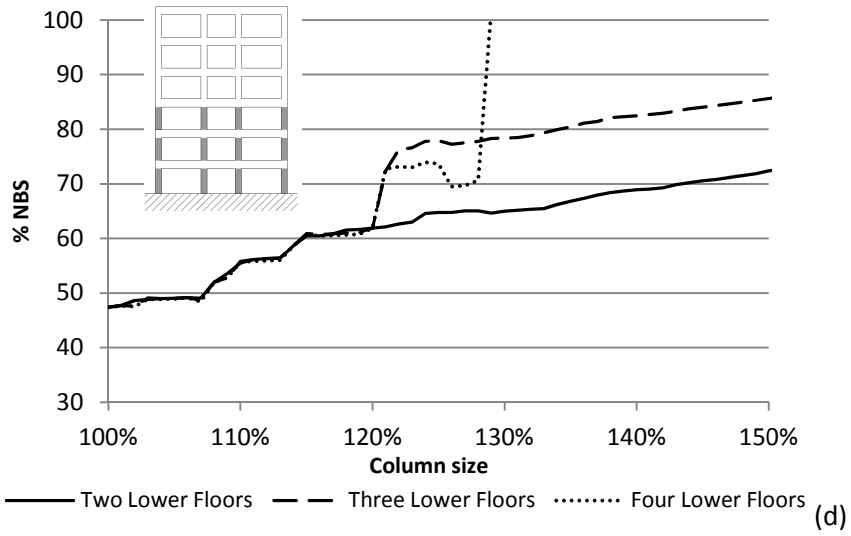

Figure 31: %NBS obtained from Pushover analyses as a function of the modified structural elements capacities for the alternative retrofit options: (a) FRP retrofit option, (b) Selective Weakening, (c) Full Selective Weakening and (d) Concrete Jacketing.

Three or four curves are presented in each graph, relating to different levels of invasiveness of the intervention, in fact the same retrofit strategy has been applied to a different number of elements (i.e. the same intervention is performed on a different number of storeys) in order to identify the minimum number of elements necessary to reach the desired performance.

Even though this procedure is simplified in nature and the analysis method is deterministic, a few considerations can be made regarding the effectiveness of the retrofit strategies.

These curves reflect the trend towards an increase of the building performance, switching from brittle failure modes to more ductile flexural plastic mechanisms. As expected, these curves appear as step-functions: in fact in some cases a minor change in the structural properties can lead to a remarkable increase in the %NBS. This means that the element(s) governing the collapse (e.g. exterior or interior joints exhibiting excessive distortions, columns or beams deflecting beyond their capacity), have been changed and hence can be located at a different level of the building. To further clarify this aspect, it is worth referring to the graph related to the FRP intervention. At first the intervention is planned on the three lower floors to try to minimize both invasiveness and cost. The increase in the external joint capacity leads to an increment of the %NBS from 47% to approximately 55%. A further increase in the joint capacity is then responsible of moving the first element reaching collapse, an exterior joint in this case, from the third to the fourth floor. Hence, at this point continuing to strengthen only

the elements of the lower floors can not lead to any effective increase in the global structural behaviour, thus representing a “cap” or upper bound for the selected strategy. The next level of performance could be achieved by either intervening on the upper fourth floor, and/or by combining (herein not shown) two different strategies and/or techniques.

Involving the next floor in then intervention, an increment in terms of performance can be observed. In fact, with reference to the same FRP graph for example, a value around 68% of NBS can be reached, with the weakest element located at the fourth floor. Hence, in principle, an intervention on the first four floors to increase the exterior joints' capacity can still be beneficial. In fact, at a further modification in the retrofitted elements corresponds a distinct increase of performance, indicating that the elements inducing failure are no longer the exterior joints pertaining to the lower four floors, but failure is governed by the interior joints at the ground level. Hence, as observed before for the case of intervention on the three lower floors, keeping on modifying the properties of exterior joints can not result in any performance upgrade. As a consequence, an additional intervention would be required on the interior joints in order to reach 100%NBS with a certain level of confidence. For this reason, for the purposes of this specific case study, it is concluded that for the FRP retrofit strategy the achievement of 100% NBS is not deemed possible with a partial retrofit solution involving only exterior joints.

Similarly, when the Selective Weakening retrofit option is considered, 59%NBS can be achieved by intervening on the three lower floors, while the fourth floor could be included in the retrofit to reach 90%NBS. A further decrease of beam moment capacity would not lead to an increase of performance as at this stage the weakest element is no longer involved in the intervention. However, even retrofitting the fifth storey, 100% of NBS will not be achieved as the structure will exhibit interstorey drifts greater than those allowed for the life safety limit state. In this case, the maximum sustained seismic intensity results 98%NBS.

The Full Selective Weakening retrofit option combines the effects of reduced flexural capacities of the beams, which ensure a more ductile global behaviour, with the beneficial effects of the insertion of external post-tensioning cables. In this procedure, it is conservatively assumed that the cables and anchorage can ony provide confinement to the joint core delaying joint cracking and concrete-wedge spalling, hence not acknowledging the beneficial contribution of the axial forces provided by the tendons on the flexural capacities of the

beams. For these reasons, based on the findings of Kam (2010), the following empirical relation is adopted to estimate the effect in terms of increased principal stresses that the joints can sustain due to the adoption of this retrofit strategy:

$$p'_{t-sw} = 0.42 \frac{h'_c}{h'_b} \sqrt{f'_c} \tag{5.1}$$

where h'_c and h'_b are the effective heights of the column and beam respectively. An upper coefficient of $0.42\sqrt{f'_c}$ MPa is taken from the recommendations of Priestley (1997) and is the same also adopted by Calvi, Magenes et al. (2002) to represent the ultimate capacity of interior (thus confined) joints.

As soon as the intervention is applied to the lower three floors, failure occurs at an exterior joint at the fourth floor, as the provided confinemennt protects the lower joints. Acting on four levels postpones the occurrence of joint failure and allows the structure to achieve around 67/68%NBS. A sudden change in the curve indicates that a higher level of performance can be obtained, but since this is associated with interior joint failure, it has to be considered as an upper bound for this retrofit strategy.

Finally, Concrete Jacketing presents a slightly different trend. In fact, conversely to what has been observed in the previous cases, even if the columns involved in the intervention and the element leading to failure do not belong to the same level, an increased degree of retrofit can still result in an improved %NBS and not in a sort of plateaux. This difference can be explained by the different effect that this retrofit strategy has on the global structural behaviour with respect to the other ones. In fact, while the previous three strategies essentially aim at increasing the ductility of the system, the concrete jacketing improves the performance by modifying also strength and stiffness. To clarify this aspect, Figure 32 represents two capacity curves in ADRS format. The blue marker indicates the performance point of the original state of the structure, intersecting the 47%NBS damped spectrum. Adopting a retrofit strategy like FRP, Selective Weakening or Full Selective Weakening the capacity curve does not change significantly in shape, but as far as the weakest element within the system is being retrofitted the performance point is shifted towards higher ductilities. On the contrary, Concrete Jacketing affects the original system by rising its capacity curve, reflecting an increase in both strength and stiffness. As a result, even if the elements governing failure are not directly

involved in the intervention, increasing the size of the columns can still modify the shape of the capacity curve, allowing the structure to reach higher performance levels.

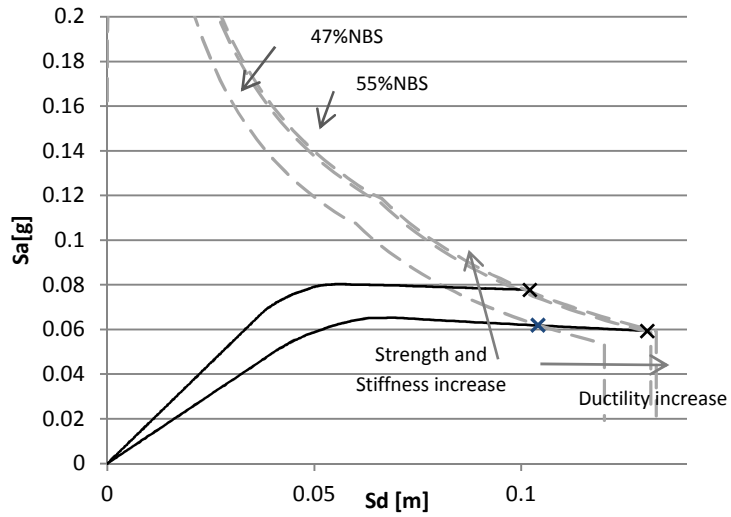

Figure 32: Effect of different retrofit strategies on the global performance.

The curves presented in Figure 31 can then be adopted for the conceptual design of the considered retrofit alternatives. Four levels of performance, namely 55%, 67%, 80% and 100%NBS, when feasible, are selected. Hence, the design is performed, for each type of intervention, by identifying the structural elements' characteristics corresponding to the targeted %NBS. In this fashion, the following retrofit options (and corresponding structural models) are identified:

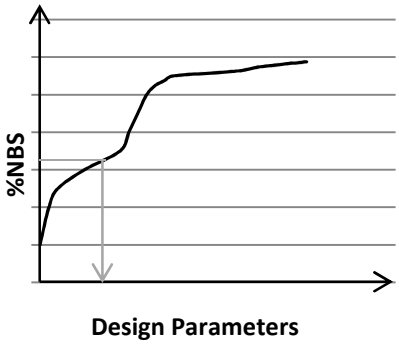

	Retrofit strategy	Achieved %NBS	Storeys involved		Retrofit strategy	Achieved %NBS	Storeys involved
1	FRP	55%	3	8	FullSW	55%	3
2	FRP	67%	4	9	FullSW	67%	4
3	FRP	78%	4	10	FullSW	80%	4
4	SW	55%	3	11	CJ	55%	2
5	SW	67%	4	12	CJ	67%	2
6	SW	80%	4	13	CJ	80%	3
7	SW	98%	5	14	CJ	100%	4

Table 3: Schematic representation of the use of the %NBS/Parameters curves to design the interventions and number of storeys involved in the interventions.

The following graphs represent the levels of interstorey drift ratio and rotations of the exterior joints corresponding to the fourteen structures considered, subdivided by retrofit strategy.

These graphs confirm the considerations made above. In fact, as an example, Figure 33 indicates that for the structure retrofitted with FRP to achieve 55%NBS failure occurs due to excessive distortion of the exterior joints at the third level. When the structure is retrofitted to reach 67%NBS the elements leading to failure are still exterior joints but are located at the fourth floor. 78%NBS can be achieved by further retrofitting the structure. In this case, the exterior joints exhibit lower rotation but at the same time the allowable rotation is exceeded in the interior joints.

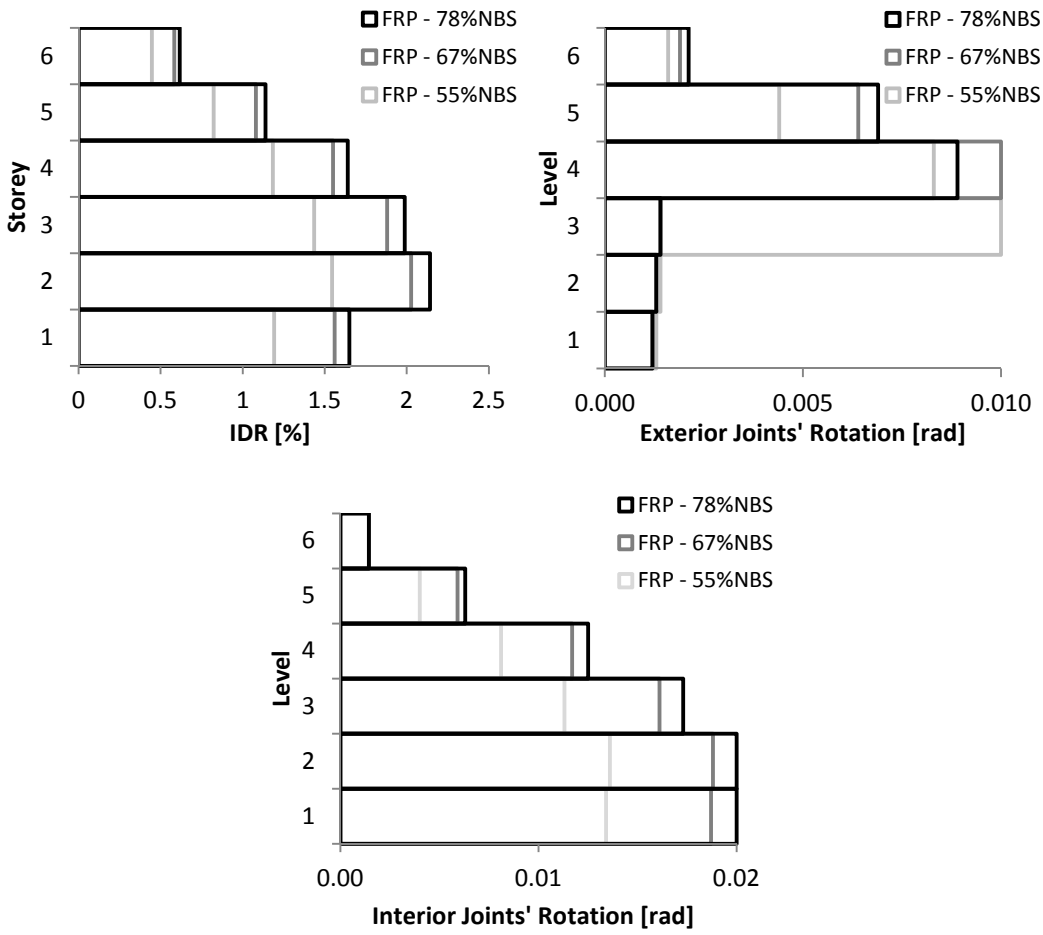

Figure 33: Interstorey drift ratios and joint rotations for the three structures retrofitted with FRP to sustain different levels of %NBS.

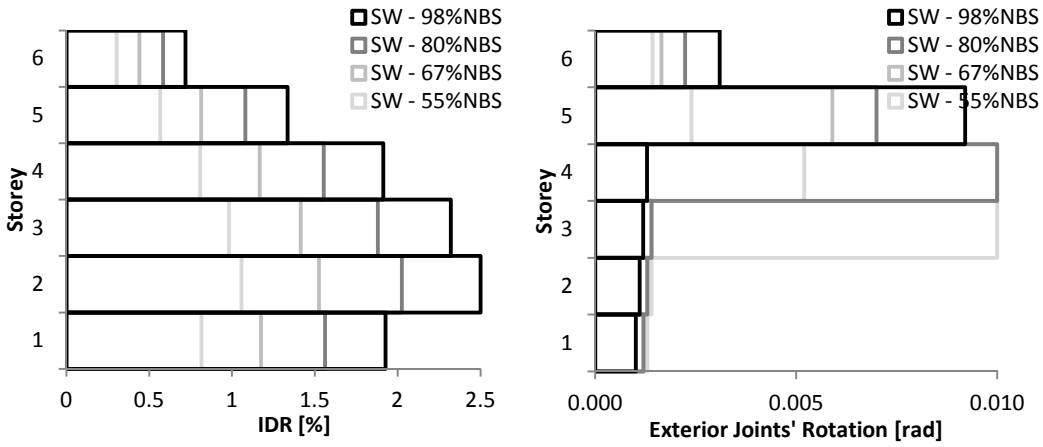

Figure 34: Interstorey drift ratios and joint rotations for the four structures retrofitted through SW to sustain different levels of %NBS.

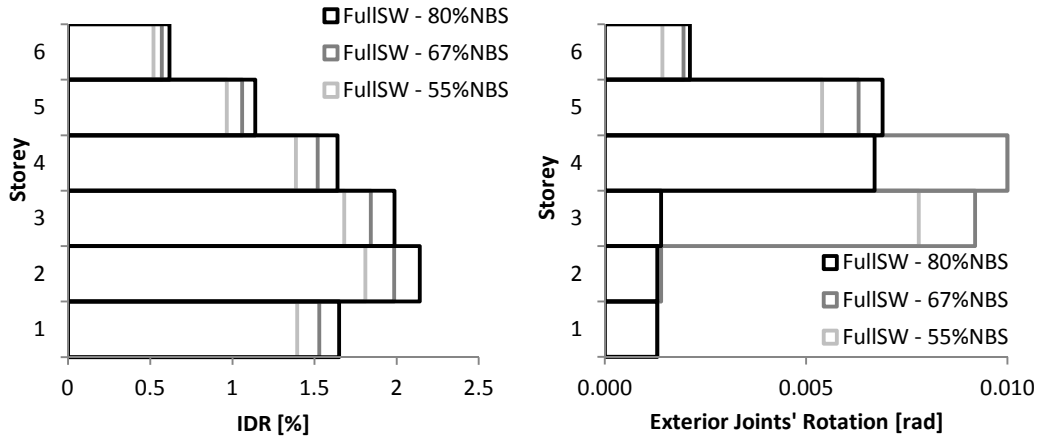

Figure 35: Interstorey drift ratios and joint rotations for the three structures retrofitted through FullSW to sustain different levels of %NBS.

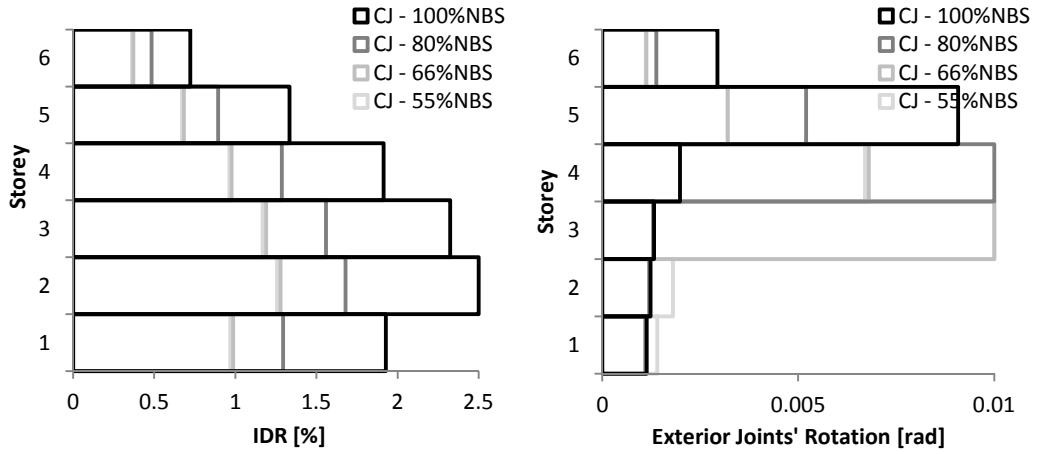

Figure 36: Interstorey drift ratios and joint rotations for the four structures retrofitted with CJ to sustain different levels of %NBS.

Finally, Figure 37 compares five different pushover curves obtained for the As-Built structure as well as the four retrofitted frames targeting 55%NBS. Conversely to what is expected for the Concrete Jacketing retrofit option, the shapes of the capacity curves representing the structures upgraded through FRP, SW and FullSW do not differ significantly from the original structure, with the weakened structure exhibiting a slightly lower level of base shear at yield. This observation confirms that these strategies affect the global performance of the structure by enhancing its ductility capacity.

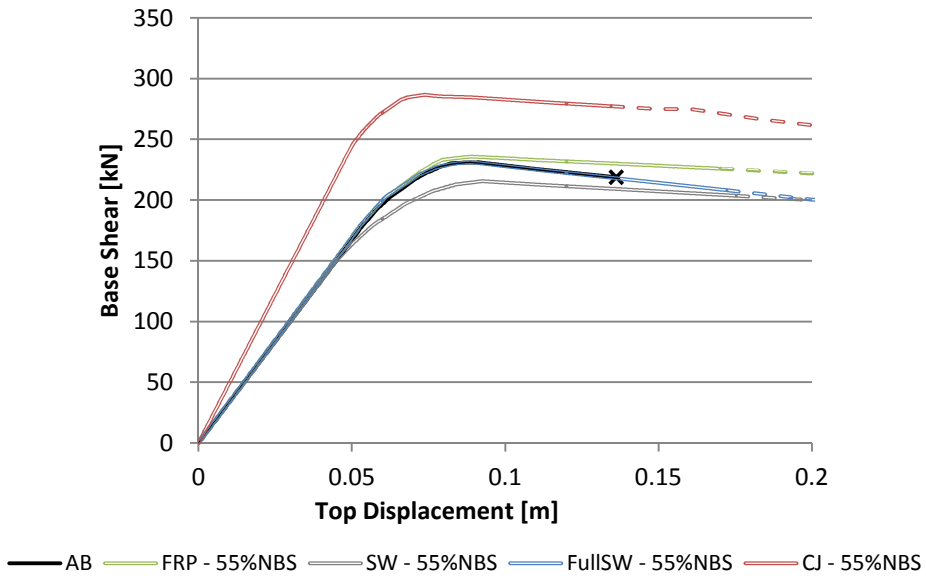

Figure 37: Example of Pushover curves obtained targeting 55%NBS through different strategies.

6. Dynamic response of existing and retrofitted frames

Introduction

The most intuitive but yet challenging method to evaluate structural behaviour under seismic excitation is represented by non-linear dynamic analyses. In this type of analysis, by subjecting the structure to a ground motion, the evolution of structural response through the loading history can be obtained integrating the dynamic equation of equilibrium. However, it is well established that the same structure could exhibit very different behaviour when excited with different ground motion, even of "comparable intensity" and this aspect can not be resolved by deterministic approaches. Hence, in order to overcome this issue and accurately estimate structural response, current seismic codes prescribe the use of groups of ground motions, either recorded from past events or simulated.

For what concerns recorded time histories, at this time there is no established procedure to select such sets of ground motions. However, current seismic codes prescribe the use of suites of records whose average pseudo-acceleration response spectrum is compatible with a given Response Spectrum (e.g. Uniform Hazard Spectrum) in an appropriate range of periods and that are representative of the seismicity at the site under consideration. This process implies that the time histories should be selected according to parameters capable of capturing intensity, frequency content and duration information that significantly affect the elastic and inelastic response of complex soil-structure systems. Unfortunately, no single parameter is ideally suited for this selection procedure, and the best choice of parameters depends, sometimes weakly and sometimes strongly, on the structural system and the performance level to be evaluated.

As ground motion record selection is considered a critical aspect in assessing structural response based on numerical dynamic analyses, a parallel study addressing this specific issue has been conducted. In particular, the main focus of this research has been the definition of a procedure for estimating reference mean structural response for non-linear structures: at first, attenuation relationships for the inelastic demand on various SDOF and MDOF structures were

defined and then a Probabilistic Seismic Hazard Analysis has been performed using the obtained models allowing to evaluate the interstorey drift levels associated with a 475 year return period. These values have then been adopted as reference response and compared to the estimates of the average response obtained by using spectrum-compatible suites of recorded accelerograms with the same return period, selected according to different criteria. As a consequence, the effect on the predicted response of the adoption of different selection criteria could be investigated. For clarity of presentation, this second aspect of the research has been reported separately in Appendix A.

A large body of research is currently under development addressing the issue of artificial time histories. The main concern regarding this type of input motions is that, when a synthetic ground motion is generated to have a response spectrum compatible with a target response spectrum, this will be characterized by too many cycles of strong motion, resulting in unreasonably high energy content (Naeim and Lew, 1995). Hence, a second category of methods for simulating acceleration time histories have been developed, relying on a more physical approach, according to which the ground motion is modelled by convolving the source, path and site effect (Aki and Richards, 1980), while some important research efforts have been devoted to the modelling of the source process (Hartzell, 1978; Irikura, 1983).

Non-linear Dynamic analyses can be adopted to evaluate, in probabilistic terms, the probability of incurring in structural collapse (or achieving any other limit state) as a function of a considered Intensity Measure. Incremental Dynamic Analysis (IDA) is an iterative procedure introduced by Vamvatsikos and Cornell in 2002 to pursue this objective, in fact it allows to evaluate the level of shaking intensity required to induce collapse in a specific building accounting for the variability of seismic demand on the structure by scaling each ground motion in a suite at increasing levels of intensity and evaluating at each of these levels the response of the structure.

The main shortcoming of this approach is that it involves a great number of structural analyses and hence it is computationally intensive. Furthermore, some researchers pointed out that scaling typical moderate-IM ground motions up to higher levels of the same intensity measure might result in unrealistic acceleration time-histories (Baker and Cornell, 2005). To overcome these issues, several approaches have been proposed in literature. As an example, truncated incremental dynamic analyses could be adopted, in which the considered accelerograms are scaled only up to a threshold value, accepting that for a certain number of ground motions the

structure does not collapse. Hence, through the maximum likelihood method the results are post-processed providing the parameters of the fragility function of interest (Baker, 2014)
Another viable strategy to assess collapse probability is adopting multiple stripes analysis (MSA). The main difference with respect to IDA is that the structural analyses are performed at a discrete set of *IM* levels, and the ground motions to be used in the analyses are independently selected to represent each of the considered *IM* levels (Jalayer, 2003).
Having said that, in this chapter, the As-Built structure and all the retrofitted frames designed according to the procedure outlined in the previous Chapter are subjected to Incremental Dynamic Analyses in order to evaluate their response under seismic excitation and estimate their capacity with regard to the collapse limit state. A reliable estimate of the collapse probability could in fact be an effective metric of structural performance, meaningful for both designers and stakeholders.

Incremental Dynamic Analyses

As already mentioned, in order to evaluate their collapse probabilities, the structural models of the original building and the retrofitted ones are subjected to Incremental Dynamic Analyses (IDA, Vamvatsikos and Cornell, 2002). This analysis technique allows for the identification of the structural capacity in probabilistic terms, capturing the different response of the system due to the natural variability of the seismic action. In order to account for the so-called record-to-record variability, a suite of recorded earthquake motions is considered. According to the IDA method, the structural model, representative of both material and geometric non-linearities, is analyzed for each ground motion record and the time-history analysis is repeated several times, with the considered accelerogram linearly scaled (in amplitude) to increasing levels of intensity to cover a wide range of shaking intensities. It is worth noticing that as the accelerograms are simply multiplied by a constant, neither the frequency content nor the duration of the ground motion are modified.

Different measures can be adopted to define the capacity of the structure to be compared with the seismic demand, e.g. maximum shear, interstorey drift, chord rotation, etc. In this study the maximum inter-storey drift and the elements' deformation demands are monitored during the analyses in order to obtain the scaling factor at which each record induces on the structure the attainment or exceedance of the considered limit state. Hence, the level of shaking intensity (described in this case by the spectral acceleration at the fundamental period of the structure) causing the failure of the structure can be identified as it is given by the

product of the scaling factor and the spectral acceleration at the natural frequency of the structure of the unscaled accelerogram.

In order to establish the scaling factor associated to the attainment of the structural failure, various iterative algorithms could be adopted. For instance, Ferracuti et al. 2009 implemented a bisection algorithm in order to reduce the width of the interval of the amplification factors including the value of interest, and the procedure is arrested when the amplitude of the interval becomes smaller than a given tolerance. Buratti (2009), conversely, implemented the iterative Brent's method (Press, Teukolsky et al., 2002), combining root bracketing, bisection and inverse quadratic interpolation, to obtain, up to the desired accuracy, the scaling factor causing structural collapse.

In the present study, a stepping algorithm is adopted, where the IM is increased by a constant step from zero to a value selected according to engineering judgement to be high enough to ensure collapse. This choice results in uniformly spaced values of spectral acceleration. The main drawback of this simple approach is that it may not be cost-efficient, as to ensure sufficient accuracy, the steps of the scaling factor must be kept very small. In fact, once the highest scaling factor not bringing the structure to collapse and the smallest scaling factor inducing collapse have been identified, linear interpolation is adopted to compute the sought value. However, this algorithm is selected as it allowed to observe both hardening behaviour and structural resurrection.

A hardening behaviour can be observed when a system showing high response at a given intensity level, exhibits the same or even lower response when subjected to higher seismic intensities. In these cases, the IDA curves are non-monotonic functions of the Intensity measure (as shown in Figure 38, where an example of IDA curves compared to the capacity of the external joints is presented). The extreme case of hardening is termed "structural resurrection": the structure experiences collapse for a given IM but it results as non-collapsing for higher intensity levels (Vamvatsikos and Cornell, 2002).

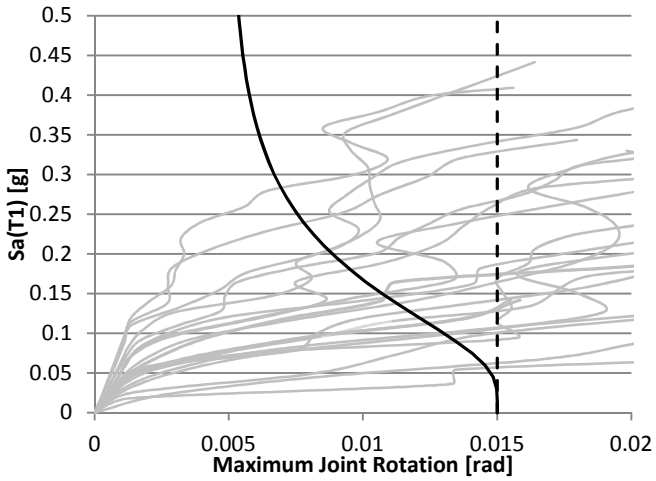

Figure 38: Example of IDA curves compared with the external joint maximum deformation capacity.

The aforementioned procedure has been automated developing a code (in the Matlab environment) that interacts with the software Ruaumoko and Dynaplot, the companion software adopted to extract the data of interest from the performed nonlinear analyses. The code allows for the selection of the required number of accelerogram, performs a sequence of nonlinear dynamic analyses at increasing levels of spectral acceleration and collects and post-processes the results of the IDA extracting the values of spectral acceleration inducing collapse for each record.

The final output of this procedure is a log-normal cumulative distribution function (approximating the discrete number of collapse capacities obtained through incremental analyses) termed collapse fragility, relating the Intensity Measure, IM, to the probability of exceeding the considered limit state. Hence, these fragility functions can be fully defined by a median value of spectral acceleration (μ) and a dispersion term (β). It is worth noticing that the β values computed through the IDA takes only into account the record-to-record variability. Modelling uncertainties can be incorporated in a simplified fashion adopting the mean estimate approach. The total dispersion term, expressed as the standard deviation of the natural logarithm, resulting from the combination of the aforementioned variabilities is calculated as follows:

$$\beta_{LN,total} = \sqrt{\beta_{LN,RtR}^2 + \beta_{LN,Mod}^2} \tag{6.1}$$

where a modelling dispersion term of the order of 0.5 is assumed following the suggestions of Haselton and Deierlein, 2007. It can be observed that this modelling variability is relatively

large as it reflects the large variability of some of the parameters adopted to model the structural behaviour. As a consequence, the total dispersion term and hence the collapse fragility is greatly influenced by these structural uncertainties.

It has been already highlighted that a relevant aspect to be taken care of when structural performance is addressed through dynamic analyses is the identification of the set of accelerograms to be used as input in the analyses. The task of selecting an appropriate suite of recorded ground motions is typically accomplished using information from the hazard analysis and more specifically from the disaggregation of the hazard at the site. This latter, in fact, allows to identify the seismic scenario (in terms of magnitude and distance) with the largest contribution to the hazard, in terms of the intensity measure considered, at the site under investigation.

It can be observed that different disaggregation charts are obtained when different return periods of the seismic action are considered. For this reason the choice of the intervals of magnitude and distance to be adopted in the case of incremental dynamic analysis is not straightforward, as the same record has to be scaled to represent seismic actions characterized by increasing return periods. For the purposes of this study, due to time constraints, a Probabilistic Seismic Hazard Analysis was not undertaken. Hence the Uniform Hazard Spectrum adopted is the one provided by the New Zealand Standards for the city of Christchurch and for a subsoil class C - Shallow soil sites, while literature disaggregation information are employed. Figure 39 shows the hazard disaggregation for Christchurch provided by Stirling, McVerry et al. (2012). From the chart it can be observed that the 475-year hazard is dominated by the distributed seismicity model, with magnitudes within the range of 5 to 6.8 at distances of less than 50 km. The disaggregation shows more than one scenario significantly affecting the hazard. However, bearing in mind that the shaking intensities inducing collapse will more probably be scaled down with respect to the 475 years return period spectrum than scaled up towards higher accelerations, and acknowledging that the hazard associated with frequent events is generally governed by low intensity but close events, the scenario in terms of magnitude and distance upon which the ground motion selection is conducted is identified in correspondence to the highest peak at lower values of magnitudes of the disaggregation chart. Then, considering a subset of the time-histories collected in the NGA-database (Power, Chiou et al., 2006), the two components of each record characterized by values of magnitude and source-to-site distance consistent with the selected scenario are scaled to allow their

geometric mean to match the uniform hazard spectrum in a range of periods including the fundamental one. The geometric mean is calculated according to the following equation:

$$S_{a,Mean} = \sqrt{S_{a,x} \cdot S_{a,y}} \tag{6.2}$$

where $S_{a,x}$ *and* $S_{a,y}$ are the spectral accelerations of the two horizontal components of the ground motion record. A further condition is introduced regarding the scatter of the two components with respect to the target spectrum. In particular, among all the pairs matching the requirements in terms of magnitude and source-to-site distance, the records are selected according to the compatibility of their geometrical mean spectrum with the UHS but also checking that the singular components are able to represent the reference spectrum in the range of periods of interest, setting a threshold value for the relative distance (computed through the root-mean-square difference) between the spectrum of the component and the reference one.

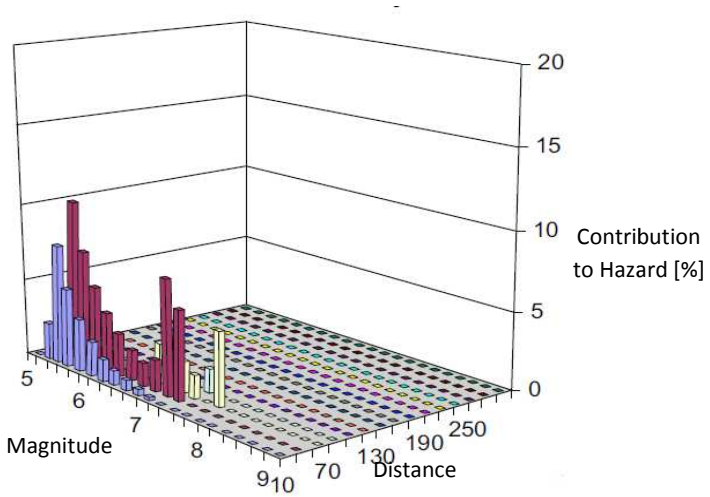

Figure 39: Hazard deaggregation in terms of PGA corresponding to a 475 years return period for Christchurch (from Stirling et al., 2012)

As for the numerosity of the ground motions to be selected, the ATC-58 (2012) recommends that at least seven ground motion pairs should be used. However if the spectral shape is not directly considered in the selection procedure, resulting in a significant scatter in the spectral shapes of the considered records, the number of pairs of ground motions should be increased up to eleven or more. In light of this, 20 ground motions from the NGA-database are considered.

As measures of building performance, local response parameters are analyzed, namely the elements deformation demands in terms of maximum curvature for beams and columns and maximum rotation in the joints.

On top of this, an interstorey drift ratio of 4% is assumed in this study as a global collapse criterion, following the recommendations of ASCE-41. It is worth noticing that since the structure is being retrofitted, its drift collapse capacity could be arguably increased when compared to the As-Built solution. However, due to the complexity of defining collapse and as the retrofit designs are performed according to the %NBS (which does not explicitly address the collapse limit state), this value is conservatively kept constant for the original structure and all the retrofit alternatives.

A few cases on numerical instability have been observed, in which the analysis failed to converge before the attainment of ultimate capacity in terms of global interstorey displacements or member deformations. In some cases, non-convergence could indicate dynamic instability and thus collapse. However, this behaviour could also be due to numerical issues related to the quality of the model and of the algorithm adopted within the analysis. For this reason the analyses that suffer from numerical instability are discharged and do not take part in the definitions of the parameters describing the collapse fragilities.

In the following paragraphs, the collapse fragilities obtained for the As-Built structure and all the retrofitted frames are shown. In particular, the fragilities displayed on the left are plotted against the results of the IDA and thus they only account for the record-to-record variability, while the cumulative distributions on the right also include the modelling uncertainty.

"As-Built" model

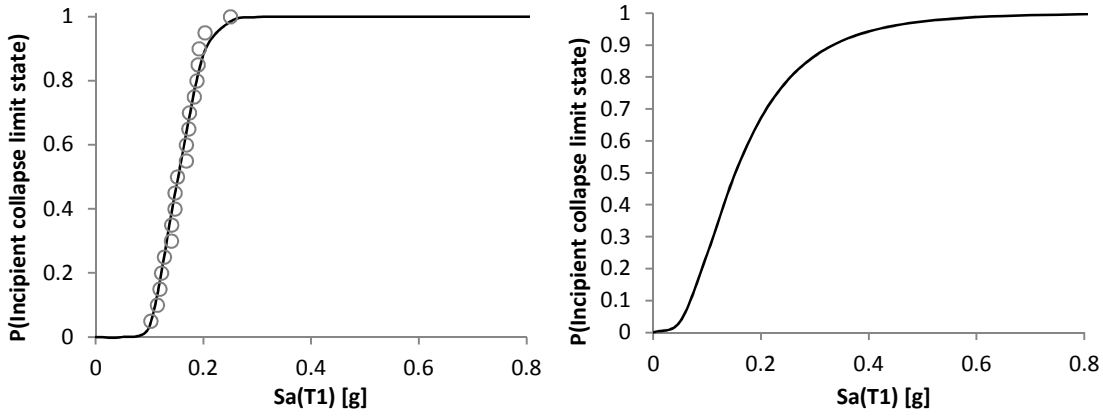

Figure 40: Collapse fragility for the existing structure incorporating record-to-record variability (left) and record-to-record variability plus modelling uncertainty (right).

FRP retrofit option

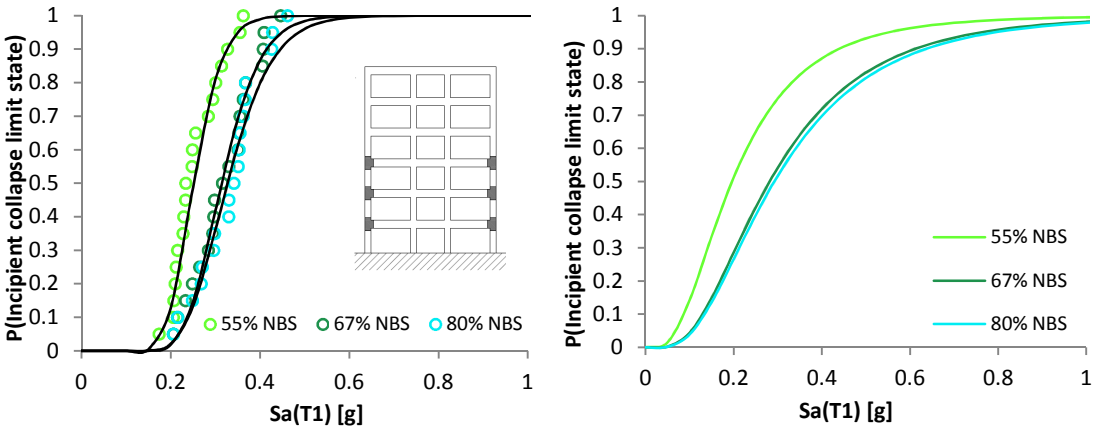

Figure 41: Collapse fragility for the structure retrofitted with FRP for the three levels of %NBS achieved, incorporating record-to-record variability (left) and record-to-record variability plus modelling uncertainty (right).

Selective weakening retrofit option

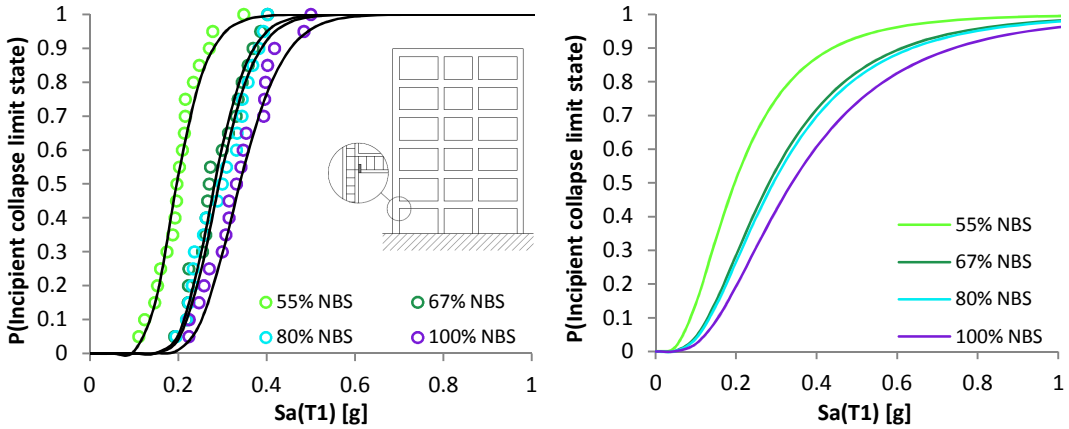

Figure 42: Collapse fragility for the structure retrofitted through Selective Weakening for the four levels of %NBS achieved, incorporating record-to-record variability (left) and record-to-record variability plus modelling uncertainty (right).

Full Selective Weakening retrofit option

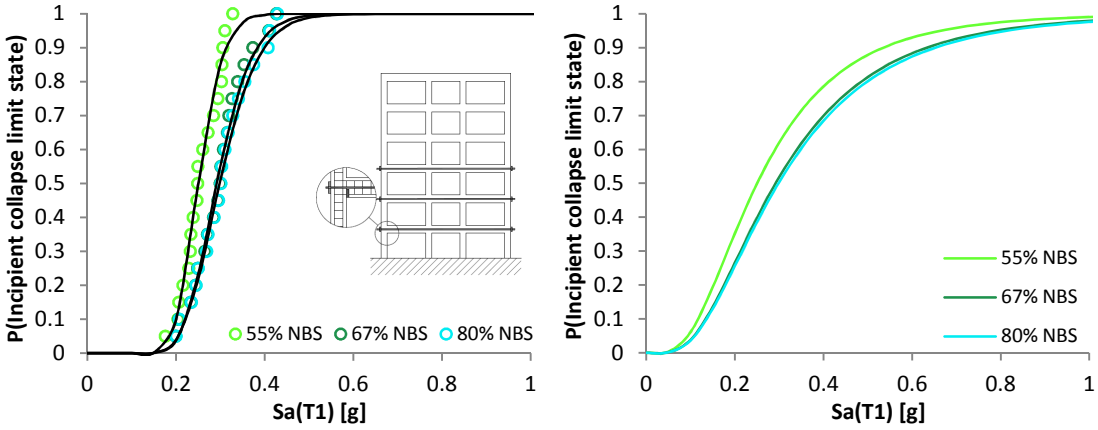

Figure 43: Collapse fragility for the structure retrofitted through Full Selective Weakening for the three levels of %NBS achieved, incorporating record-to-record variability (left) and record-to-record variability plus modelling uncertainty (right).

Concrete Jacketing retrofit option

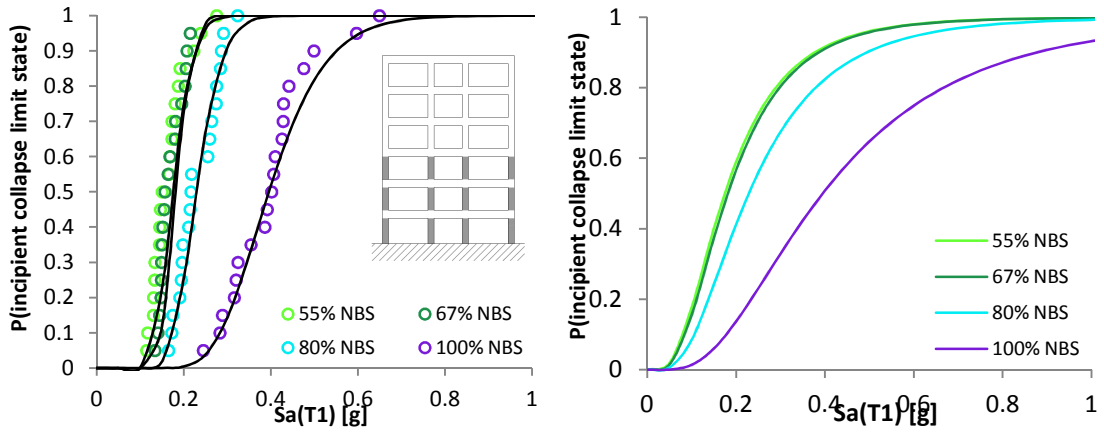

Figure 44: Collapse fragility for the structure retrofitted through Concrete Jacketing for the four levels of %NBS achieved, incorporating record-to-record variability (left) and record-to-record variability plus modelling uncertainty (right).

The parameters defining the collapse fragilities are summarized in the table below. Moreover the median spectral accelerations inducing collapse are represented in Figure 45, together with the minimum and maximum value obtained in the analyses.

	μ	β_{tot}		μ	β_{tot}
As Built	0.153	0.6425			
FRP 55%	0.242	0.6246	FullSW 55%	0.250	0.6248
FRP 67%	0.298	0.6385	FullSW 67%	0.292	0.6364
FRP 80%	0.302	0.6404	FullSW 80%	0.298	0.6417
SW 55%	0.196	0.6594	Col 55%	0.175	0.6331
SW 67%	0.282	0.6371	Col 67%	0.181	0.6212
SW 80%	0.292	0.6389	Col 80%	0.229	0.6334
SW 100%	0.339	0.6419	Col 100%	0.395	0.6535

Table 4: Summary of parameters (median and lognormal standard deviation) defining the collapse fragilities for the considered structures.

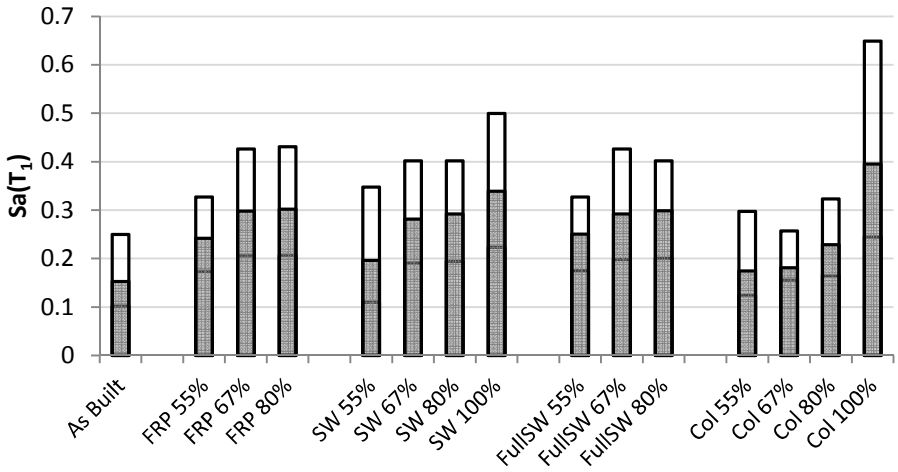

Figure 45: Minimum, median end maximum value inducing collapse on the fifteen structural models considered.

Interestingly, from the families of collapse fragilities presented in Figure 41 to Figure 44 (the same trend can be observed in the fragilities related to the Life safety limit state) it can be observed that some curves are almost overlapped. This typically occurs for those cases where the pushover analysis identified a significant benefit due to a minimal change in the characteristics of the structural elements (mainly in correspondence of a step change in the curves in Figure 31) or when the next level of performance was achieved without modifying the number of storeys involved in the intervention. In fact, while from a non-linear static analysis point of view the changes introduced on the structure produce a distinct increase in performance, addressing the same issue with a non-linear dynamic response and probabilistic approach can significantly change the outcome. In fact, although designed to reach two different levels of %NBS, the structures might be extremely similar and hence their expected performances can not be very different. Based on the above considerations, in order to take advantage of the step increase of performance derived from pushover analyses, it is suggested to perform non-linear dynamic analyses to verify the actual performance to be expected.

A further aspect requires consideration. Contrarily to what happens in the case of pushover analyses, where a single failure mode can be identified for each structure, the Incremental dynamic analyses might provide a range of different inelastic mechanisms leading to the development of the considered limit state. As an example, it was observed that besides those cases where failure is due to excessive distortion in the exterior and interior joints, the life safety performance level could be achieved due to excessive inter-storey drift, aspect that was no captured by the pushover analysis method. Similarly, for the collapse limit state, the IDA

predicted in some cases (as the one shown in Figure 46) different mechanism occurring with comparable likelihood. In such cases the limitations of assessing structural behaviour according to a deterministic manner becomes apparent, as it can fail in identifying the most probable failure mode.

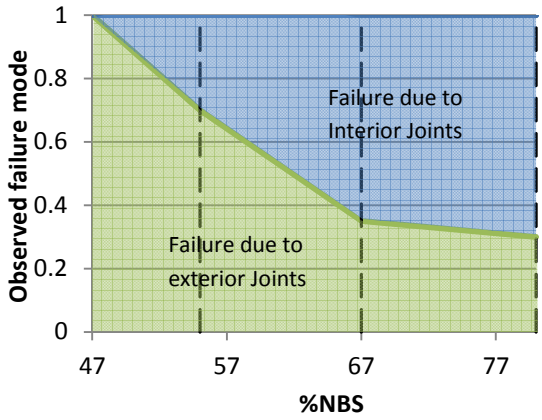

Figure 46: Different mechanisms leading to collapse for the FRP retrofit option.

Evaluation of collapse probability for the original and retrofitted structures

Finally, the collapse fragilities can be adopted to evaluate the actual probability of incurring in collapse for all the considered structure and hence compare the effects of the different retrofit option and of the different %NBS targeted during the design phase in terms of collapse risk. One way of expressing this probability could be to evaluate the collapse probability under the design level earthquake. This would give an indication of what could be expected to happen under a specific earthquake scenario. However, more significant information could be obtained by taking also into account the probability of occurrence of that intensity within a time frame that could be meaningful for the facility stakeholders. Hence, the collapse probability are obtained by considering the collapse risk due to a range of shaking intensities that could contribute to the local hazard and weigh them according to the associated probabilities of occurrence (refer to Figure 47). As a result, the collapse probability is no longer conditioned to a predefined intensity, but it is referred to a selected period of time.

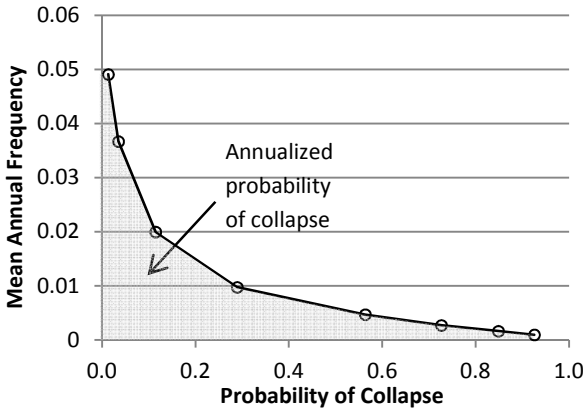

Figure 47: Evaluation of the annualized probability of collapse combining information from the collapse fragility and local hazard.

Figure 48 summarizes the annualized probability of reaching collapse for all the examined structures, providing the investigated correlation between achieved %NBS and collapse risk. The same data, once the probabilities have been made adimensional, can be represented in the format of the Performance-Risk graph provided by the NZSEE2006 guidelines, confirming for this specific case-study building the qualitative trend suggested by the aforementioned guidelines. As expected, in fact, an increase in the targeted performance in terms of %NBS result in a more than proportional reduction of risk.

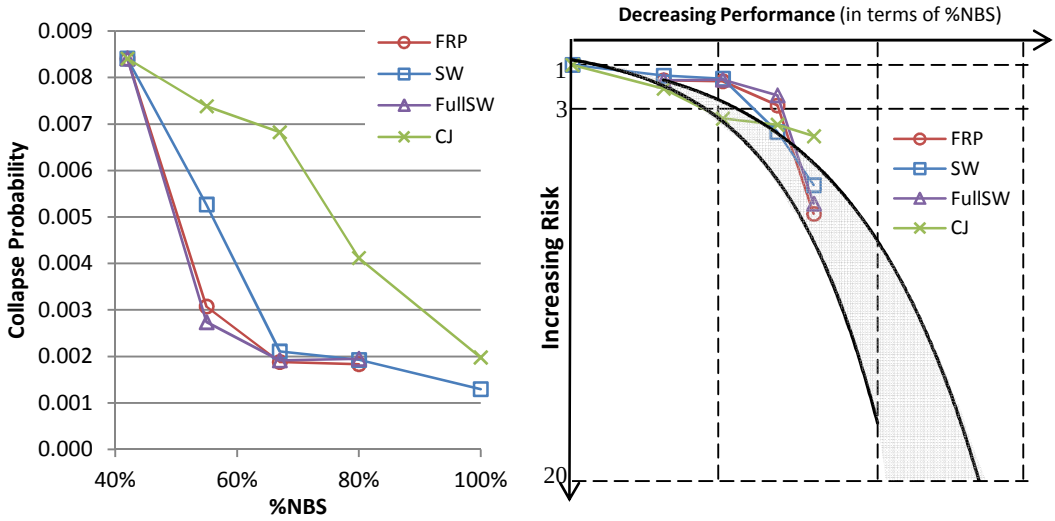

Figure 48: Annualized probabilities of collapse as a function of the targeted %NBS for the four retrofit strategies considered and comparison of the results with the Performance-Risk graph from the NZSEE2006 guidelines.

This comparison suggests that all retrofit strategies would lead to a reduction in risk, but with different trends. This reduction seems to be concentrated within the lower levels of %NBS for the strategies directly involving the joint region (i.e. FRP, FullSW and SW) and hence aiming at improving structural performance through an increase in the ductility capacity. In fact, reflecting the trend observed in the fragility functions, beyond 67% NBS an increase in retrofit effort does not appear to be effective in reducing collapse probability, implying that, in order to achieve higher performance level, an alternative retrofit scheme should be considered. Conversely, the variation in collapse probability tends to be more evenly distributed when the size of the columns is modified through Concrete Jacketing (CJ). It should be observed that even though the collapse fragilities for this latter retrofit option resulted shifted towards higher intensities with respect to the previous ones, the value of spectral acceleration representing the shaking intensities provided by the hazard curve are also greater as a consequence of the stiffening effect of increasing the column size. Hence, the performance improvement in terms of collapse probabilities moving from the original condition to the structure upgraded up to 100%NBS through concrete jacketing is in line with the other retrofit options, conversely to what could appear at first sight comparing these fragilities.

7. Assessment of earthquake-induced direct and indirect Losses

Introduction

In the past decades, increasing research efforts have been devoted to the evaluation of the economic impact of seismic activities and their consequences in terms of loss of lives and downtime, usually referred as “the three D’s”: Deaths, Dollars and Downtime. In fact, it has been acknowledged that a reliable estimate of these quantities could provide precious information at various levels. At a regional scale, predictions of the consequences of the occurrence of a certain earthquake scenario could assist in the definition of efficient mitigation strategies, prioritizing the necessary interventions on the basis of available resources. At a single building level, estimates of earthquake induced losses could provide guidance on the retrofitting scheme to be adopted and perhaps even motivate building owners to improve the seismic behaviour of their structures, providing evidences of the long-term benefits that could be obtained by an initial investment.

The following sections will briefly review the possible strategies that have been proposed to estimate the three components of loss.

Damages and direct monetary losses

The first source of loss investigated is the one associated to earthquake damages and consequent repair or replacement costs, which are commonly referred to as Direct economic losses. Different methodologies can be adopted to predict seismic damage, depending on the aim of the assessment. In fact some methods are better suited for single building analysis but would become unfeasible for a larger building stock.

The two main categories of empirical models describe damage either by Damage Probability Matrices or through continuous vulnerability functions that are based on observational data. In the former case, for a defined structural typology, the rate of buildings expected to experience a certain level of structural and non-structural damage when subjected to a given level of earthquake intensity have been estimated based on data from field surveys and expert

judgement. A discrete number of damage states are defined adopting the damage ratio, which represents the ratio of cost of repair to total replacement value.

Continuous vulnerability functions, on the other hand, represent the probability of exceeding a given damage state as a function of earthquake intensity. Since the macroseismic intensity is not a continuous variable, it was initially replaced by the Parameterless Scale of Intensity (PSI) (Spence, Coburn et al., 1992) and later by the Peak Ground Acceleration (PGA). Then, a further development of these functions allowed to correlate the damage probability with the spectral acceleration at the fundamental period of the structure.

Damage State	Damage Factor Range (%)	Central Damage Factor (%)	Probability of Damage in Percent By MMI and Damage State						
			VI	VII	VIII	IX	X	XI	XII
1 - NONE	0	0	95	49	30	14	3	1	0.4
2 - SLIGHT	0 - 1	0.5	3	38	40	30	10	3	0.6
3 - LIGHT	1 - 10	5	1.5	8	16	24	30	10	1
4 - MODERATE	10 - 30	20	0.4	2	8	16	26	30	3
5 - HEAVY	30 - 60	45	0.1	1.5	3	10	18	30	18
6 - MAJOR	60 - 100	80	-	1	2	4	10	18	59
7 - DESTROYED	100	100	-	0.5	1	2	3	8	38

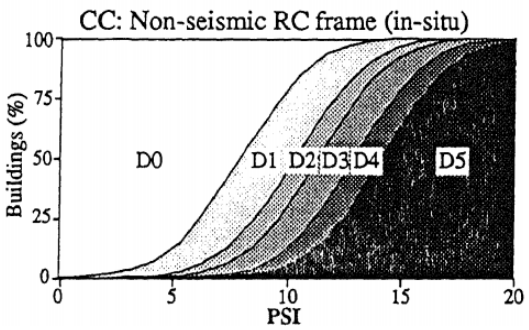

Figure 49: Example of Damage Probability Matrix (from ATC-13) and continuous vulnerability functions (Spence et al., 1992)

Even though the reliability of empirical approaches in case of a single structure might be questionable as they refer to brad classes of buildings and depend on the quality of the data available, they can still be adopted to provide useful information at a territorial scale.

However, if a loss assessment is required for a limited number of buildings, other methods could be adopted in order to better represent the specific features of the structures of interest. Analytical models, as suggested by the name, are not based on observational data but rely on the development of a structural model which is used to evaluate parameters of seismic response at different intensity levels. Then, structural response can be correlated to a measure of damage. By dividing the parameter adopted to quantify damage into appropriate ranges, a discrete number of damage states can be defined and hence the probability of reaching or exceeding each of them can be computed for every intensity level considered.

A mechanical approach has been implemented in Hazus (FEMA, 1999), a software developed to evaluate losses at a territorial scale as a consequence of different possible hazards. In particular, adopting the Capacity Spectrum Method (ATC-40, 1996), capacity curves developed for different building classes are compared with the seismic demand in the ADRS domain. The identification of the performance point allows for the definition of the value of displacement

required as input in vulnerability functions derived from expert opinion, field survey and data from experimental campaign. Hence, the probability of experiencing a certain level of damage can be computed.

Besides these force-based approaches, assessment procedures based on the Displacement-Based design principles are also being developed (Calvi 1999, Crowley and Pinho, 2004). Relying on the assumption that a MDOF system can be transformed in a substitute appropriate SDOF system, the proposed approach is computationally efficient and suitable for parametric studies (Calvi, Pinho et al., 2006).

Lately, several building specific loss assessment studies have been carried out considering component-based fragilities. Instead of relating the structural response of a building with global damage states using building-level fragility functions, which are typically obtained only considering damages to the structural components, this latter approach allows to incorporate in the assessment all possible damageable elements, structural and non-structural, that might affect the total loss. Hence, separate vulnerability functions should be associated with each damageable component within the system. In order to do so, an inventory of all the components of the facility is required and it is usually based on its architectural layout (if known) or expert judgement. Then, recalling the steps of the PEER methodology, given a certain level of shaking intensity, building response parameters can be obtained through structural analyses or from other assessment methods and serve as input to the component-based fragilities, which usually derive from experimental campaigns or field observations merged with expert judgement. A function representing the cost of the required repair effort can be associated to each of the damage states and each of the components. In other words, each damage state is coupled with a specific repair intervention necessary to restore the component to its undamaged condition, and the cost of the intervention might be described by a probability distribution to take under consideration possible cost differences among contractors. This last step of the procedure allows for the evaluation on the expected repair costs associated with the selected shaking intensity.

Monetary losses could also be computed through a time based assessment. In this case the assessment is undertaken by identifying all the possible shaking intensities that could affect the building site through the hazard curve. Then, expected losses are computed for each of the intensities and weighed according to their probability of occurrence in the time frame of interest, which is usually taken as one year. In this fashion, annualized values of losses can be estimated.

This loss estimate methodology has been adopted by the ATC-58 (2012) and implemented in the provided Performance Assessment Calculation Tool described in the following sections.

Interestingly, Ramirez and Miranda (2009) proposed a simplified version of the loss assessment procedure that allows to avoid the damage evaluation step in the loss assessment by providing functions that relate structural response and the decision variable (cost in this case) directly. This procedure will be described in more detail in the following chapter.

A final aspect requires consideration when dealing with costs of earthquake repairs. Demand surge can be defined as the inflation in costs as a result of sudden excess of demand following a catastrophic event. Loss assessment methods do not currently cover this aspect, as numerical models to describe this phenomenon are still to be developed. However, for the comparative analysis performed as part of this study, this issue is not expected to induce particular bias.

It should be pointed out that the economic cost related to elements' repairs is not the only source of possible monetary loss to be accounted for. In fact, in order to evaluate the economic impact of the occurrence of seismic events, losses associated to possible collapse or to the need of demolishing the building must be considered, as they could contribute significantly to the predicted total loss, especially in the case of buildings that are not compliant with the current seismic codes.

Loss of functionality and downtime

Downtime can be defined as the time frame between the occurrence of a damaging earthquake and the end of the repairs required to restore functionality. Within this interval, different operations can be undertaken, from the inspection of the facility, the damage assessment to the design of the necessary intervention and the time required to repair or re-build the construction. Hence repair/rebuilding is only one component of the total downtime, and might not be the more relevant one.

To this regard, Comerio (2006) divided downtime in two components. The first one is termed "rational" as it accounts for the time effectively required to repair/replace damaged buildings and make them suitable for occupancy. The second, termed "irrational" might include the time required to source the necessary foundings, and depends on the availability of construction resources and skilled labour following the event among other factors. Hence this time component accounts for all the operations required before the beginning of the repair effort, as well as all possible sources of delay. Comerio undertook several studies aiming at identifying

and quantifying the various components of downtime (Comerio, 2000 and 2006; Comerio and Blecher, 2010).

Table 5 describes the assumptions underlying the downtime assessment methodology undertook by Comerio and Blecher (2010) at the Berkeley university campus. In particular, values of downtime are shown for different building types based on the Vision 2000 structural performance rating.

Vision 2000 Structural Rating	Damage description	Small < 7500m^2	Large > 7500m^2	Wood (all)
		Time in Months		
9-10	Minimal Effort	0	0	0
7-8	Cleanup	0.25	0.5	0.25
6	Minor Repair	2	3	1
5	Minor/Major	4	6	3
4	Major Repair	20	24	6
1-3	Replacement	36	40	24

Table 5: Simplified method for estimating downtime for the U. C. Berkeley campus (Comerio, 2000)

These estimates will be adopted as reference values within the loss assessment to be undertaken.

Injuries and loss of lives

Minimizing earthquake induced injuries and fatalities is arguably the main focus of Performance Based Earthquake Engineering. Reliable collapse assessment procedures can provide essential information to predict to which extent the life of building occupants is endangered. However, this can be considered only the first step to evaluate possible fatalities induced by seismic activity. In fact structural collapse does not necessarily imply that all the occupants will be killed, as this will depend on many factors, like the type of construction, the severity of the earthquake, the availability and readiness of rescue teams and the reaction of people. In 1972, the NOAA published a study titled “A study of Earthquake losses in the San Francisco area: Data and Analysis” (1972), providing one of the first attempts to address fatalities estimates. Later, the ATC-13 (1985) refined that methodology in order to predict the rate of building occupants that are likely to be killed or injured based on the building damage state, and a revised version of these rates have been considered in Hazus (2003).

Earthquake	Richter Magni-tude	Max MMI	Date	Time of Occur-rence	Deaths Per 100,000 Population	Serious Injuries Per 100,000 Population
Owens Valley, CA	-	-	Mar 26, 1872	-	-	-
Lone Pine			"		8,000	-
Charleston, SC	-	X	Aug 31, 1886	9:51PM	45 outright 113 total	-
San Francisco	8.3		Apr 18, 1906	5:12AM	-	-
San Francisco	"	XI	"	"	124	104
Santa Rosa	"	-	"	"	116	69
San Jose	"	VIII	"	"	80	38
Santa Barbara, CA	6.3	VIII-IX	Jun 29, 1925	6:42AM	45	119
Long Beach, CA	6.3	IX	Mar 10, 1933	5:54PM	26	1,300
Imperial Valley, CA	7.1	X	May 18, 1940	8:37PM	18	40
Puget Sound, WA	7.1	VIII	Apr 13, 1949	11:56PM	1	-
Kern County, CA	7.7	XI	July 21, 1952	4:52AM	-	-
Tehachapi	"		"	"	500	-
Bakersfield, CA	5.8	VIII	Aug 22, 1952	3:41PM	3	47
Alaska	8.4	XI	Mar 27, 1964	5:36PM	-	-
Anchorage	"		"	"	9	315
Seattle-Tacoma, WA	6.5	VIII	Apr 29, 1965	7:29AM	1.5	-
San Fernando, CA	6.4	XI	Feb 9, 1971	6:01AM	-	180
Excl. Vet. Adm. Hosp.	"		"	"	12 total	-
Incl. Vet. Adm. Hosp.	"		"	"	64 total	-

Table 6: Death and injury rates for selected earthquakes (from ATC-13, 1985)

Damage State	CDF(S) (%)	Fraction Injured		Fraction Dead
		Minor	Serious	
1	0	0	0	0
2	.5	3/100,000	1/250,000	1/1,000,000
3	5	3/10,000	1/25,000	1/100,000
4	20	3/1,000	1/2,500	1/10,000
5	45	3/100	1/250	1/1,000
6	80	3/10	1/25	1/100
7	100	2/5	2/5	1/5

Table 7: Death and injury rates as a function of damage state: 1: None; 2: Slight; 3: Light; 4: Moderate; 5: Heavy; 6: Major; 7: Destroyed (from ATC-13, 1985). Noticeably, for light steel or woof-frame constructions the expected injuries and fatalities are one tenth of the provided values

While these predictions could be associated to any structural typology, Coburm, Spence et al. (1992) suggested a general model to predict earthquake casualties subdividing buildings in classes. The model relies on the definition of five factors which are believed to significantly affect the lethality ratio. According to the proposed model, for a class of building *b,* the number of people killed can be expressed as:

$$Ks_b = D5_b \cdot \left[M1_b \cdot M2_b \cdot M3_b \cdot \left(M4_b + M5_b \right) \right]$$

Where $D5_b$ is the total number of collapsed structures (damage level 5) of buildings pertaining to class b*,* M1 is the population of the building, M2 is the occupancy rate at the time of the earthquake, M3 is the percentage of occupants trapped by collapse, M4 represents the rate of entrapped people immediately killed and is highly dependent on the considered structural system while M5 describes the percentage of entrapped people that died before they could be rescued and is a measure of the effectiveness of post-event activities. Other methodologies have been proposed in recent years, however, given the particular nature of the topic, they are inevitably affected by great uncertainty and often rely on expert opinion. On top of this, other studies have highlighted that, unfortunately, loss of lives could also occur for reasons not strictly related to structural failures, as they can occur as a consequence of falls, heart attacks, car accidents, fire and other causes not directly attributable to structural or non-structural collapse. These casualties should also be considered when the global impact of an earthquake is assessed.

Loss assessment through the Performance Assessment Calculation Tool

Direct monetary losses, downtime, injuries and fatalities are evaluated for the original and all the retrofitted structures adopting PACT (ATC-58, 2012). The software allows to perform probabilistic loss computations, in line with the PEER framework, for the most common structural systems and building occupancy types using component-based fragility data collected from multiple sources.

The program can be used in several ways, in fact a scenario-based assessment as well as an intensity-based or a time-based assessment can be undertaken. Moreover, it allows to input structural analysis results obtained from dynamic analyses but also from simplified methods such as the non-linear static analyses. In this study, a time based assessment has been performed, and the response of the structures considered has been described through time-history analyses.

Figure 50 shows a screenshot of the graphical interface of the tool, while the input data required are summarized in Figure 51. It should be pointed out that a large amount of information is needed for the assessment, however the ATC-58 (2012) document provides guidance on how to reasonably assume data that might be not known.

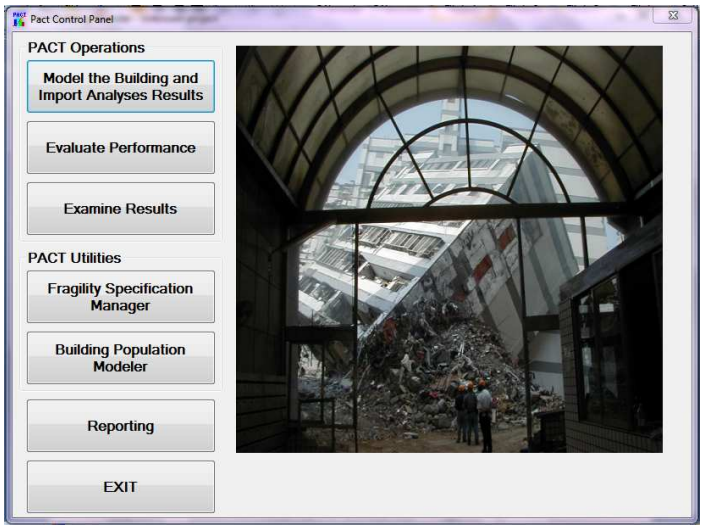

Figure 50: Screenshot of the Performance Assessment Calculation Tool (PACT)

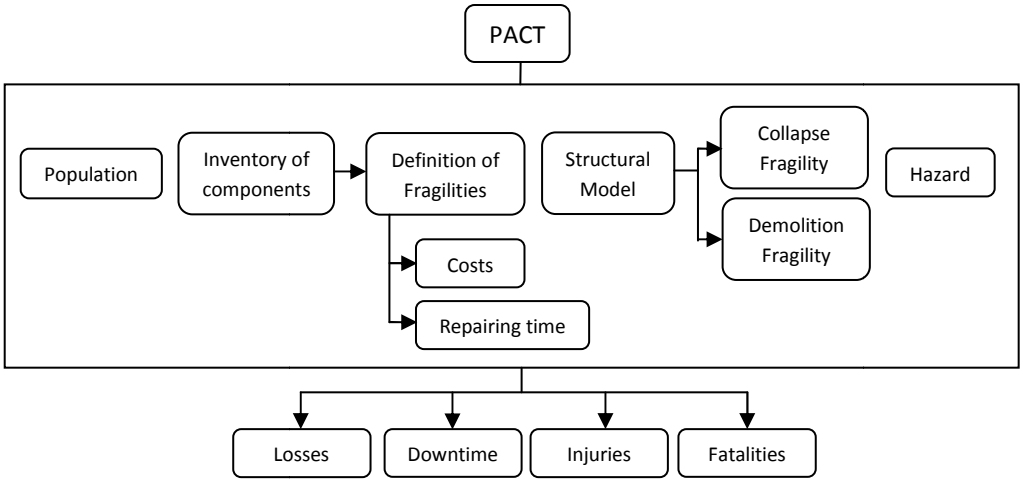

Figure 51: Required input for the performance assessment

With reference to Figure 51, the basic inputs to be provided are described in the following sections.

Population

At first, a model describing the amount and distribution throughout the day, the week and months of the occupants of the building needs to be defined. This allows for the evaluation of

the number of persons that could be found inside the building and hence that might be threatened by an earthquake occurring at a random time and day.

The model depicted in **Figure 52** is been adopted, following the suggestions by the ATC-58 in case of office buildings. The same document gives also indications on the peak number of people to be expected in the building based on its occupancy type and floor area. This peak number is adopted for all the floors a part from the ground level. In fact it seems reasonable assuming that a smaller number of people would be at risk at this level for two reasons: first, it is usually employed, at least in part, for different purposes with respect to the other floors, as the mail entrance, the reception and other common facilities could be located here. Furthermore, in case of an earthquake, the occupants of this level might be able to exit the building during the shaking and hence they should not be considered at risk. This assumption derives from the fact that PACT has been designed to evaluate injuries and fatalities occurring within the building and does not account for those that might happen outside the facility as a consequence of falling objects or other secondary hazards. Hence, 2/3 of the occupants of each of the higher floors is assumed to be at risk at the ground level.

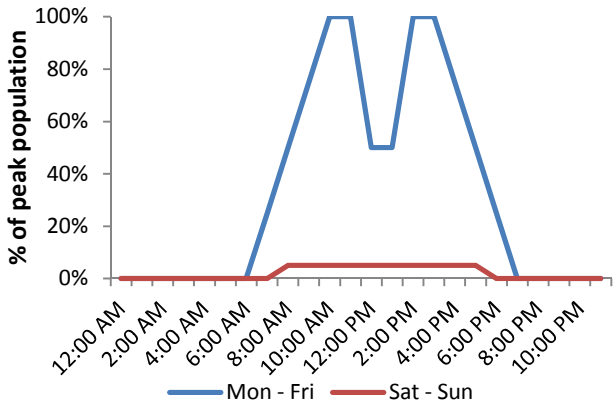

Figure 52: Weekly Population model for office buildings (from ATC-58)

Definition of building components and identification of fragilities

The quantities of structural and non-structural components, including equipment, plumbing, heating/cooling and electrical systems etc., are estimated according to normative quantities provided by ATC-58 for the considered occupancy type. These data have been collected analyzing approximately 3000 buildings representing typical occupancies to assist the users of the tool. In fact it has been recognised that the exact quantities of such damageable component are typically known only at the later stages of the design procedure and might still

be uncertain when the loss assessment is performed. In the normative quantities tables, the vulnerable components are organized in fragility groups, homogeneous subsets of items characterized by similar construction characteristics, details and installation techniques, similar susceptibility and modes of damage and represent similar threat to building occupants. As a consequence, different fragility groups might exhibit sensitivity to different demand parameter, meaning that the elements comprised in a group might be damaged as a consequence of excessive interstorey drifts, while components pertaining to other fragility groups might be susceptible to floor accelerations or other demand parameters.

The amount of components in each fragility group has to be further subdivided in smaller assemblies, termed performance groups. The elements pertaining at the same performance group are all subjected to the same earthquake demands, in a particular direction and at a particular floor level. “Exterior Non-structural walls” is an example of fragility group. The associated performance groups might include Exterior Non-structural walls at the first storey in the N-S direction, Exterior Non-structural walls at the first storey in the E-W direction, Exterior Non-structural walls at the second storey in the N-S direction and so on, indicating that all the elements within a specified performance group will be subjected to the same level of seismic demand (interstorey-drift ratio in this case). It should be pointed out that the elements that are acceleration sensitive (typically equipment) are not considered affected by the direction of this acceleration, hence in this case performance groups are only required to subdivide the elements of the fragility group among the storeys of the building, and do not account for directionality.

Once all the damageable components have been identified and their quantities have been estimated for each storey and each direction (if applicable), the software associates to each of them the already mentioned component fragilities, relating the probability of exceeding a discrete number of damage states to the seismic demand parameter that best represents the damageability of that fragility group.

Costs, Repair Time and threat to life

In the methodology implemented in PACT, each of the aforementioned damage state is coupled with a unique probable repair action, which is in turn associated with cost and repair time consequences. Moreover, each damage state is also related to a unique potential effect on the number of injuries and victims.

Repair costs are intended to cover all the required phases to restore the damaged components to their pre-earthquake condition, hence no upgrade of non-conforming elements is considered. Costs hence depend on the repair measure required and on the number of elements that necessitate of the same intervention. In fact, increasing the number of repairs of the same type that have to be performed, the cost of the single intervention is expected to decrease. An example of consequence function for repair cost is shown in Figure 53.

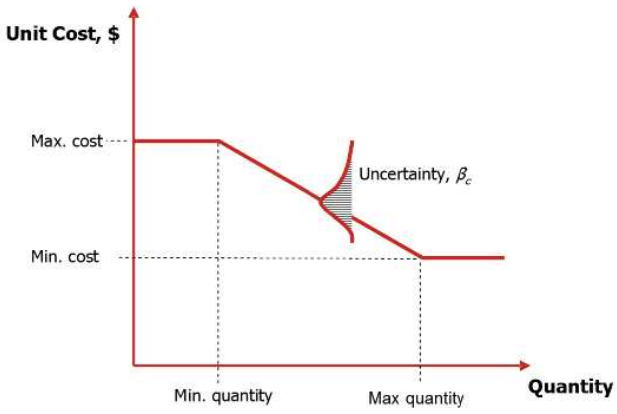

Figure 53: Generic cost function (from ATC-58)

Similarly, repair times are given for each repair action and hence damage state, and a lower and upper bound are provided together with a measure of uncertainty. Hence repair times are estimated based on the number of workers engaged in the building at the same time. This information, however, is associated with great uncertainties as it is affected by many factors, first of all demand surge that might generate lack of available skilled workers or the fact that the building might be occupied during the repair works rather than empty. PACT uses a "maximum worker per square foot" parameter. Although this value can be input by the users, the implementation guide suggests to adopt the default value of 0.001.

Due to the complexity and uncertainty related to evaluating downtime, which depends on both rational and irrational time frames, only the former is evaluated. This repair times is evaluated twice, reflecting two opposite conditions. At first repair are assumed to be performed sequentially between floors, then simultaneously. These two strategies provide an upper and lower bound to the actual repair time that should be expected.

Damage to both structural and non-structural components can result in hazards to building occupants. In fact, besides collapse, falling of debris, equipment or even release of material from pipings could affect life safety. Hence, each damage state of the fragility functions is

correlated to its potential deadly consequence, usually in terms of an area around the specific component where people could be injuries or killed by the occurrence of damage. The evaluation of casualties associated to building collapse require the definition of possible collapse modes, a number of mutually exclusive failure mechanisms that could be expected to develop when structural collapse is predicted. In this study, a number of failure modes are considered for the case study building based on the mechanisms observed performing the incremental dynamic analysis. In particular a combination of soft-storey mechanisms involving one or two of the lower storeys is considered for the as built structure, while more ductile failure modes are also considered to represent the improved behaviour of the retrofitted structures. The Collapse modes are defined through the fraction of floors subjected to collapse debris, that are coupled with a Mean Fatality rate and mean injury rate estimated from the values provided by the ATC-13 (1985) (Table 7) to evaluate the consequences in term of loss of lives and injuries.

Hazard and Building response

In order to perform a time based assessment, a discrete number of intensities, in terms of spectral acceleration, have to be selected from the seismic hazard curve associated to the fundamental period of the structure. Hence, for each of these intensities, non linear time history analyses have to be performed using a suite of ground motions. As for the case of the Incremental Dynamic Analysis described in the previous chapter, recorded accelerograms are selected and scaled in order to ensure the compatibility, within a range of periods including the fundamental one, among the geomean spectrum of the two components and the uniform hazard spectrum representing the return period of interest.

The ATC-58 (2012) guidelines recommend the use of 8 intensities to discretized the hazard curve, while 11 pairs of ground motions should be employed to evaluate the seismic response at each intensity level. However, it is important to point out that, as it will be clarified in the following sections, the values of building response required by PACT are used to describe the behaviour of the building if collapse does non occur. Hence, a higher number of ground motion pairs and analyses are required in order to find at least 11 time histories that do not induce collapse in the building. Especially in the case of those intensities associated with a particularly low frequency, a great number of non-linear analyses have been necessary to achieve the required number of non-collapsing responses.

The results of these analyses have to be given as input to PACT in terms of those response parameters that are relevant to the fragility groups, e.g. the Interstorey drift ratios and the peak floor accelerations as well as the residual interstorey drifts.

Collapse and Demolition Fragility

Collapse and demolition fragilities have to be provided. The former have been obtained through IDA (refer to the previous Chapter), while the latter, describing the probability of a building being demolished as a consequence of excessive residual drifts, can be obtained following the suggestion by Ramirez and Miranda (2012): the authors indicate a median value of 0.015 and a dispersion (logarithmic standard deviation) of 0.3, as shown in Figure 54. The proposed values result in a probability of having to demolish a building of approximately 10% if the maximum residual interstorey drift is 1% while they indicate a virtual certainty of demolition if the structure experiences a residual interstorey drift of 3% or more.

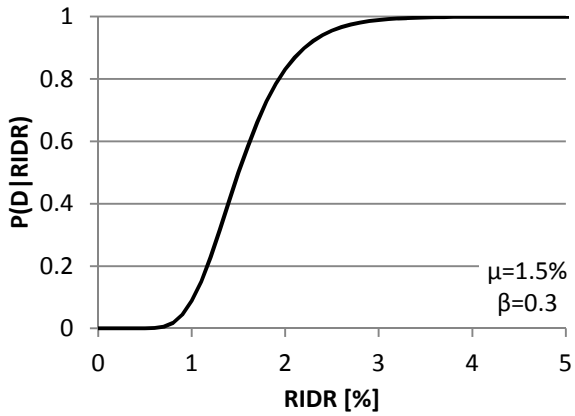

Figure 54: Probability of Demolition given Residual Interstorey Drift Ratio (after Ramirez and Miranda, 2012).

Finally, global building parameters have to be defined. The total replacement cost assumed here was calculated by Beetham (2013) for the same case study building, based on cost information obtained from Rawlinsons (2012) and it includes the cost of demolition/removal of collapse debris from the site as well as the building replacement value. Furthermore, a two years total replacement time was assumed. This value is adopted by PACT in conjunction with the repair times evaluated according to the possible damage states of each component. Hence, in order to allow for a consistent use of these times, the total time is chosen to represent only the rational component of downtime.

Performance Calculation

Once all the required input data have been provided, the performance evaluation can take place. This is carried out by the program adopting Monte Carlo simulations which replace the triple integrals of the original loss assessment methodology proposed by the PEER. The internal repetitive procedure followed by PACT is represented in the flowchart of Figure 55.

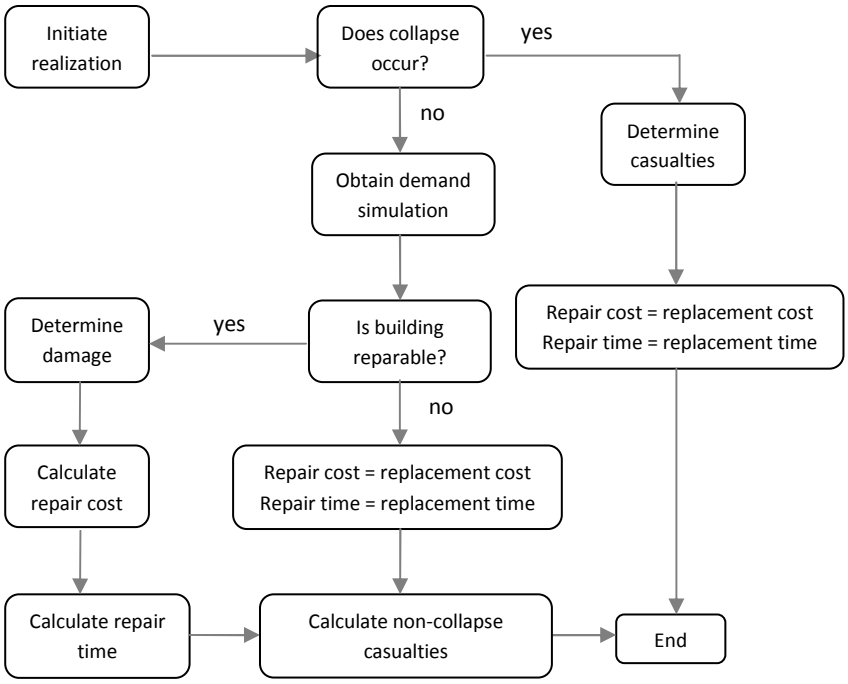

Figure 55: Flowchart for the identification of building performance at each realization (after ATC-58)

The procedure starts associating to each realization of the Monte Carlo approach a unique value of spectral acceleration and a unique set of structural response parameters. These structural parameters (drifts, accelerations, residual drifts,…) are simulated to reflect the correlation between the response parameters obtained through the non-linear analyses. Moreover, a time of day and day of the week for each realization is randomly generated. Then, for each realization, the collapse fragility is compared with the value of spectral acceleration, which gives a probability of collapse. Using random number generation it is determined whether collapse occurred or not. If collapse occurred, the time and the date of the realization are used to evaluate the number of people at risk and randomly choosing a collapse mode, casualties and injuries are computed. The repair time is set as the total replacement time and similarly the repair cost is equated to the total replacement cost.

If collapse did not occur, the residual interstorey drift associated with the realization is adopted to evaluate the probability of having to demolish the building. Again, using a random

number it is decided if the structure has to be demolished or is repairable. In the former case, repair costs and repair times are assumed equal to the corresponding replacement values, in the latter case damage has to be evaluated.

If the building is deemed repairable, the simulated vectors of structural response are adopted together with the fragility functions to evaluate each component's damage state. In fact, the fragilities provide the probability for each damageable component within the building of exceeding different possible damage states. Using a random number, a specific damage state is selected and associated to the realization. Hence, repair costs, times and casualties that might occur in this non-collapsing scenario are computed. Finally, a total loss threshold value is compared with the repair costs just evaluated. This value represents an upper bound on the repair effort beyond which the building will likely be replaced rather than repaired, and for this case study it has been set to 70% of the total replacement cost. Hence, if the repair cost associated to the simulation exceeds this threshold, total replacement costs and times will be attributed to the realization.
The number of repetitions of this procedure has been selected by gradually increasing the number of realizations until it was observed that a further increase did not lead to a significant change in the estimated performance.

From Intensity-based assessment to time based assessment

2000 realizations have been performed for each intensity level, providing a full range of possible consequence outcomes. As an example, Figure 56 and Figure 57 show the results (for the original structure) in terms of repair costs for each repetition for two intensity levels corresponding to a return period of 20 and 100 years respectively. As it can be observed from the graphs, for the same intensity, the computed repair cost can vary greatly ranging from values as low as 0.3% up to 100% of the total replacement cost in the cases where structural collapse is predicted. However, as expected, the probability of incurring in collapse is significantly lower for the frequent event with respect to the rarer one. The pie charts represent the mean contributions to repair costs of the damageable components in case of repairability of the structure. For low intensity earthquakes, this deaggregation shows that, as far as collapse is not occurred, exterior non structural walls and windows, partitions and ceilings have an higher impact on cost than the structural elements. On the contrary, for moderate to severe shakings, damage of structural element becomes the more relevant contribution of the total loss.

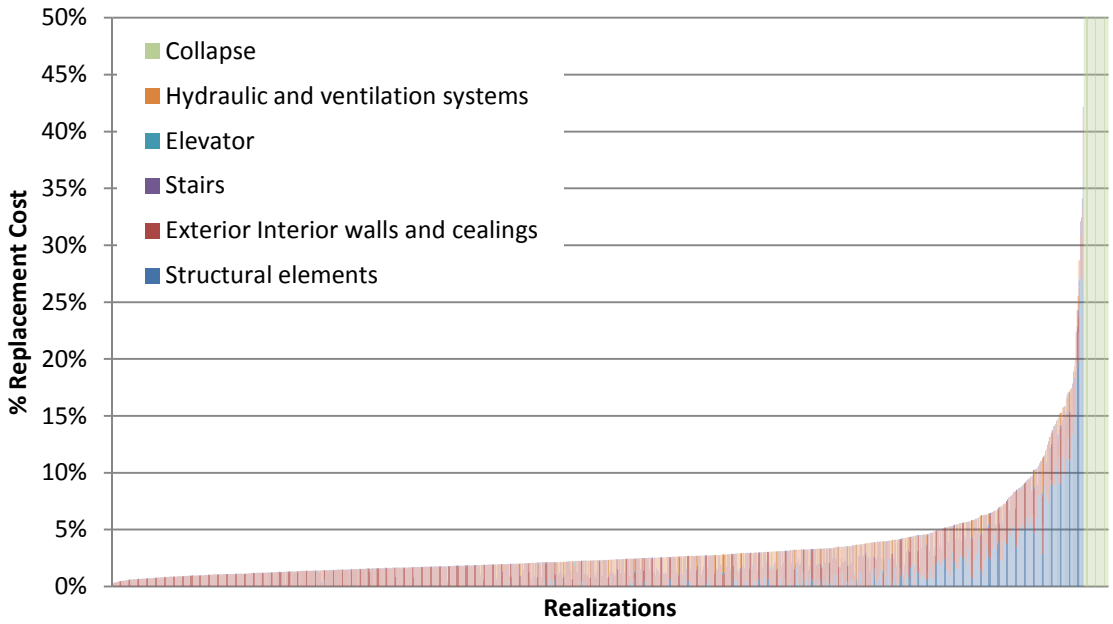

Figure 56: Repair costs from the Monte Carlo simulations (Return Period of the intensity level: 20 years). The vertical axis is limited to 50% of the total replacement cost to show the contributions of noncollapsing realizations, however both collapse and demolition are associated to the full replacement cost of the structure).

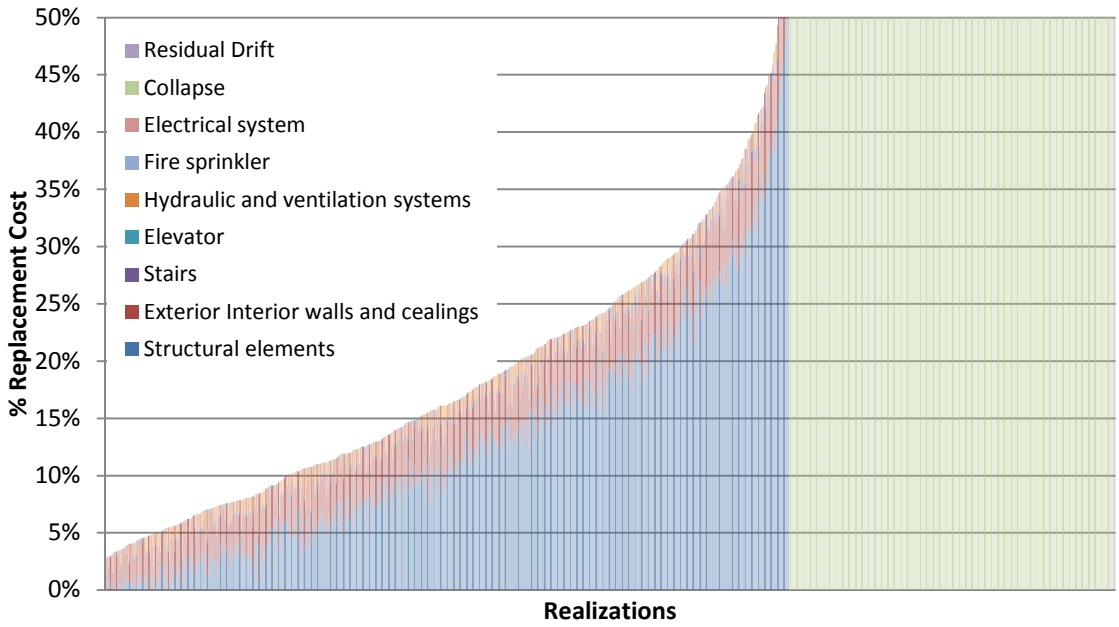

Figure 57: Repair costs from the Monte Carlo simulations (Return Period of the intensity level: 100 years).

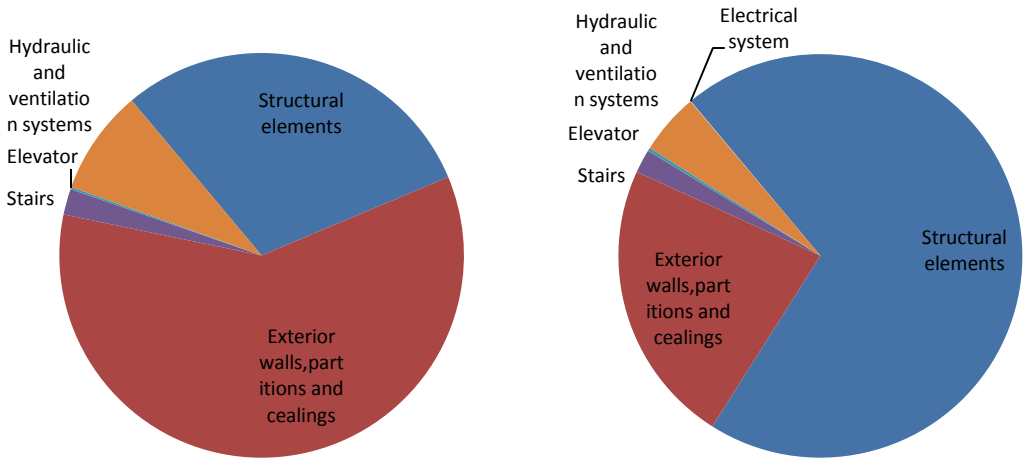

Figure 58: Contribution of different types of damageable components to repair cost predicted for a shaking intensity corresponding to a return period of 20 years (a) and 100 years (b)

Figure 59 and Figure 60 illustrate the contribution of repair cost, losses due to collapse and losses due to demolition on the total predicted loss along all the considered intensities. In particular, it can be observed from Figure 60 that the loss at lower intensities is almost entirely attributable to the cost of the repairing effort, while at higher intensities repair becomes less influent, as the total loss is dominated by the higher probabilities of experiencing collapse.

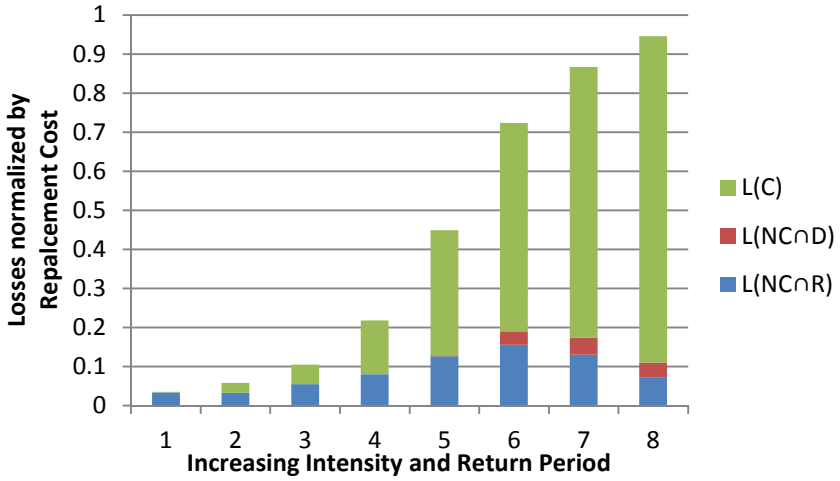

Figure 59: Incidence of repair cost, losses due to collapse and demolition on the total economic loss at different intensity levels for the As-Built structure. L(C): Losses associated to collapse; L(NC∩R): Losses associated to non-collapse of the building and repair; L(NC∩D): Losses associated to non-collapse of the building and demolition.

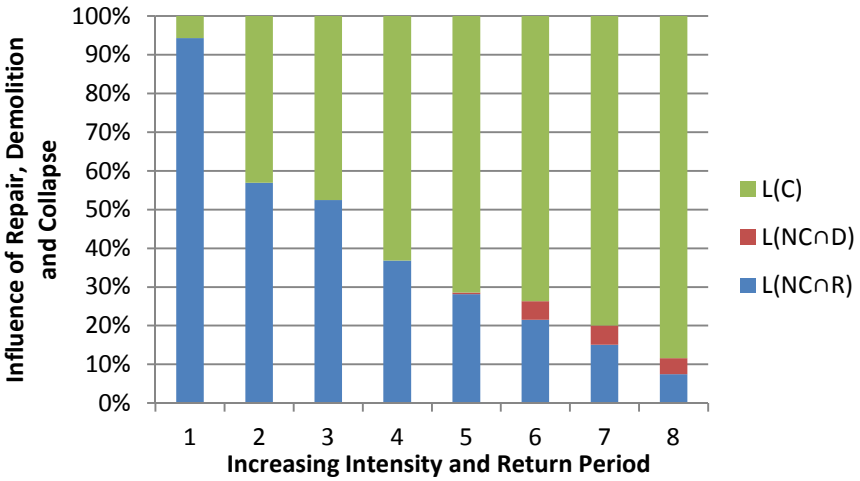

Figure 60: Percentages of the three sources on loss at different intensity levels for the As-Built structure.

Finally, the time-based assessment results are evaluated weighing the results obtained for each intensity according to its mean annual frequency. This is graphically represented in Figure 61 which is a piecewise approximation of the total loss curve. By computing the area enclosed by the curve, the Expected Annual Loss is evaluated. Similarly, repeating the same procedure for the other performance metrics of interest (repair time, casualties and Injuries) annualized values of indirect losses can be estimated.

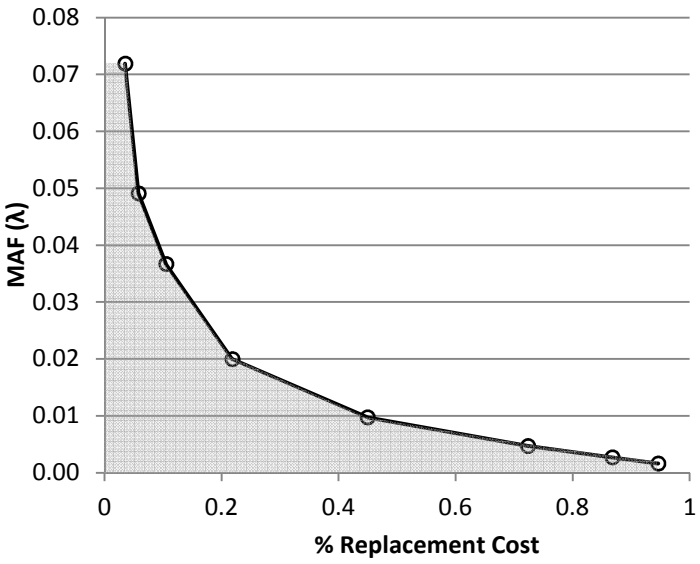

Figure 61: Total Loss curve for the As-Built structure. The area enclosed by the curve represents the Expected Annual Loss.

An Expected Annual Loss of 1.54% of the total replacement cost is estimated for the case study building. The Loss calculation has then been performed for all the upgraded structures, providing the values summarized in the graph below.

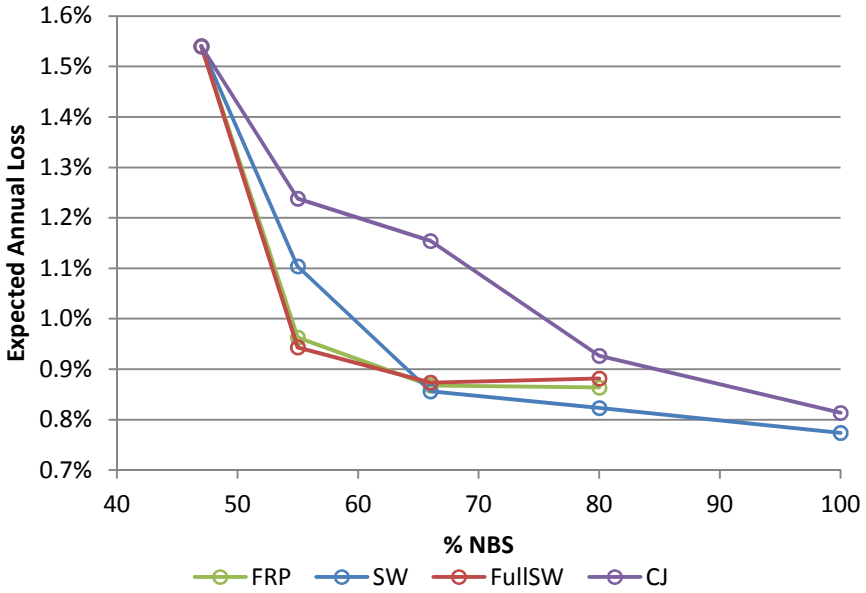

Figure 62: Expected Annual Losses for the As-Built and retrofitted structures, as a function of the achieved %NBS

As it can be expected, the EAL values follow closely the trend observed for the collapse probabilities presented in the previous chapter, as total losses are extremely sensitive to the total replacement cost. In fact, it was observed that for the structures where the retrofit intervention aimed at increasing their ductility, losses associated with repairability of the structure were slightly increased as an effect of higher demands on the building. However, the lower incidence of collapse still governs the final trend of the predicted total loss. On the other hand, the stiffening effect of the column size increase resulted in lower levels of damage, with a positive effect on the computed EAL. However, this aspect has a limited impact on the values of economic loss mainly due to the fact that loss is made of the contribution associated with repair and the total replacement cost which takes into account both demolition and rebuilding costs. Hence, once the costs of the required repair interventions are added to the ones associated with collapse or demolition, their contribution might induce limited changes on the overall loss. For this reason, the improvement in performance associated with the concrete Jacketing retrofit option is more evident when expressed in terms of the annualized repair times presented in Figure 63, where the chosen total replacement time is probably more “in

scale" with the repair times, allowing to capture the contribution of a change in the required repair interventions.

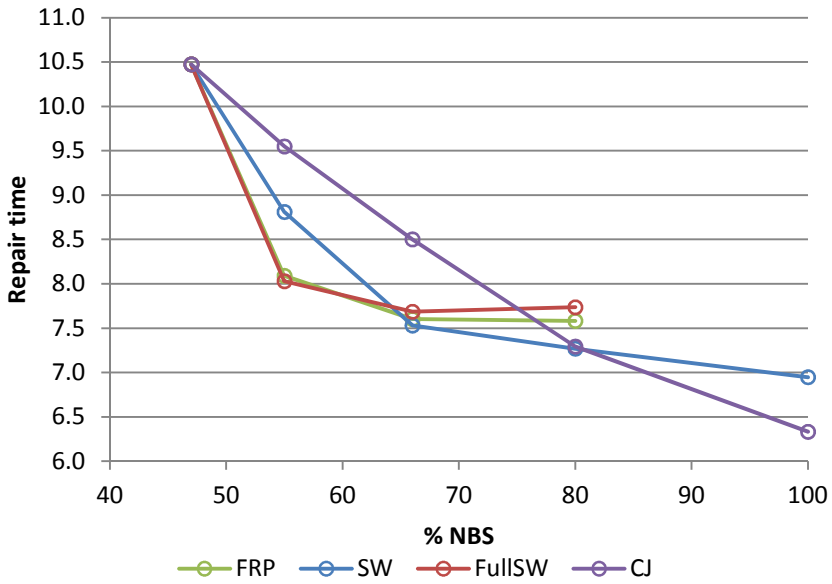

Figure 63: Annualized repair times for the As-Built and retrofitted structures, as a function of the achieved %NBS

Finally Figure 64 collects the injuries and fatality rates obtained in the assessment. These values are affected by great uncertainties, as they are obtained from judgement-based data. However, they still reflect the trend of collapse probabilities and are positively effected by the predicted change in the collapse mechanism obtained through retrofit.

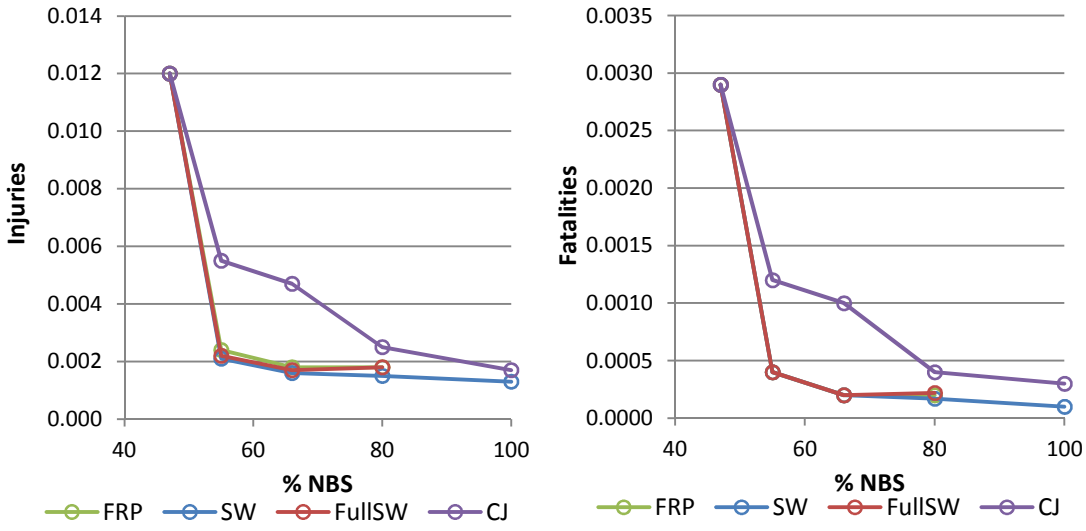

Figure 64: Annualized injury and fatality rates for the As-Built and retrofitted structures, as a function of the achieved %NBS

These results were found to be in line with benchmark studies published in the last few years. For example, Ramirez and Miranda (2009) present values of Expected Annual Losses evaluated for a large variety of code-conforming reinforced concrete frame buildings, characterized by different design choices, geometries and heights, with the number of storeys ranging from 1 to 20. The authors report values of EAL extremely dispersed, from values as low as 0.5% up to 2.5% of the replacement cost of the building. However, these researchers indicate 1% of the replacement cost as an approximate estimate of the mean expected annual loss for office buildings. Similar values have been reported by Mitrani-Reiser (2007), which also compared two design variants with and without Strong Column – Weak Beams provisions observing an increase of 70% in the predicted EAL in the case where capacity design principles were ignored.

Finally, Liel and Deierlein (2008) evaluated expected losses for non-conforming reinforced concrete frames, obtaining values ranging from 1.2 to 5.2% of the total replacement cost, with an average value of 2%, double with respect to those predicted for modern and more ductile structures (refer to Figure 65), providing confirmation on the values obtained within this study.

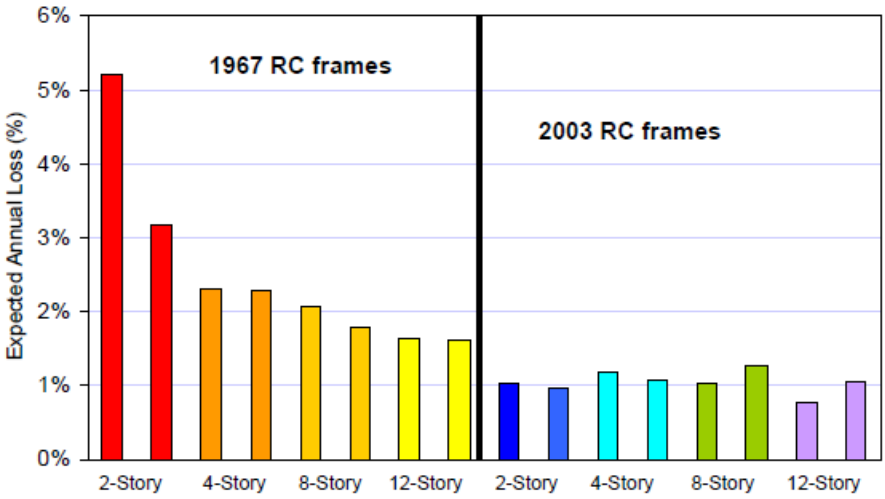

Figure 65: Comparison of EAL for different non-conforming and conforming structures (Liel and Delerlain, 2008)

8. Simplified Loss-Assessment procedure

Introduction

The widely accepted Pacific Earthquake Engineering Research (PEER) Centre's Loss Assessment framework, although comprehensive, is arguably too onerous to be adopted by design professionals. For this reason, in recent years numerous research efforts were carried out, aiming at the definition of simplified procedures for building specific loss estimations (Porter, Beck et al., 2004; Solberg, Dhakal et al., 2008; Sullivan and Calvi, 2011; Welch, Sullivan et al., 2014). For the purposes of this study, a simplified loss model introduced by Sullivan and Calvi (2011) and then further developed by Welch, Sullivan et al. (2012), has been considered and implemented. As the latter method focused on modern RC frames, the procedure has been slightly modified in order to capture the performance of the existing non-ductile structure under examination, including some suggestions by the aforementioned contribution by Sullivan and Calvi and by Beetham (2013).

The methodology presented relies on several simplifying assumptions and thus it should not be intended as a rigorous assessment procedure. Loss estimates are obtained through a deterministic procedure, while uncertainties are incorporated "a posteriori" using the SAC/FEMA approach (FEMA-350, 2000, Fajfar and Dolšek, 2010). Hence, as observed by Beetham (2013), the obtained results should only be considered suitable for comparison among retrofit alternatives at the preliminary design phase of a project.

The method is based on the principles of Direct Displacement Based seismic Assessment (DDBA), which is an extension of the Direct Displacement Based Design (DDBD) methodology to evaluate the performance of existing structures. Conversely to the DBD procedure, where a target displacement is set and the detailing of structural members can be performed accordingly in order to ensure the achievement of the desired performance, the DBA methodology follows the inverse path. In fact, in the case of assessment, the procedure starts with the evaluation of the likely inelastic mechanism which leads to the identification of the displaced shape corresponding to a considered limit state. The

structure is then transformed into an equivalent SDOF system characterized by dynamic properties specific to the limit state of interest. Once the expected base shear and yield displacement are estimated, the effective stiffness and ductility demand can be determined. These parameters can then be used to evaluate the effective period and equivalent elastic spectral displacement of the SDOF substitute structure accounting for the non-linear behaviour at the limit state under consideration through an equivalent viscous damping term. Finally, the seismic intensity inducing the development of the considered limit state can be calculated and the return period or probability of exceedance of that specific intensity can be obtained based on the regional hazard at the building site.

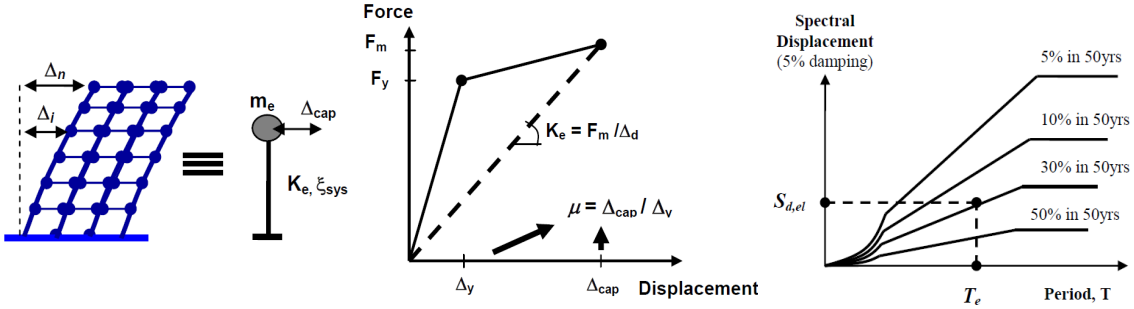

(a) (b) (c)

Figure 66: Direct Displacement Based Assessment: (a) Equivalent SDOF representation of structure at critical limit state; (b)Force-Displacement curve for equivalent SDOF system; (c) Identification of seismic intensity that would induce the development of the considered limit state (from Sullivan and Calvi, 2011)

Outline of the procedure

The aim of the present methodology is to evaluate direct losses expected on a specific building within a certain time frame as a result of the hazard at the building site. These losses are defined as monetary loss, meaning the amount an owner could expect to pay on average in a given time frame to repair earthquake damage or replace its building, considering all possible earthquakes at the site and their probabilities of occurrence, while losses due to possible injuries, casualties, business disruption and downtime are excluded.

Assessment of global response of the building and definition of Performance Levels

In order to perform the loss assessment, the global response of the existing building must be evaluated. To keep the procedure as simple as possible, this analysis is performed "by hand" representing the structural behaviour in terms of a bi-linear pushover curve, the parameters of

which are obtained based on the displaced shape prior to and following yield and hence on the expected inelastic mechanism.

Then, different limit states are selected as they are required to perform a piecewise linear approximation of the continuous total loss curve. According to Welch et al. (2012), four performance levels should be considered, corresponding to:

- Zero Loss (or fully operational)
- Operational
- Life safety
- Near collapse

However, introducing a minor change in the original methodology in order to adapt it to the existing structure of interest, a fifth performance level is considered necessary for the assessment. This is mainly due to a different failure mechanism expected to develop in the case study building being addressed and the consequent value of expected losses at the near collapse limit state. The details and motivations of this choice will be detailed in the following sections.

Adopting the DBA approach, the properties of an equivalent SDOF system corresponding to each one of the performance levels are estimated, as well as the intensity measure (spectral acceleration at the fundamental period of the structure, $S_a(T_1)$), required to reach or exceed the same performance level.

For each performance level, the structural response in terms of Interstorey drift ratio (IDR), peak floor acceleration (PFA) and Residual interstorey drift ratio (RIDR) can then be estimated. IDR and PFA are generically referred to as Engineering Demand Parameters, EDPs. Damages in structural components are usually assumed to be related to the Interstorey drift ratios experienced by the building, while Peak floor accelerations (PFAs) together with the IDRs are usually considered responsible for damages and losses of non-structural components and buildings contents.

Simplified approaches are adopted to evaluate these quantities, in particular:

- The interstorey drift ratio at each performance level can be derived from the assumed structural displaced shape. The peak IDR can be calculated at each storey and each performance level using the following equation, where $\Delta_{i,j}$ is the displacement at

storey i at performance level j; and H_i is the height from the ground level of the i^{th} storey.

$$IDR_{i,j} = \frac{\Delta_{i+1,j} - \Delta_{i,j}}{H_{i+1,j} - H_{i,j}} \tag{8.1}$$

- Peak floor accelerations are determined through the "First Mode Reduced" method (Rodriguez, Restrepo et al., 2002). As the proposed method is deemed too onerous for routine design, the authors also present a simplified version of the approach in the same contribution. This latter procedure, summarized by the equations below, is adopted within this study.

$$C_{pn} = \sqrt{\left[\frac{\eta_1}{R_1} C_h(T_1,1)\right]^2 + 1.75\ln(n)C_{h0}^2} \tag{8.2}$$

where:

$$R_1 = \max\left[\frac{\mu}{2};1\right] \tag{8.3}$$

$$\Omega_i = C_{pn} / C_{h0} \quad \text{if } 0.2 < H_i / H_n \le 1 \tag{8.4}$$

$$\Omega_i = 5\left(\frac{H_i}{H_n}\right)\left(\frac{C_{pn}}{C_{h0}} - 1\right) + 1 \quad \text{if } 0 \le H_i / H_n \le 0.2 \tag{8.5}$$

C_{pn} is the basic horizontal coefficient for a part or diaphragm; η_1 is the first mode contribution coefficient and can be assumed equal to 1 for single-storey buildings and equal to 1.5 for multi-storey buildings; R_1 is the first mode reduction factor; μ is the ductility demand, $C_h(T_1; 1)$, is the elastic spectral acceleration for 5 per cent damping expressed at the fundamental period in units of g; n is number of the levels in the building; C_{ho} is the peak ground acceleration in units of g.

Ω_i is the floor acceleration magnification factor at level i and gives the predicted mean peak floor acceleration at level i (PFA_i) when multiplied by the peak ground acceleration (PGA):

$$PFA_i = \Omega_i \cdot PGA \tag{8.6}$$

- Residual interstorey drifts are estimated adopting the simplified relation proposed by ATC-58 (2002), which is based on the results of a high number of research efforts conducted in the last few years in this topic (Christopoulos and Pampanin (2004) and

Ruiz-Garcia and Miranda (2004) among others). The relation estimates the residual displacement as a function of the peak transient drift experienced by the structure and the expected yield drift of the given storey.

$$\begin{aligned} \Delta_r &= 0 && \Delta \le \Delta_y \\ \Delta_r &= 0.3\left(\Delta - \Delta_y\right) && \Delta_y < \Delta \le 4\Delta_y \\ \Delta_r &= \left(\Delta - 3\Delta_y\right) && \Delta > 4\Delta_y \end{aligned} \tag{8.7}$$

where Δ_r is the residual inter-storey drift, Δ is the peak transient storey drift and Δ_y is the median story drift ratio calculated at yield.

Direct Losses expected on the structure as a consequence of the development of each performance level need to be evaluated. Recalling that through the DDBA principles a specific value of intensity measure required to reach each limit state has already been calculated, the discrete number of losses to be calculated can be directly associated with the corresponding earthquake intensities.

Monetary losses at each limit state can be considered as the result of three different contributions:

- costs associated with building repair, given that the structure did not collapse under the specified earthquake intensity;
- losses associated with the demolition of the building, given that the structure did not collapse, but exhibits levels of residual drift such that is deemed irreparable;
- expected losses associated with the collapse of the building;

These three contributions are highlighted in the following equation:

$$L_T\left(PL\right) = L_{NC\cap R}(PL) + L_{NC\cap D}(PL) + L_C(PL) \tag{8.8}$$

where L_T is the total loss at the considered performance level (PL); $L_{NC\cap R}$ is the loss given that the structure did not collapse (NC) and the building is repaired (R); $L_{NC\cap D}$ is the loss given that there is no collapse (NC) but the building is demolished (D) and L_C is the loss due to collapse (C).

This formulation, suggested by Ramirez and Miranda (2012) represents an advancement with respect to previous loss assessment methodologies, as it acknowledges the importance of considering demolition as a possible outcome of a seismic event. Even though the incorporation of this source of losses would have a greater impact on the expected losses in the case of ductile buildings, this aspect is incorporated in the methodology.

Given the three mutually exclusive outcomes, the total probability theorem gives:

$$\begin{aligned} E\left[L_T \middle| PL\right] = & E\left[L_T \middle| NC \cap R, PL\right] \cdot \left\{1 - P\left(D \middle| NC, PL\right)\right\} \cdot \left\{1 - P\left(C \middle| PL\right)\right\} + \\ & + E\left[L_T \middle| NC \cap D, PL\right] \cdot \left\{P\left(D \middle| NC, PL\right)\right\} \cdot \left\{1 - P\left(C \middle| PL\right)\right\} + \\ & + E\left[L_T \middle| C, PL\right] \cdot \left\{P\left(C \middle| PL\right)\right\} \end{aligned} \tag{8.9}$$

From this equation it is apparent that, in order to compute the total expected loss associated with a performance level, the following quantities have to be estimated:

- Repair costs;
- Loss in case of demolition;
- Loss in case of collapse;
- Probability of demolition given that the structure survived the earthquake;
- Probability of collapse;

Repair costs

In order to keep the procedure as simple as possible, repair costs are evaluated adopting storey-based fragility function, introduced by Ramirez and Miranda in 2009. In this contribution, functions correlating the structural response parameters directly with the Decision Variable (DV), the monetary cost needed to return a building to its original (undamaged) state after an earthquake, have been derived. This result allows to simplify the loss assessment methodology suggested by the PEER by performing in advance its third step, i.e. the damage estimation, and thus reducing the amount of data and computational effort required by the design professionals (refer to Figure 67).

In order to develop these functions, assumptions were made by the authors regarding the building's inventory based on its occupancy and structural system which in turn gives information about the cost distribution among the building levels.
As different building components are not equally sensitive to all demand parameters, each component's damage should be evaluated according to its more relevant EDP. For this reason, different functions were generated for each type of EDP sensitivity.

The EDPs chosen in this study are the same selected by Ramirez and Miranda: the interstorey drift ratio (IDR) and peak floor accelerations (PFA). In fact, the authors categorized components as either drift-sensitive or acceleration sensitive. Moreover, components were further differentiated between structural and non-structural. Assuming that structural damage

could be mainly attributed to high interstorey drift demands, the following sensitivities have been developed:

- drift-sensitive structural components;
- drift-sensitive non-structural components;
- acceleration sensitive non-structural components.

A fourth typology of component was also identified by the authors, in facts some parts of the building were assumed to be damaged only in case of collapse of the entire structure. For this reason, these components, termed “rugged,” were not expected to give any contribution to the loss in case of non-collapse.

Each of the considered damageable components was assigned a fragility function to estimate damage based on the level of structural response. By integrating fragility functions with repair costs, storey EDP-DV functions have been computed for drift-sensitive structural components, drift-sensitive non-structural components and acceleration sensitive non-structural components.

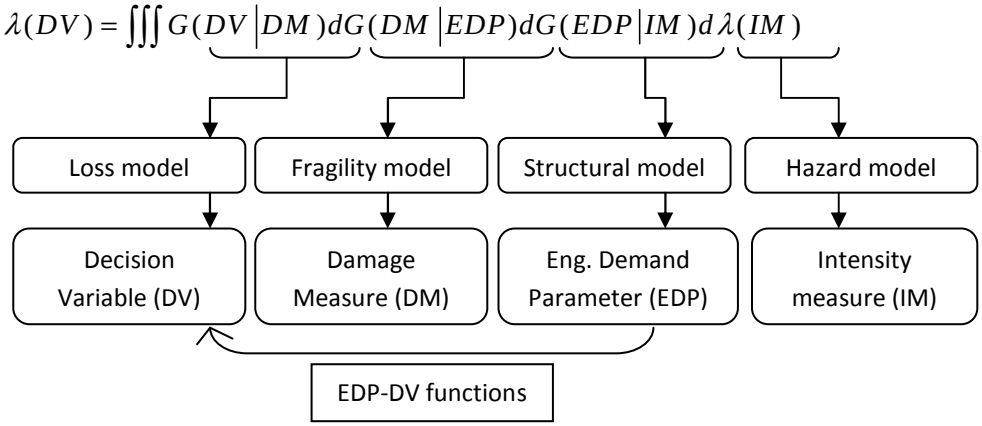

Figure 67: Simplification of the PEER methodology through EDP-DV functions.

Ramirez and Miranda (2009) provided EDP-DV functions for office buildings with ductile and non-ductile reinforced concrete (RC) moment resisting frames. Both space frame and perimeter frame structures were considered along with low-rise, mid-rise and high-rise buildings.

Hence, selecting the appropriate EDP-DV functions, the expected losses due to non-collapse can be obtained from the values of IDR and PFA already evaluated in the previous stages of the simplified loss assessment methodology.

Losses in case of demolition or collapse

For the purposes of this study, loss due to demolition and loss due to collapse are assumed equal. These losses, in particular, include the cost of demolition/removal of collapse debris from the site and the replacement value. This assumption, although simplistic, is consistent with the approach suggested by the ATC-58 and implemented in PACT. Demolition and site clearance are assumed to have an impact on the building replacement cost of 20%, following the indications of the ATC-58. Similarly to the assumption adopted in the probabilistic loss assessment procedure, a total loss threshold of 70% is also introduced.

Probability of demolition

The evaluation of the probability of demolition for a building that survived an earthquake has been the topic of a large amount of recent research contributions. Experience from past earthquake events (Mexico City, 1985 and Kobe, 1995 among others) suggest that excessive residual deformation can trigger the decision of demolishing buildings and other structures even in cases where damage was only moderate. In light of this, several methodologies have been developed to explicitly consider residual displacement into both performance-based design and assessment. Among these, the findings of Ramirez and Miranda (2012) are included in this simplified displacement-based performance assessment methodology. The authors propose a fragility function correlating the probability of having to demolish a building that has not collapsed and the peak residual IDR (RIDR), termed Residual Inter-storey Drift Ratio Demolition Fragility. This fragility function, assumed to follow a lognormal distribution with median of 0.015 and dispersion (logarithmic standard deviation) of 0.3, is the same also adopted in the probabilistic loss assessment procedure. This distribution can be interpreted as the number of professionals that would suggest demolition of a building that has survived an earthquake but exhibits a given level of peak residual interstorey drift.

Hence, for each performance level considered in the simplified loss-assessment procedure, the probability of demolition can be readily obtained from the values of RIDR already evaluated.

Probability of collapse

Lastly, the probability of collapse has to be estimated by means of a collapse fragility function, which expresses the probability of building collapse as a function of the earthquake intensity (IM). Typically these fragilities are assumed to follow a lognormal distribution and as such can be fully described by a median IM and a dispersion term.

The development of collapse fragilities can take place with different methods, from the most rigorous and computationally expensive, the Incremental Dynamic Analysis (IDA), to the least onerous where the collapse fragilities are estimated thanks to engineering judgement. Besides the method adopted to obtain these fragilities, defining collapse itself can be challenging. In fact, collapse is generally associated with either local or global failure of the gravity load resisting system, but the criteria adopted to indicate failure are often affected by great degree of uncertainty and conventionality. Especially when non code-conforming existing buildings are assessed, uncertainties in collapse capacity reflect both record-to-record variability and limited knowledge of the parameters governing the elements' post-elastic behaviour.

In this study, a judgement-based fragility has been adopted. Its median value is chosen as the spectral acceleration associated with the development of the near-collapse limit state introduced before, and the dispersion of 0.7 has been assumed, given the regular layout of the structure.

Earthquake hazard definition

Once the expected losses have been evaluated for each performance level, they can be assigned a Mean Annual Frequency (MAF or λ) knowing the earthquake hazard at the building site. Recalling that each performance level was associated with a corresponding value of shaking intensity, the mean annual frequency at which each damage state will be reached (or exceeded) is calculated introducing the power law reported in Equation (8.10).

$$\lambda(IM) = k_0 IM^{-k} \tag{18.10}$$

This numerical model was first proposed by (Sewell, Toro et al.) in 1996 and, since then, it has been improved and refined in order to achieve higher levels of accuracy in the estimation of the hazard. Nevertheless, the original Sewell's model was used within this methodology, for the sake of simplicity, as it is extremely fast to implement. In order to increase the precision of the method, the fitting of the curve is done considering the two data points at IM values closest to the point of interest using the following equations:

$$k = \ln\left(\frac{\lambda_1}{\lambda_2}\right) \Big/ \ln\left(\frac{IM_2}{IM_1}\right) \qquad k_0 = \lambda_1 (IM_1)^k \tag{8.11}$$

Figure 68 shows the hazard curve obtained for Christchurch and the fitting points are highlighted.

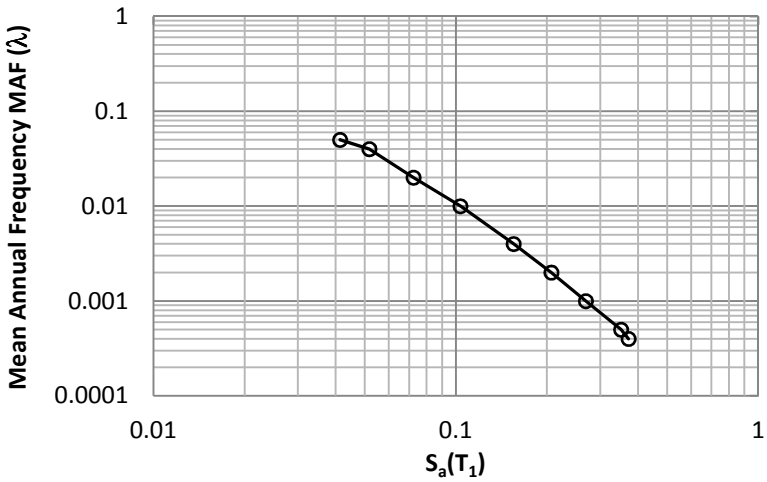

Figure 68: Hazard curve for Christchurch, New Zealand, according to NZS 1170.5:2004 at the fundamental period of the structure.

Performance calculation

Finally the performance calculation can take place. These calculated losses are each associated with a mean annual frequency of the earthquake intensity considered in the loss estimate. Each of these loss calculations represents a point on the approximated total loss curve, as illustrated in Figure 69 and the expected annual loss (EAL) can be calculated as the area enclosed by the total loss curve.

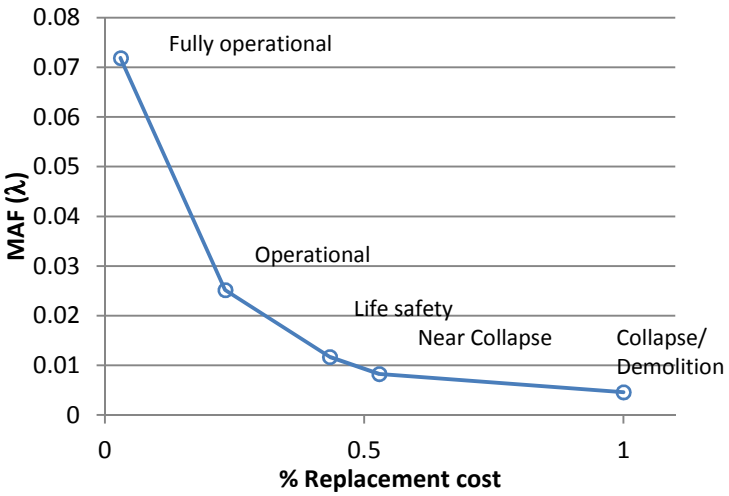

Figure 69: Approximation of the total loss curve to evaluate the expected annual loss (EAL)

A flow-chart representing the simplified loss-assessment procedure is shown in Figure 70.

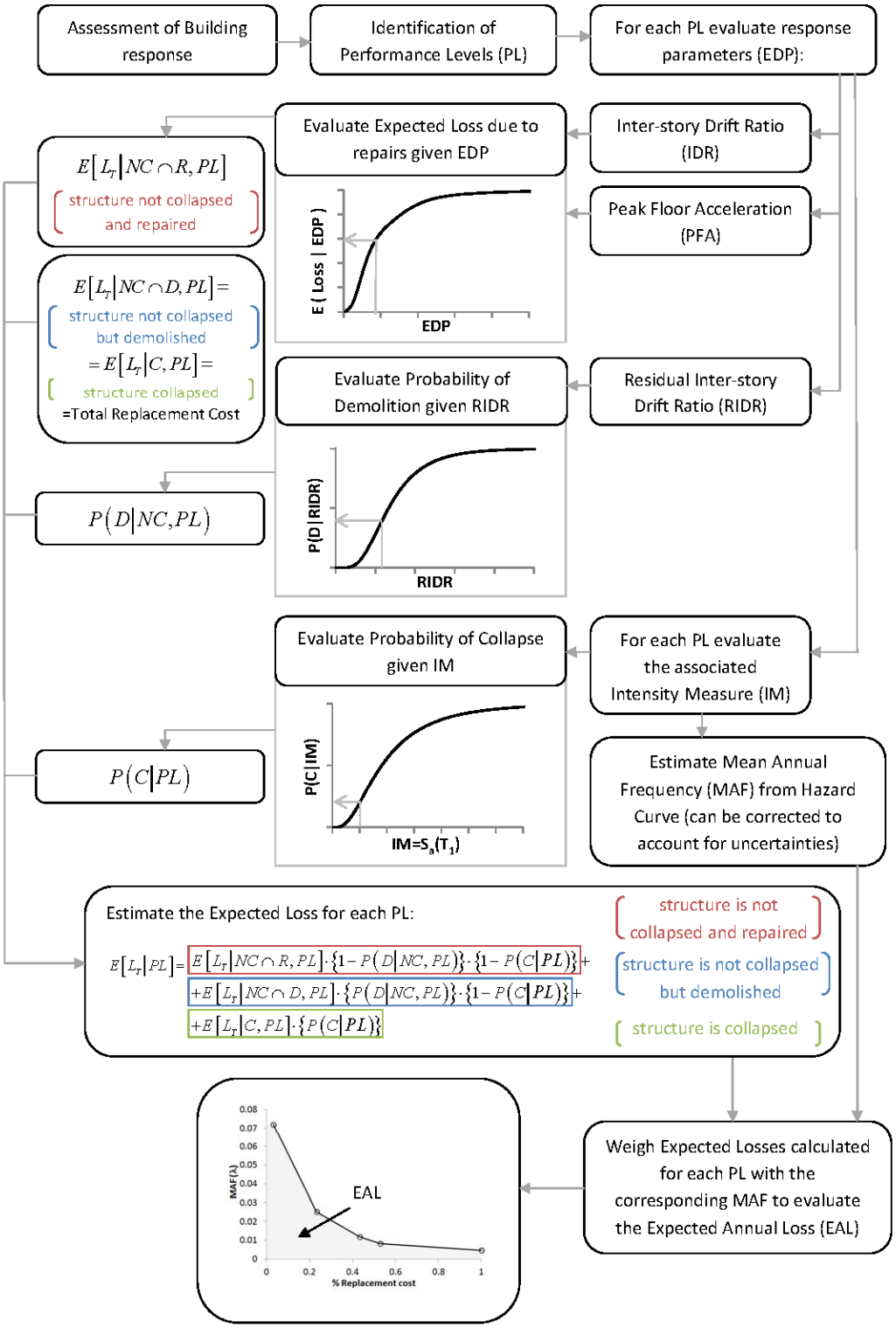

Figure 70: Flow chart of the simplified loss assessment procedure.

Assessment of global building response

The simplified procedure begins with the assessment of global building response, which will be represented by an idealized bi-linear pushover curve. In order to do so, the probable inelastic deformation mechanism of the structure being analyzed must be identified. This aspect, as highlighted by many authors (Priestley and Calvi (1991), Priestley (1997)and more recently Priestley, Calvi et al. (2007) among others), has a key role in the assessment of the seismic behaviour of existing buildings. In order to achieve this goal, the authors suggest to compare, through the Sway potential index $S_{p,}$ the relative capacities of beams and columns referring to the same storey, to establish whether a beam-sway or column-sway mechanisms is likely to develop. The Sway potential index is defined in Equation (8.12):

$$S_{P,i} = \frac{\sum_j \left(M_{bl,i} + M_{br,i} \right)}{\sum_j \left(M_{ca,i} + M_{cb,i} \right)} \tag{8.12}$$

where $M_{bl,i}$ and $M_{br,i}$ are the beam moment capacity to the left and to the right of each joint *j* at the *i*-th storey of the building, while $M_{ca,i}$ and $M_{cb,i}$ are the column moment capacities above and below each joint, with reference to the same level *i*. It has to be pointed out that all moment capacities have to be extrapolated to the joint centroid.

According to the authors, a value of S_p greater than one suggests that a column-sway mechanism has to be expected, while if S_p results smaller than one a beam-sway mechanism is predicted. However, in order to account for uncertainties in material properties and higher mode effects, it is conservatively suggested that a column-sway mechanism has to be assumed when S_p>0.85.

However, it has already been shown that due to the lack of proper detailing affecting the joint region, the full flexural capacities of both beams and columns might not be able to develop before the activation of a more brittle failure mode involving the joints. For this reason, values of S_p were also obtained considering the possible development of a joint shear hinging mechanism, conservatively assuming that this failure mode could lead to a column-sway mechanism (Sullivan and Calvi, 2011). In this case, the indices were evaluated considering the joint equivalent column moments instead of the column moment capacities as done earlier.

For the case study building, the two sets of sway potential indices are summarized in Table 8. The values of Sp for column hinging indicates that a column-sway mechanism will unlikely develop below the 4th storey, while joint shear hinging has to be expected at all levels.

Storey	$S_{p,i}$ - column hinging	$S_{p,i}$ - joint shear hinging
6	2.098788	5.212633
5	0.937673	2.211243
4	0.850577	1.954348
3	0.787064	1.770218
2	0.736757	1.629926
1	0.69978	1.518449

Table 8: Sway potential indices for the 6-storey RC frame case study building.

As a column-sway mechanism cannot develop at each floor, the level at which the mechanism is more likely to form has to be identified. With this respect, a Sway-demand index (SD_i) taking into account the relative capacities of adjacent storeys was introduced by Sullivan and Calvi (2011).

The index can be evaluated for each level according to the following equation:

$$SD_i = \frac{V_{i,D}}{V_{i,R}} \cdot \frac{V_{b,R}}{V_{b,D}} \tag{8.13}$$

where $V_{i,D}$ and $V_{i,R}$ are the storey shear demand and resistance at level *i*, and $V_{b,D}$ and $V_{b,R}$ are, namely, the base shear demand and resistance. The actual shear demands are still unknown but, as can be seen in Equation (8.13), only the distribution of shear demands is required. Assuming a triangular lateral force distribution up until the formation of a mechanism, the ratio $V_{i,D}/V_{b,D}$ can be obtained using the following equations:

$$V_{i,D} = \sum_{j=i}^{n} m_j H_j \tag{8.14}$$

$$V_{b,D} = \sum_{j=1}^{n} m_j H_j \tag{8.15}$$

The storey shear resistances $V_{i,R}$ and $V_{b,R}$ do not refer to the column section shear resistance but are the shears associated with the formation of the expected mechanism and can be evaluated as follows:

$$V_{i,R} = \frac{\sum (M_{c,j,i} + M_{c,j,i-1})}{2\left(H_i - H_{i-1}\right)} \tag{8.16}$$

$$V_{b,R} = \frac{\sum \left(\frac{M_{c,j,1}}{2} + M_{col,b}\right)}{H_1} \tag{8.17}$$

where H_i is the height above ground of the i-th level and $M_{c,j,i}$ is the equivalent column moment associated to the joint shear resistance extrapolated to the joint centroid at level i, as failure in the joints is expected to occur before any other failure mechanism.

The Sway-demand indices presented in Table 9 predict a column-sway mechanism activating within the second storey of the case-study building, because at that level corresponds the maximum value of SD.

Storey	SD_i
6	0.713532
5	1.134436
4	1.385064
3	1.518432
2	1.562922
1	1

Table 9: Sway-demand indices for the 6-storey RC frame case-study building.

The shear forces at each level, corresponding to the incipient formation of the probable inelastic deformation mechanism just computed, were obtained by scaling the lateral force distribution, which is assumed to vary linearly with the height while the structure is still behaving elastically, until the storey shear demand equals the storey shear capacity at yield in at least one level. As it can be observed in Figure 71, the shear demand matches the value of resistance at the second storey, which was found to be the critical level also according to the sway-demand index approach.

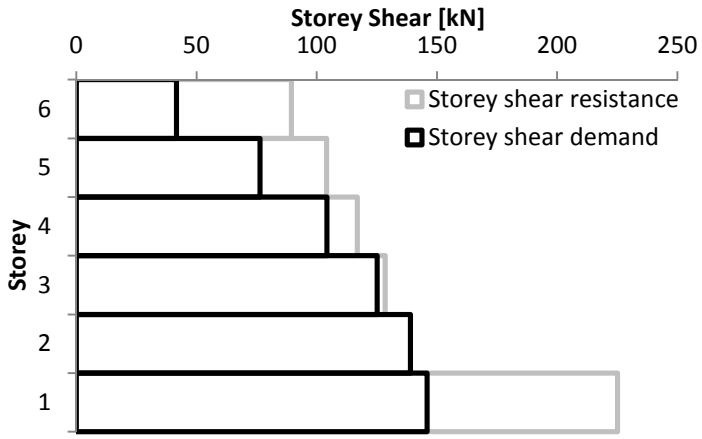

Figure 71: Shear demand vs. shear resistance

The shear profile is then known and the base maximum shear corresponding to the imminent formation of a mechanism (column-sway due to shear hinges failure at the second storey) was found to be 146kN while the shear value associated with the attainment of the ultimate joint capacity in the interior joints resulted 207kN.

The corresponding yield displacement at the critical storey can be estimated following the suggestions by Priestley, Calvi et al. (2007) as:

$$\Delta_y = \chi_y \cdot H^2 / 3 \tag{8.18}$$

which refers to a cantilever. Assuming that the point of contra-flexure is at 0.6 of the storey height (*H*), the displacement is evaluated according to Equation (8.19):

$$\Delta_y = \chi_{y,1} \cdot (0.6 \cdot H)^2 / 3 + \chi_{y,2} \cdot (0.4 \cdot H)^2 / 3 \tag{8.19}$$

where $\chi_{y,1}$ and $\chi_{y,2}$ are the curvatures associated with the formation of the joint shear hinge at the first and second level respectively. In order to obtain the aforementioned curvatures from the joint equivalent column moment, the cracked section modulus was taken as $0.6I_g$, in which I_g is the column gross section modulus, following the recommendations of Paulay and Priestley (1992). The resulting yield displacement, 9.6mm at the critical storey, can be divided by the same storey height giving an interstorey-drift at yield (θ_y) of 0.32%. Assuming an idealized bi-linear elasto-plastic Base Shear-Displacement behaviour, the interstorey yield drift becomes 0.45% as shown in Figure 72.

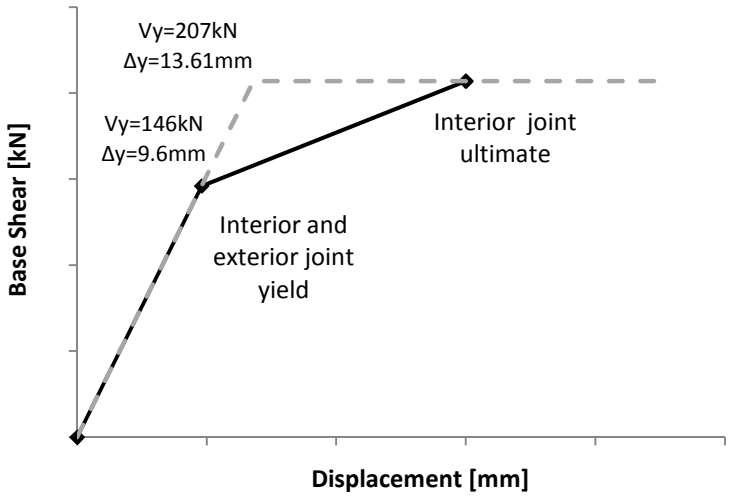

Figure 72: Idealized bilinear response in terms of yield displacement of the critical storey.

Identification of four performance levels: Zero loss, Operational, Life Safety and Near collapse

In order to perform the simplified loss-assessment procedure which is based on the approximation of the total loss curve using a tri-linear model, as proposed by Welch, Sullivan et al. (2012), the definition of the following four performance levels is required:

- Zero Loss (or fully operational)
- Operational
- Life Safety
- Near collapse

The performance levels are defined according to the recommendations by Pampanin, Magenes et al. (2003) as well as the Vision 2000 Report (SEAOC, 1995). In particular, the values of interstorey drift have been correlated with the joint shear deformation in the exterior beam-column joints, as these are expected to govern the seismic performance of the building. Joint shear distortions of 0.01rad and 0.015rad were associated, namely, with the development of Life Safety Limit State and Incipient Collapse. On the other hand, according to the Vision 2000 Report (SEAOC, 1995), a building is considered to be Fully Operational when the earthquake induced damage to both structural and non-structural components is negligible, which in turn means no loss of functionality for the building. In this case, the assumed peak transient drift corresponds to 0.20%. Finally, within the framework of Vision 2000, the operational limit state is defined as a performance level in which moderate damage to non-structural elements and

light damage to structural elements has occurred. The document indicates a threshold inter-storey drift ratio (IDR) of 0.50%. However, as the yield drift has been estimated to be lower than 0.50%, the operational performance level will be precautionary associated with the value of structural yield drift: 0.45%.

The critical inter-storey drift values and the joint shear deformation are assumed to be linearly related for values of deformation below joint 'yield' at γ_y =0.0015. In light of this, the exterior joint shear deformation is supposed to be related to the inter-storey drift ratio (θ) through Equation (8.20) and (8.21) (Beetham, 2013).

$$\frac{\theta}{\theta_y} = \frac{\gamma}{\gamma_y} \quad \text{where } \gamma \leq \gamma_y \tag{8.20}$$

$$\theta = \gamma + \theta_y - \gamma_y \quad \text{where } \gamma > \gamma_y \tag{8.21}$$

The resulting performance levels are summarized in Table 10 and illustrated on the bi-linear pushover curve in Figure 73.

Performance Level	Inter-storey drift θ	Exterior joint shear deformation γ [rad]
Zero Loss	0.20%	0.00094
Operational	0.45%	0.0028
Life Safety	1.17%	0.0100
Near Collapse	1.67%	0.0150

Table 10: Performance Levels in terms of Inter-storey drift and Joint shear deformation for the 6-storey RC frame case-study building.

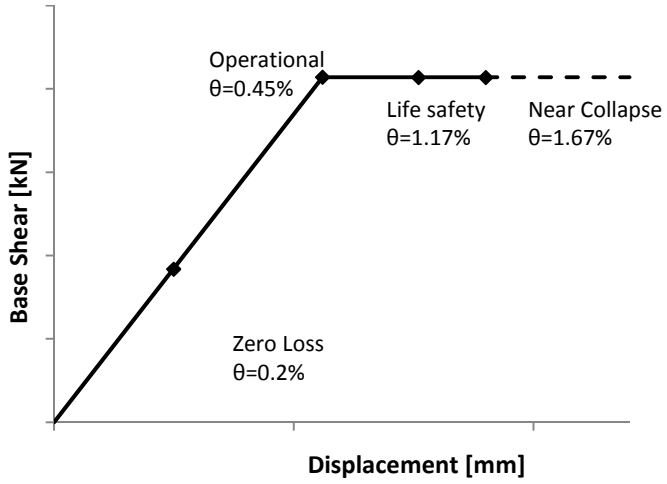

Figure 73: Performance Levels represented on the idealized bilinear response curve.

Once the inter-storey drifts were identified for each of the four performance levels required by the simplified loss-assessment procedure, the characteristics of the same number of equivalent single degree of freedom substitute structures were computed according to the Direct Displacement Based Assessment principles. In particular, the characteristics of each Single Degree of Freedom system can be determined through equations (8.22) to (8.26), assuming a linear displaced shape for the first two limit states and the development of a soft-storey mechanism for the remaining ones.

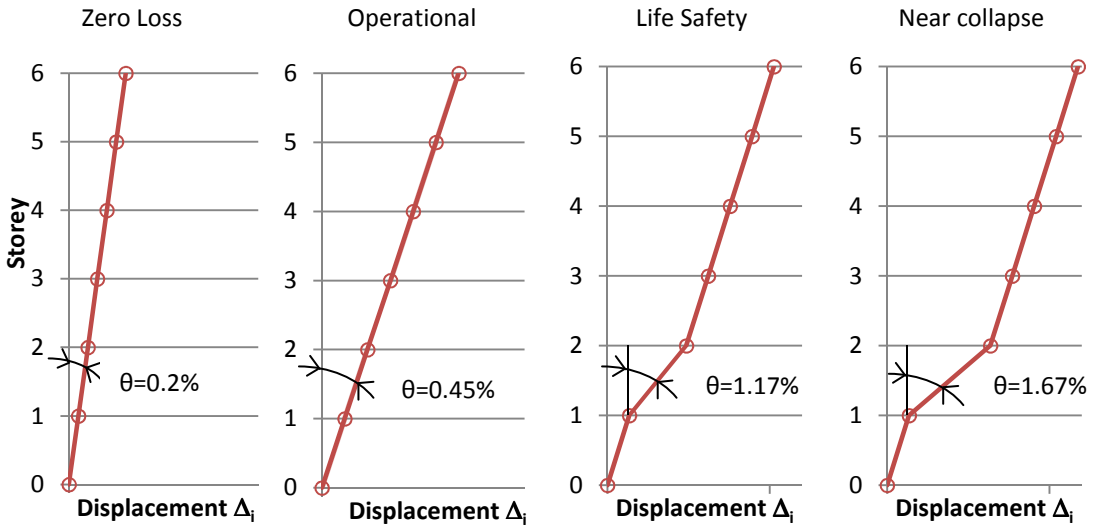

Figure 74: Displaced shapes for the considered performance levels.

$$\Delta_c = \frac{\sum_{i=1}^{n}\left(m_i \cdot \Delta_i^2\right)}{\sum_{i=1}^{n}\left(m_i \cdot \Delta_i\right)} \tag{8.22}$$

$$m_e = \frac{\sum_{i=1}^{n}\left(m_i \cdot \Delta_i\right)}{\Delta_c} \tag{8.23}$$

$$H_e = \frac{\sum_{i=1}^{n}\left(m_i \cdot \Delta_i \cdot H_i\right)}{\sum_{i=1}^{n}\left(m_i \cdot \Delta_i\right)} \tag{8.24}$$

$$K_e = \frac{V_y}{\Delta_c} \tag{8.25}$$

$$T_e = 2\pi \cdot \sqrt{\frac{m_e}{K_e}} \tag{8.26}$$

where m_i and Δ_i are the seismic mass and displacement at level i respectively, Δ_c is the displacement capacity of the structure, m_e is the effective mass, H_e is the effective height, K_e is the effective stiffness and T_e is the effective structural period of the equivalent substitute structure. It has to be pointed out that, within the DBA procedure, the effects of non-linear behaviour and energy dissipation are considered introducing an equivalent viscous damping term (ξ_{eq}). This parameter accounts for the additional damping, beyond the 5% conventional elastic value, associated with the yielding of the system. This term is related to the ductility demand of the system and can be calculated according to Priestley, Calvi et al. (2007) as:

$$\xi_{eq} = 0.05 + 0.565\left(\frac{\mu - 1}{\mu\pi}\right) \tag{8.27}$$

In the original methodology, at the Near Collapse limit state is expected to correspond an earthquake induced loss comparable with the total replacement value of the building, or at least a value of loss greater than the loss threshold, suggesting that the building would more likely be replaced than repaired. However, for the case-study building, a soft storey mechanism is expected to develop as failure mode. For this reason, at the near collapse limit state losses due to repair are much lower than the ones expected in a code-conforming building, as they are mainly expected at one storey rather than distributed along the height of the building. As a consequence, at the Near Collapse limit state the total loss threshold might not be reached and a further performance level is required as closure point of the Loss-Mean Annual frequency total loss curve. Hence, a fifth performance level will be defined in the following sections selecting an Interstorey Drift value at the critical storey corresponding to an unacceptable level of residual deformation, following the recommendations of ATC-58.

Building response at each performance level: EDP-IM Relationship for the existing building

The calculation performed returns the equivalent elastic spectral displacement associated to the effective period of the SDOF structure, $S_d(T_e)$. From this information, the return period of the seismic action required to reach each of the selected limit states can be determined, together with the associated spectral acceleration at the fundamental period of the structure, $S_a(T_1)$, which represents the Intensity Measure (IM) selected within this methodology.

The equivalent SDOF system properties and spectral acceleration values calculated for each performance level are reported in Table 11.

	Zero Loss	Operational	Life Safety	Near Collapse
θ [%]	0.2	0.45	1.17	1.67
V_b [kN]	92	207	207	207
Δ_c [mm]	25	57	76	90
m_e [kN]	3124	3124	3225	3250
H_e [m]	12.56	12.56	12.30	12.19
K_e [kN/m]	3662	3662	2718	2291
T_e [s]	1.84	1.84	2.16	2.37
μ [-]	-	-	1.35	1.60
$S_a(T_1)$ [g]	0.030	0.068	0.099	0.117

Table 11: Properties or the SDOF systems corresponding to the four Performance Levels considered.

Figure 75 shows an example of the displaced shape adopted and the Engineering Demand Parameters (EDP's) evaluated at each performance level: the inter-storey drift ratio, the residual inter-storey drift and the peak floor acceleration.

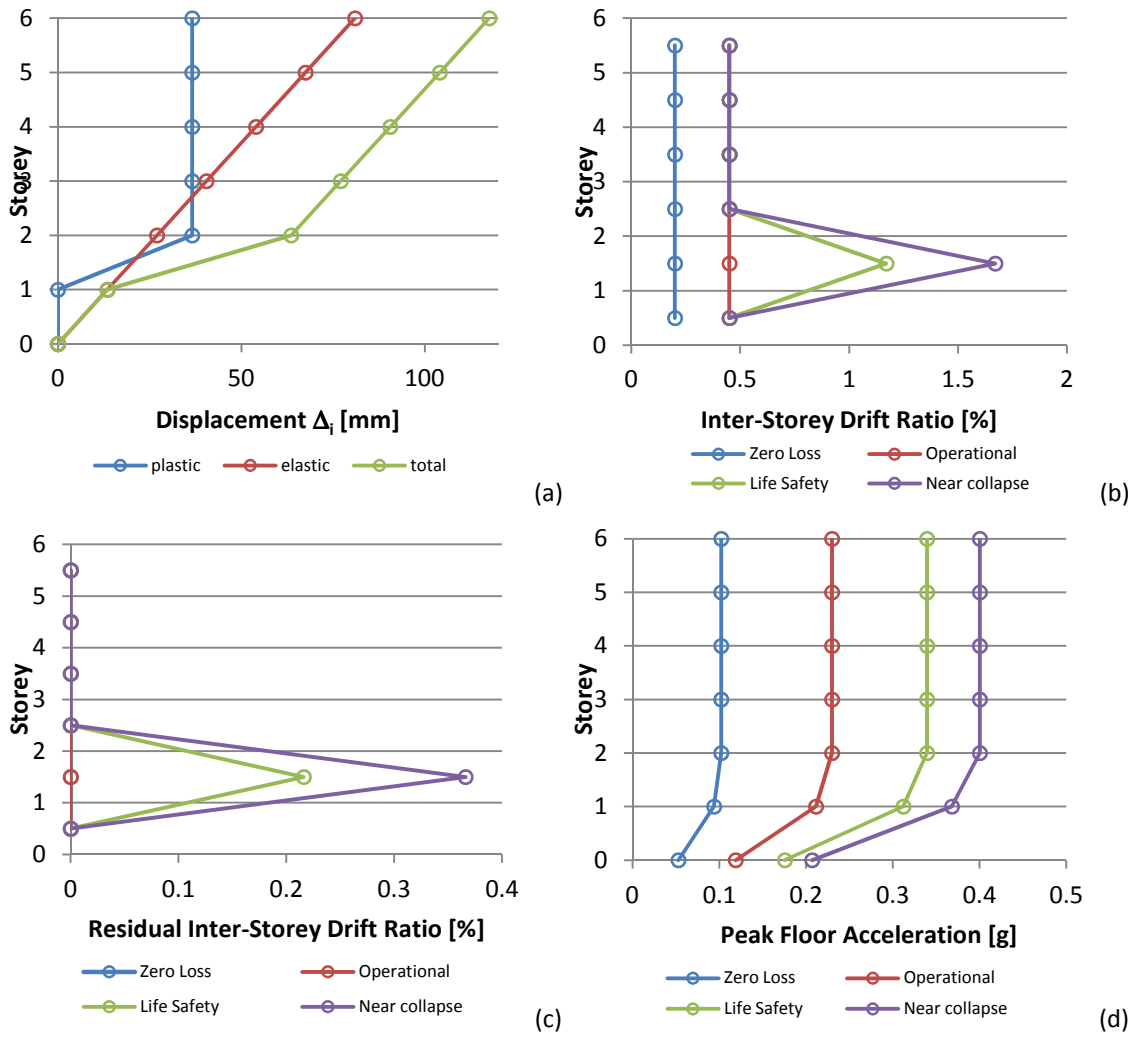

Figure 75: Displaced shape (a) and Engineering Demand Parameters calculated for the existing structure at each performance level (b, c and d).

Earthquake hazard: relating Intensity Measures to their Mean Annual Frequencies

The mean annual frequency at which each damage state will be reached (or exceeded) is calculated adopting the power law:

$$\lambda(IM) = k_0 IM^{-k} \tag{8.28}$$

The power law coefficients are summarized in Table 12, while Table 13 shows the Mean Annual Frequencies obtained for the limit states.

Return Period [years]	MAF [1/years]	$S_a(T_1)$ [g]	k	k_0
20	0.05	0.0432	1	2.1582E-03
25	0.04	0.0540	2.0600	9.7726E-05
50	0.02	0.0755	1.9434	1.3210E-04
100	0.01	0.1079	2.2599	6.5296E-05
250	0.004	0.1619	2.4094	4.9728E-05
500	0.002	0.2158	2.6419	3.4816E-05
1000	0.001	0.2806	2.5838	3.7484E-05
2000	0.0005	0.3669	3.9039	9.9769E-06
2500	0.0004	0.3885	/	/

Table 12: Power law empirical constants k, the logarithmic slope of the hazard curve, and k_0.

Performance Level	$S_a(T_1)$ [g]	λ [1/years]
Zero Loss	0.0300	0.0719
Operational	0.0676	0.0252
Life Safety	0.0995	0.0117
Near Collapse	0.1173	0.0083

Table 13: Spectral acceleration and Mean Annual Frequency for the first four Performance Levels.

Storey-based Engineering Demand Parameter (EDP) - Decision Variable (DV) Functions

Once that the building response corresponding to different limit states has been evaluated, the economic loss due to repairing costs can be estimated. The direct correlation between the engineering demand parameters and the Decision Variable, the economic loss expressed as a fraction of the storey replacement cost, can be obtained using the Storey-Based Building specific functions introduced by Ramirez and Miranda (2009).

The graphs presented in Figure 76 were developed for non-ductile mid-rise reinforced concrete perimeter frames. It can be observed that, normalizing the curves by the total value of structural drift-sensitive components, non-structural drift-sensitive components and non-structural acceleration-sensitive components respectively, the resulting functions exhibit little dependence on the floor level considered.

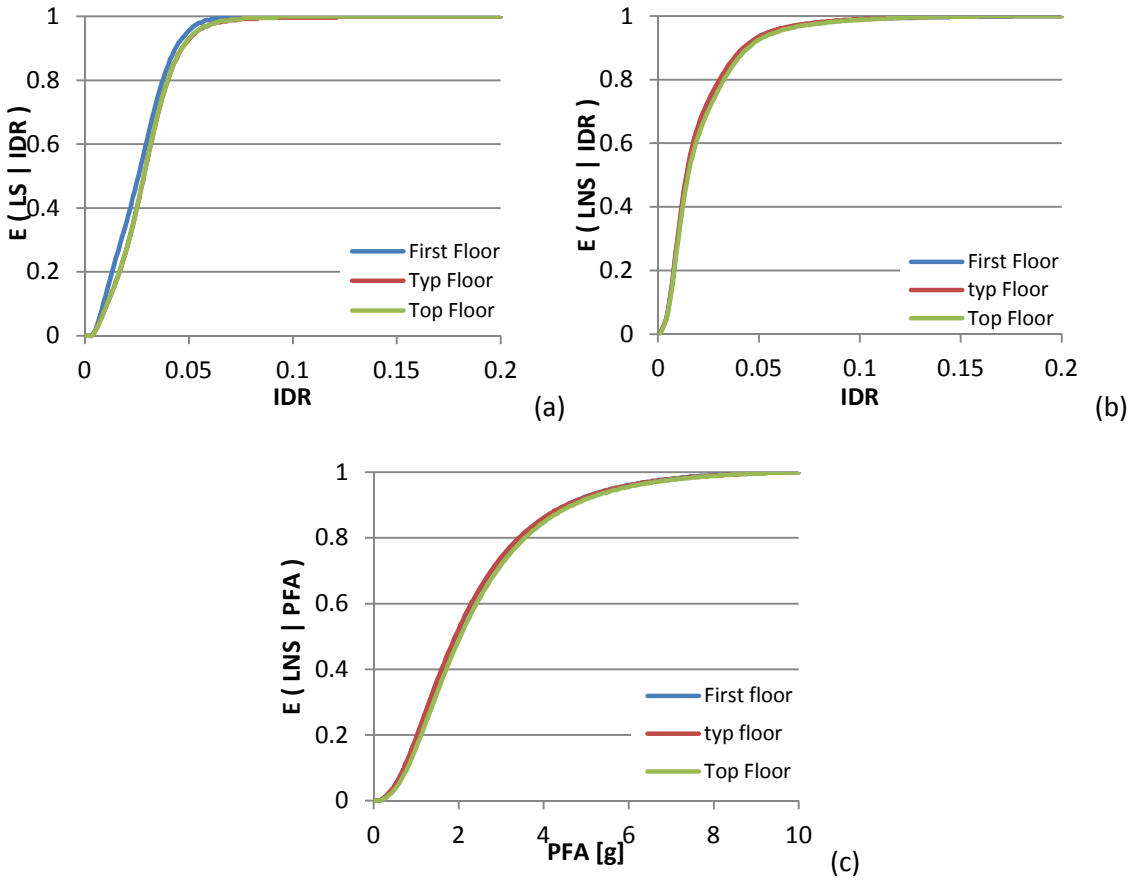

Figure 76: Fragility functions for drift-sensitive structural components, drift-sensitive non-structural components and acceleration-sensitive non-structural components (normalized by the total value of the fragility group for each floor)

Entering the EDP-DV functions with the values of interstorey drift and peak floor acceleration calculated in the previous paragraph, the repair costs can be evaluated once a storey cost distribution is assumed.

Establishing the storey cost distribution requires that assumptions are made regarding the architectural layout of the building considered. The cost distribution assumed here was calculated by Beetham (2013) (Table 14) for the same case-study building, and already adopted in the probabilistic procedure.

Fragility Group	1st Floor	Typ Floor	Top Floor	Total
Structural	1.49	1.49	0.95	8.4
Non-structural Drift Sensitive	6.52	6.88	3.89	37.93
Non-structural Acceleration Sensitive	6.51	7.03	3.8	38.43

Total	14.52	15.4	8.64	84.76

Table 14: Building and storey cost distribution as a percentage of the replacement cost for the case study building - from Beetham (2013).

As it can be observed from Table 14, only approximately 85% of the building replacement cost could be categorized as 'structural', 'non-structural drift-sensitive' or 'non-structural acceleration-sensitive'. The rest of the cost was in either 'rugged' items , site preparation and exterior works or was included in items such as project management or professional fees.

Collapse Fragility and Demolition Fragility

Collapse fragility functions indicate the probability of reaching collapse at increasing levels of intensity measure. It is widely accepted that these function can be described through cumulative lognormal distributions, and as such characterized by a median value and dispersion factor (lognormal standard deviation).

Paulay and Priestley (1992) define a stability index Θ_Δ which compares the magnitude of the P-Δ effect to the design base moment capacity of a structure and suggest that beyond a threshold value of 0.33 the structure becomes unstable. This stability index, according to Beetham (2013), could be used to estimate the structural collapse capacity.

$$\Theta_\Delta = \frac{P\Delta}{M} \tag{8.29}$$

$$\Delta_{\max} = \frac{0.33 \cdot V_b \cdot H_e}{P} \tag{8.30}$$

Although this approach, associated with the Displacement-Based Assessment principles, can certainly be considered viable, it returns values of inter-storey drift ratios associated to a 50% probability of collapse that are particularly high. In fact, the spectral acceleration required to reach the P-Δ instability is 3.25 times higher than the spectral acceleration needed to achieve the near collapse limit state and almost 4 times the value associated to the attainment of the life safety limit state. According to the recommendations of the ATC-58 (2012), a scale factor of the order of three between the spectral acceleration corresponding to the maximum allowable Inter-storey drift (set at 2% of the storey height) and the one expected to cause collapse in the structure can be considered reasonable for buildings conforming to the

requirements of recent building codes, which is not the case of the existing structure under examination.

For this reason, the median value of the judgment-based collapse fragility is precautionary assumed as the spectral acceleration associated to the near collapse limit state (μ=0.117g), while the dispersion is taken as 0.7 (see Figure 78a).

Figure 78 also shows the judgment-based demolition fragility assumed referring to the findings of Ramirez and Miranda (2012).

The median value of the demolition fragility has also been adopted to characterize the fifth SDOF system required for the assessment. In fact, from equations (8.7), assigning a value of 1.5% to the Residual IDR, the value of transient interstorey drift required for the definition of this last limit state can be estimated (as shown graphically in Figure 77).

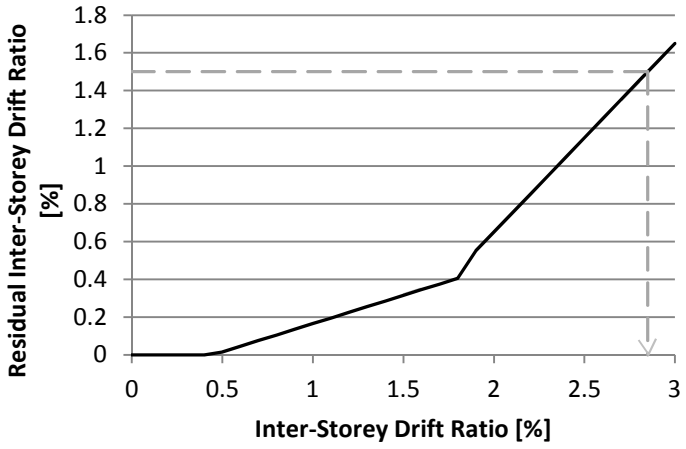

	RIDR=1.5%
θ [%]	2.85
V_b [kN]	207
Δ_c [mm]	125
m_e [kN]	3265
H_e [m]	12.04
K_e [kN/m]	1662
T_e [s]	2.785
μ [-]	2.20
$Sa(T_1)$ [g]	0.152

Figure 77: Evaluation of the inter-storey drift ratio related to a Residual Inter-storey drift of 1.5% and parameters of the SDOF characterized by the just calculated IDR value.

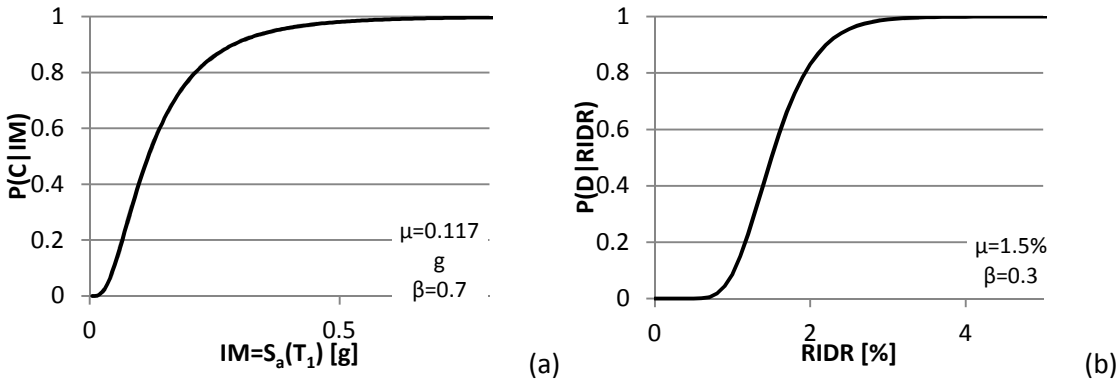

Figure 78: (a) Collapse fragility and (b) Demolition fragility assumed for the case-study building.

Performance Evaluation

The Loss was finally calculated for each performance level, taking into account the repair costs, the losses due to possible demolition and the ones expected in case of collapse, according to the equation below:

$$L_T = L_{NC\cap R} + L_{NC\cap D} + L_C \tag{8.31}$$

where $L_{NC\cap R}$ is the expected loss, given that the building did not collapse and was deemed repairable, $L_{NC\cap D}$ is the loss due to demolition caused by excessive residual displacement and L_c is the loss due to collapse.

The five limit states considered are correlated to a specific value of pseudo acceleration at the fundamental period of the structure. As a result, a discrete number of losses on the building is obtained, each of them associated to its mean annual frequency of occurrence, as reported in **Table 15**.

	IM	λ	L(NC∩R)	L(NC∩D)	L(C)	E[L_T|PL]
Zero Loss	0.030022	0.071888	0.46%	0.00%	2.58%	3.04%
Operational	0.06755	0.025178	1.66%	0.00%	21.54%	23.20%
Life Safety	0.099495	0.01171	2.65%	0.00%	40.71%	43.36%
Near collapse	0.117268	0.008287	2.90%	0.00%	49.99%	52.89%
Demolition	0.152068	0.004606	1.38%	17.77%	64.47%	83.61%

Table 15: Expected losses evaluated for each performance level investigated.

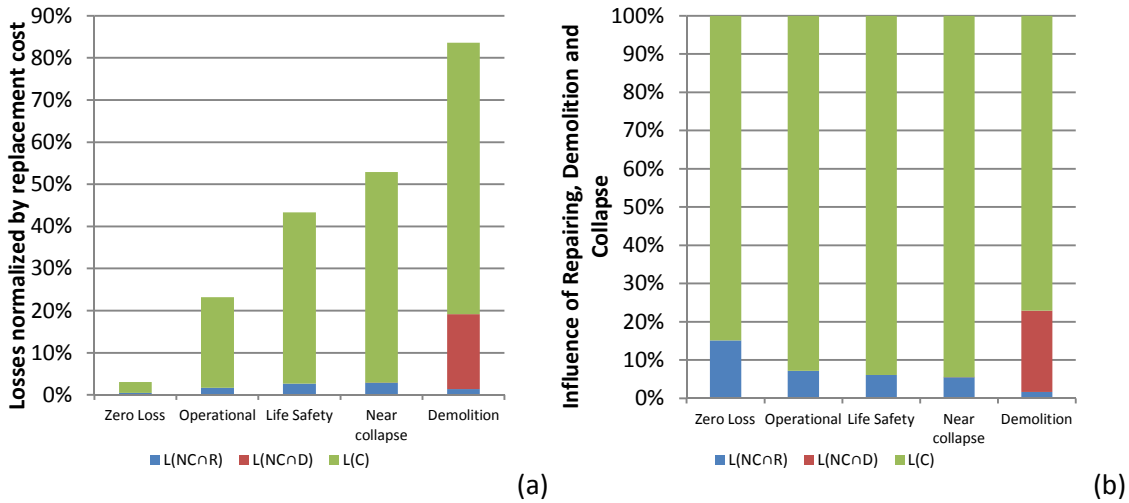

Figure 79: (a) Losses normalized by the replacement cost; (b) Percentage of influence on the expected total losses at each performance level of repairing costs, demolition and collapse losses.

Figure 79(a) and (b) illustrate the total losses disaggregated, in order to clarify the impact of repairing, demolition and collapse costs on the global value for each level of shaking intensity considered.

It can be observed that, even if the intensity measure associated to the Zero loss limit state is particularly low (but frequent), it is still sufficient to induce on the structure losses that are not negligible, around 3% of the building value. This result reflects the relatively high chance of incurring in structural collapse even at the lower levels of intensity. In fact, over 80% of the just mentioned total loss comes from possible collapse of the building (Figure 79(b)).

The Demolition limit state realization returns an expected total loss in the order of 80% of replacement cost and a 65% probability of collapse. In such circumstances, the ATC-58 (2012) document suggests, based on past studies, that the building owner would more likely replace the building instead of repairing it. For this reason, the full replacement cost was attributed to this performance level.

Each of these loss calculations performed is a point in the total loss curve, as shown in Figure 80, and the area underlying the curve represent the approximation of the Expected Annual Loss.

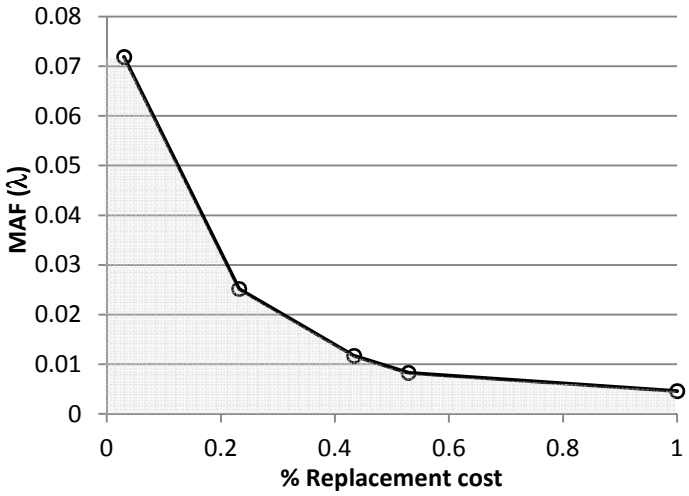

Figure 80: Approximated total loss curve.

The Expected Annual Loss predicted in this study for the existing building is 1.97%, around 30% higher than the same value obtained through the probabilistic approach. This result was to be

expected, given the number of simplifying and precautionary assumptions introduced as well as the deterministic nature of this approach. In particular, the definition of the collapse fragility has a great influence in the evaluation of the losses, particularly in the case of existing buildings, since a high probability of collapse characterizes each performance level. Hence, the effect of different assumptions regarding the definition of the collapse fragility will be further investigated in the following sections.

Evaluation of the percentage of NBS achieved by the existing building

The New Zealand built environment is commonly assessed referring to the percentage of the new building standard (% NBS) (New Zealand Building Act (2004) and NZS 1170.5:2004). This parameter indicates the percentage of the design level earthquake, relative to a newly designed structure, that the existing building can sustain without exceeding a certain limit state. As a result, structures can be graded as either potentially earthquake prone (NBS less than 33%), potentially earthquake risk (NBS greater than 33% but smaller than 67%) or unlikely to be an earthquake risk building (NBS above 67%).

The existing building was assessed to determine the percentage of the New Building Standard (NBS) that the structure could achieve at each performance level. Figure 81 graphically presents the results of the assessment undertaken, showing the design spectrum scaled to match the required limit states.

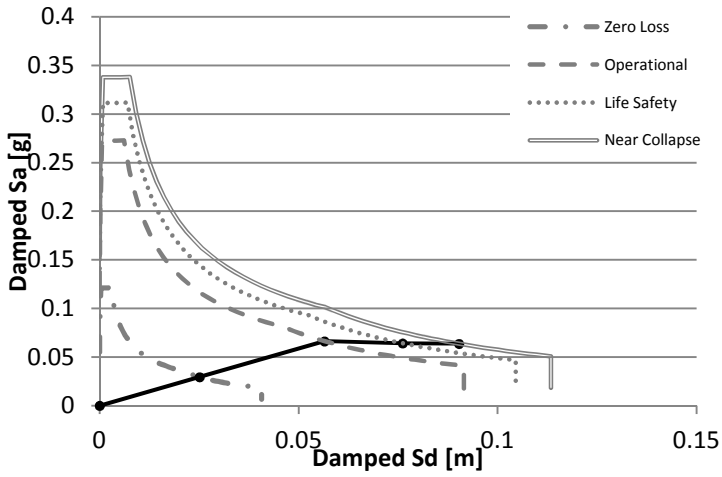

	NBS
Zero Loss	14%
Operational	31%
Life Safety	39%
Near collapse	45%

Figure 81: Existing Building Percentage of NBS for the four performance levels.

The Life safety limit state is reached at 39% of the New Building Standard, thus, in principle, no building upgrade is required according to the current codes.

Upgrade to 100% of the New Building Standard: effect on the EAL of different retrofit strategies

Given the particularly brittle nature of the failure expected to develop, various retrofit strategies were taken into account, aiming at modifying the structural behaviour to prevent complete structural collapse under the design level earthquake. This performance target is in line with the ASCE-41 rehabilitation objectives for existing structures, where it is referred to as Limited Rehabilitation Objective (LRO). By removing the critical structural weaknesses and preventing soft-storey collapse, human fatalities are minimized, while accepting significant structural and non-structural damages.

The strategies do not refer to a specific retrofit technique and include: increase of ductility, increase of strength, decrease of stiffness and a combined modification of strength and stiffness. For each of these strategies, the values of EAL are compared in Table 16.

	Δ_y [mm]	V [kN]	EAL [%]
Ductility	84.1	207	1.06%
Stiffness	131.6	207	1.30%
Strength	131.7	324	1.09%
Stiffness and Strength	84.1	523	0.84%

Table 16: Predicted values of Expected Annual Loss for different retrofit strategies.

It should noticed that one aspect differentiates the evaluation of the Expected Annual loss for the 'as-built' structure and the upgraded ones. In particular, in the retrofitted buildings a beam-sway mechanism is expected to develop, hence, the displaced shape is modified accordingly. Although a beam-sway mechanism implies higher repair costs, due to drift demands that are not concentrated in a single critical storey but are distributed along the height, it is also associated with a reduction of losses due to collapse or demolition. In fact, the spectral accelerations required to reach the selected limit states are shifted toward higher intensities. As expected, the existing structure exhibits annualized total losses that are greater than the ones calculated for the four retrofit strategies considered.

Effect of dispersion in Collapse Fragility and Demolition Fragility

While the median value of the collapse fragility was evaluated through Displacement Based Assessment, the dispersion β was taken as 0.7 following the indications from the ATC-58 (2012) document. Similarly, the median value of the demolition fragility was chosen as the spectral intensity able to induce on the structure residual drifts of the order of 1.5%, while the dispersion was judgementally assumed as 0.3.

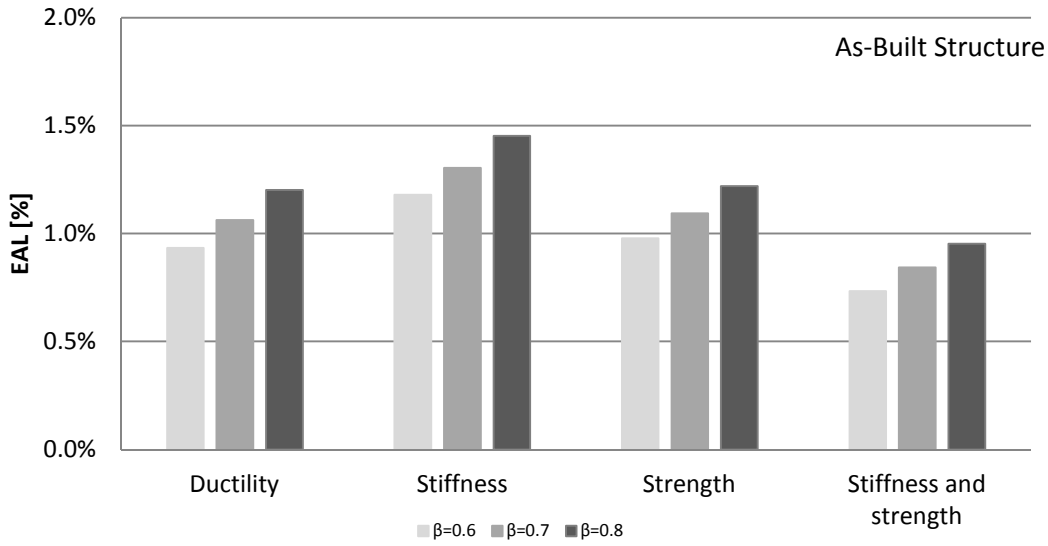

Figure 82: Sensitivity of the EAL value to the dispersion of the collapse fragility.

In Figure 82, values of EAL corresponding to different values of dispersion of the collapse fragility are compared.

From this comparison, the result of the Loss Assessment appears to be quite sensitive to the collapse fragility dispersion, with the maximum difference as high as 10% with an increase of 0.1 in the β value. On the other hand, a variation of the demolition dispersion does not affect the EAL value. In fact, the Loss value is almost independent from the demolition dispersion. This is a consequence of the fact that losses due to demolition are only relevant for the fifth limit state considered, where, by definition, the probability of the structure being demolished is 50%, regardless of the dispersion value adopted.

Introduction of uncertainties

The current methodology does not account for any source of uncertainty, in fact both aleatory randomness and epistemic uncertainty have been neglected so far. Aleatory uncertainties are

uncertainties that cannot be reduced through improved methods or more accurate measurement (e.g. record-to-record variability). By comparison, epistemic uncertainty is solely due to a lack of knowledge and it can arise, for example, from the assumptions introduced or from the mathematical model used to represent the physical processes. As a consequence, this source of variability could in principle be reduced by gaining better understanding on the phenomenon of interest.

In particular, the simplified approach assumes that a unique set of Engineering demand parameters will correspond to a given level of Intensity Measure, thus ignoring the demand variability on the structure.

In order to account for the sources of uncertainties and randomness inevitably present, without compromising the simplified nature of the methodology, a simplified version of the SAC-FEMA approach (FEMA-350,2000) is adopted, in line with Sullivan and Calvi (2011).

The formal basis behind the probabilistic performance evaluation approach presented in the aforementioned guidelines are described by Cornell, Jalayer et al. (2002). In particular, according to the authors, the ground motion intensity as well as the demand parameter D and the capacity parameter C have to be treated as random variables, and the corresponding uncertainties need to be accounted for in the performance assessment. The proposed procedure is illustrated in Figure 83, taken from the reference article:

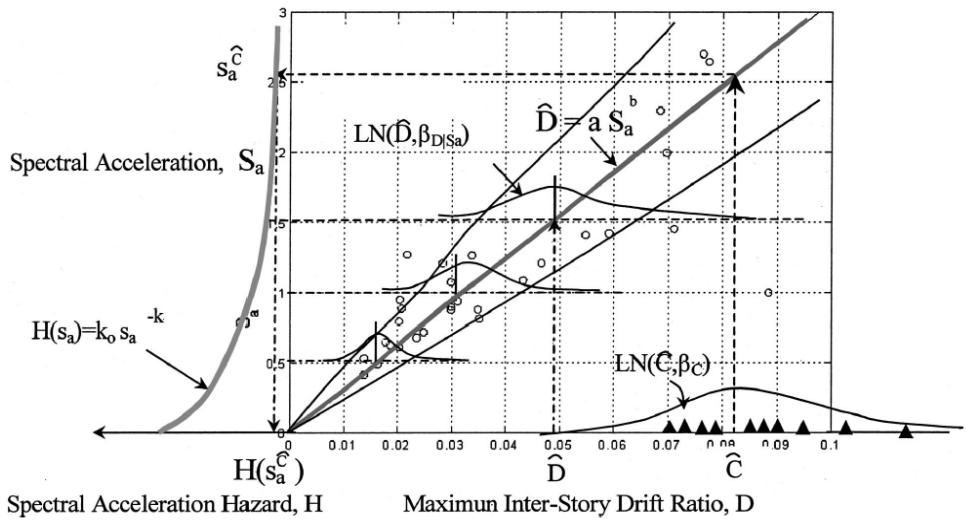

Figure 83: Incorporation of uncertainties in the performance assessment following Cornell et al.(2002).

The all procedure have been described in terms of annual probability of exceedance of a given intensity measure. However, for small values of the exceedance rate, the probability can be approximated with the Mean Annual Frequency λ. In fact, according to the Poisson model, the probability of observing at least one event in a period of time t, one year in this case, is equal to:

$$P(n_{events} \geq 1) = 1 - e^{-\lambda t} = 1 - e^{-\lambda} \tag{8.32}$$

and can be approximated using the first two terms of the Taylor series expansion for the exponential, resulting:

$$P(n_{events} \geq 1) = 1 - e^{-\lambda} \cong \lambda \tag{8.33}$$

This approximation can be considered accurate for values of λ smaller than 0.1. As this condition is always verified for the applications presented, the annual probability will be substituted with the corresponding annual frequency in the following of the procedure.

The figure above summarizes the key aspects of the approach. Firstly, it is assumed that the site hazard curve, giving the mean annual frequency of the random intensity measure (S_a) reaching or exceeding the value s_a, can be approximated using the power law already presented and reported here for clarity:

$$\lambda(IM) = k_0 IM^{-k} \tag{8.34}$$

where IM is the value of spectral acceleration at the fundamental period of the structure.

The uncertainties associated with the ground motion hazard curve are usually presented in the form of "confidence bands" on the mean annual frequency of exceedance of any intensity level. To a 50% confidence level corresponds the median estimate of the annual probability $\hat{\lambda}(s_a)$. The values of mean annual frequency are assumed to be lognormally distributed and hence can be described by the mean estimate $\overline{\lambda}(s_a)$ and the standard deviation of the natural logarithm, the dispersion term β_H. The mean value can be obtained from the median estimate using the equation below:

$$\overline{\lambda}(s_a) = \hat{\lambda}(s_a) \cdot \exp\left[\frac{1}{2}\beta_H^2\right] = \hat{\lambda}(s_a) \cdot C_H \tag{8.35}$$

Moreover, the relationship between the intensity measure and the median of the Engineering Demand Parameter is approximated as follows:

$$\hat{D} = a\left(S_a\right)^b \tag{8.36}$$

The EDP are again assumed to be lognormally distributed about the median, thus the distribution can be fully described introducing a dispersion value accounting for the record-to-record randomness, termed β_{DR}, associated with a specific level of spectral acceleration. This record-to-record variability is not the only source of dispersion affecting the structural demand. In fact, additional uncertainties reflecting the effective knowledge available for the estimation of the demand have to be considered. The letter uncertainty, epistemic, is termed β_{DU}. Similarly, two values of dispersion can be introduced to describe the structural capacity, β_{CU} and β_{CR}, namely, the dispersion representing the epistemic uncertainty and the one representing the aleatory randomness.

From probability theory, the mean annual frequency of exceedance of a given limit state is given by:

$$\overline{\lambda}_{PL} = \overline{\lambda}(s_a^{\hat{C}}) \cdot \exp\left[\frac{1}{2}\frac{k^2}{b^2}\left(\beta_{DR}^2 + \beta_{DU}^2 + \beta_{CR}^2 + \beta_{CU}^2\right)\right] \tag{8.37}$$

While the estimate of the annual frequency associated with the confidence level x can be obtained from the following equation:

$$\lambda_{PL}^x = \overline{\lambda}(s_a^{\hat{C}}) \cdot \exp\left[\frac{1}{2}\frac{k^2}{b^2}\left(\beta_{DR}^2 + \beta_{CR}^2\right)\right] \cdot \exp\left[K_x \frac{k^2}{b^2}\left(\beta_{DU}^2 + \beta_{CU}^2\right)\right] \tag{8.38}$$

The equation above can be rearranged in a more compact form as follows:

$$\lambda_{PL}^x = \hat{\lambda}(s_a^{\hat{C}}) \cdot C_H \cdot C_f \cdot C_x \tag{8.39}$$

where $\hat{\lambda}(s_a^{\hat{C}})$ is the median estimate of the mean annual frequency of the spectral acceleration corresponding to the median capacity. C_H considers the distance between mean and median hazard values, C_f accounts for the dispersion in structural demand and capacity and C_x is a function of the selected confidence level through the parameter K_x, the standardized Gaussian variation associated with probability x of not being exceeded.

$$C_H = \exp\left[\frac{1}{2}\beta_H^2\right] \tag{8.40}$$

$$C_f = \exp\left[\frac{1}{2}\frac{k^2}{b^2}\left(\beta_{DR}^2 + \beta_{CR}^2\right)\right] \tag{8.41}$$

$$C_x = \exp\left[K_x\frac{k^2}{b^2}\left(\beta_{DU}^2 + \beta_{CU}^2\right)\right] \tag{8.42}$$

Fajfar and Dolšek (2010) suggest a number of simplifications to the approach just briefly described above based upon the following observations:

- the mean and median values are usually not very different and, as such, the distinction between mean and median values is omitted in the case of hazard curves as well as demand and capacity estimates. The value of C_H is then set equal to 1;
- for practical purposes a 50% confidence level is considered acceptable and consequently Cx becomes unity;
- the spectral intensity is assumed to be linearly related to the demand, hence, the value of b is taken equal to one;
- default values for the dispersion values for randomness were proposed by the authors to overcome the lack of reliable data. The adopted value for the total dispersion was: $\beta_{DR}^2 + \beta_{CR}^2 = 0.2025$.

Hence, this simplified procedure allows to incorporate the uncertainties into the loss assessment methodology by scaling the mean annual frequencies corresponding to the considered limit states by a coefficient C_f, function of the slope of the hazard curve, thus leading to an increase of the Expected Annual Loss, as showed in Figure 84 and Figure 85.

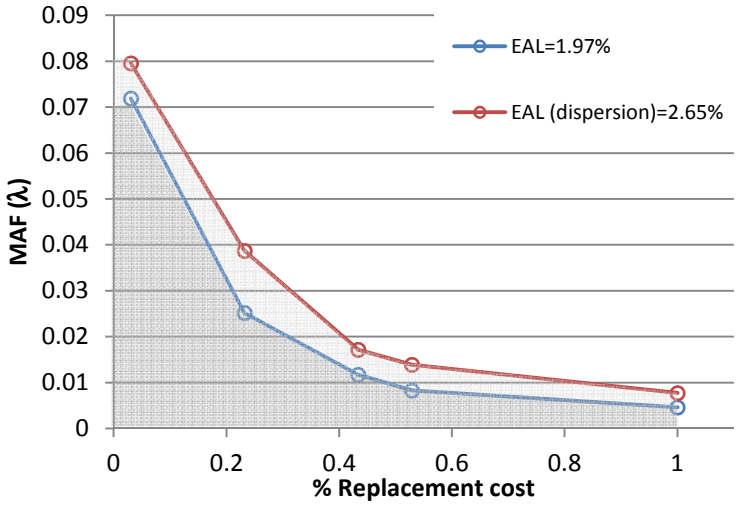

Figure 84: Total loss curve, and results in terms of EAL, for the As-Built structure.

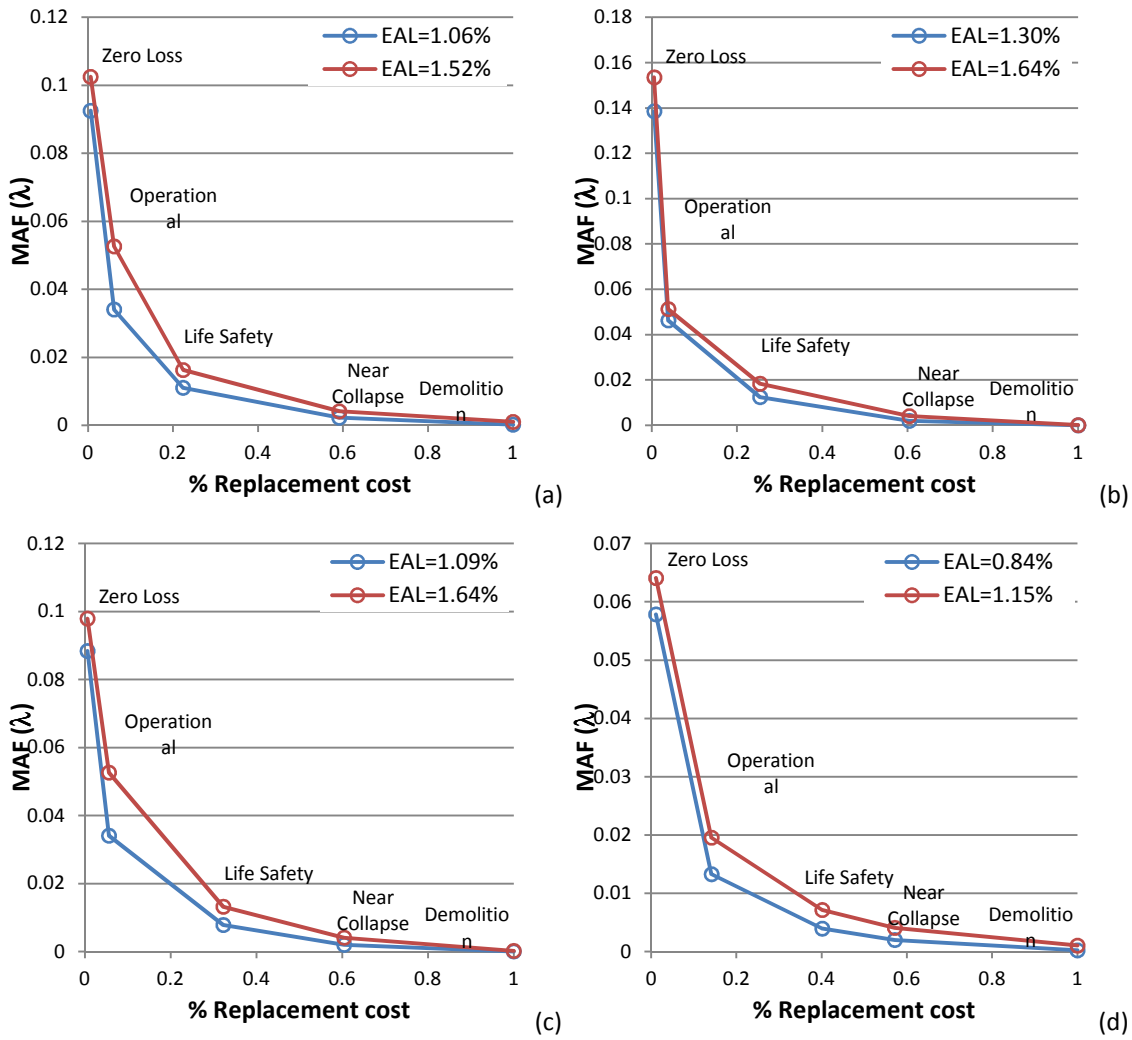

Figure 85: Total loss curve and EAL for the retrofit strategies considered: (a) ductility increase, (b) stiffness decrease, (c) strength increase and (d) a combined modification of stiffness and strength.

Assessment of retrofitted frames: FRP intervention and Selective Weakening

The simplified loss assessment methodology has been applied to two of the retrofit alternatives already introduced in the previous chapters. In particular, at first the DBD principles were adopted to design two retrofit interventions on the existing structure, then the Expected Annual Losses could be computed and compared with the values obtained by the probabilistic Loss Assessment carried out using PACT.

An intervention with FRP involving only the exterior joints was first designed. By increasing the moment capacities of the exterior joints, the development of a beam-sway failure mechanism could be ensured, enabling the structure to achieve 80% of NBS (it has already been shown that 100%NBS can not be obtained by intervention on the exterior joints alone, but retrofit on the interior node panels would also be required in order to achieve this performance). Similarly, the second retrofit scheme was designed to allow for the same failure mechanism to develop, but in this latter case the flexural capacities of the beams pertaining to the exterior joints were decreased simulating Selective Weakening. In this second case the design was performed to enable the structure to reach 100% of NBS.

In order to compute the Expected Annual Loss, the collapse capacity of both structures must be assessed. The median value of the collapse fragilities was assumed to be the lesser between:

- the Spectral acceleration inducing at the critical storey an unacceptable level of residual inter-storey drift (1.5%);
- the Spectral acceleration inducing a peak IDR value at the critical storey that is expected to lead to instability due to second order effects (P-Δ instability);
- twice the value of Spectral acceleration inducing on the structure the development of the Life safety limit state. This last condition was judgementally adapted from a method for estimating the median collapse capacity proposed in the ATC-58. According to this guideline, the median collapse capacity can be approximated as three times the intensity corresponding to the maximum allowable drift limit outlined by ASCE-7, where this drift threshold corresponds to 2.0% of the storey height, assuming an importance class I. This recommendation refers to building designed according to modern building codes. However, in case of buildings designed only to resist to gravity loadings, the residual capacity beyond the

"allowable drift" limit state is unknown while the retrofit only addresses the shaking intensity required to reach the Life safety limit state. For this reason, a factor of two between the Spectral acceleration at collapse and at Life safety has been precautionarily assumed.

Figure 86 shows the idealized bi-linear pushover curve of the structure retrofitted with FRP, while Figure 88 shows the same curve for the Selective Weakening intervention. Figure 87 and Figure 89 show the corresponding Total Loss Curves and values of EAL.

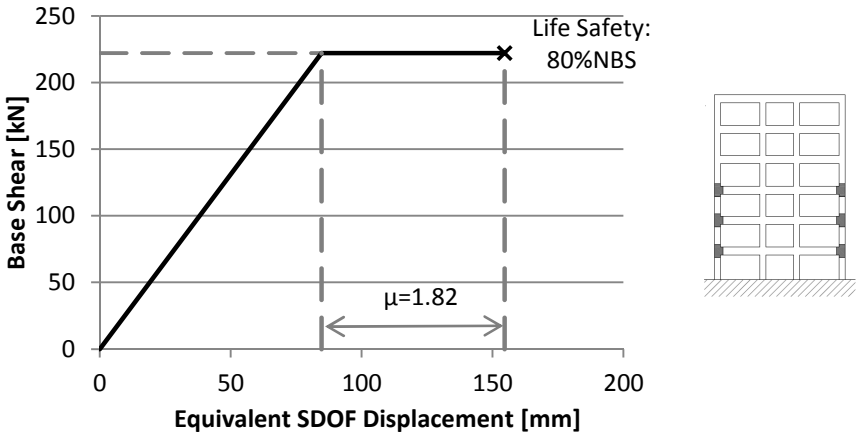

Figure 86: FRP intervention on the exterior joints.

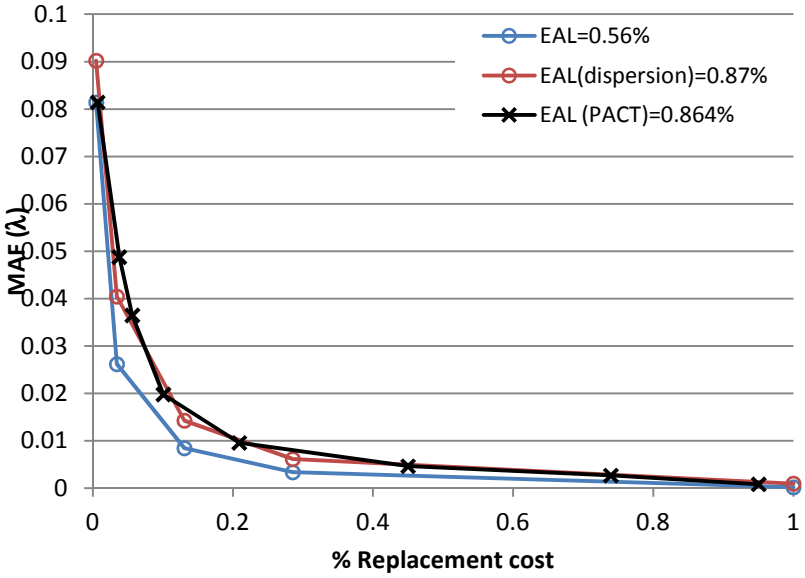

Figure 87: Total loss curve: FRP intervention on the exterior joints.

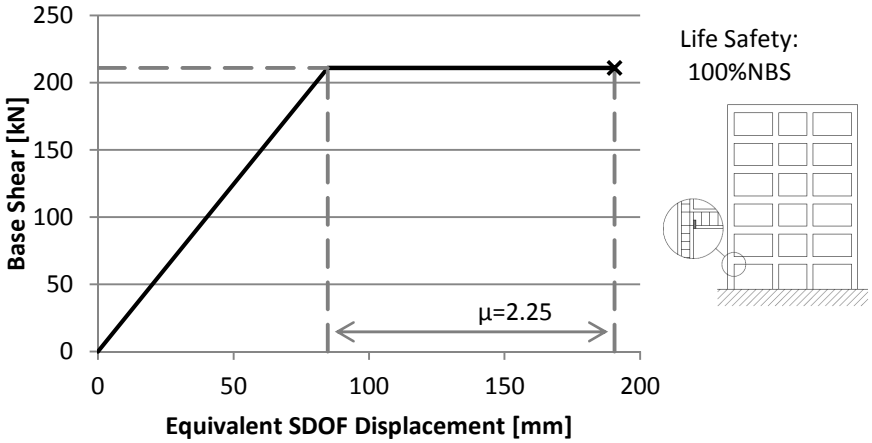

Figure 88: Selective Weakening intervention on the exterior joints.

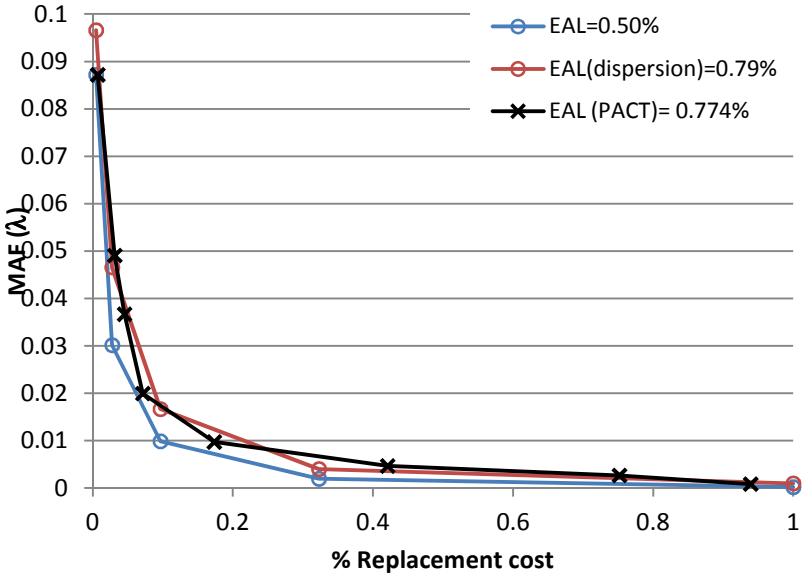

Figure 89: Total loss curve: Selective Weakening intervention on the exterior joints.

Interestingly, a good agreement can be observed from these graphs, particularly between the values of Expected Annual Loss obtained with the simplified method accounting for uncertainties and the same values obtained from the probabilistic procedure. This correspondence is much more apparent in the case of retrofitted structures in comparison with the "As-Built" one. It is believed that this difference is due to the effect of collapse on the total loss. In fact, in both cases (as-built and retrofit) the collapse fragility was judgement-based, however in the latter case, thanks to the effect of retrofit, collapse appears to have a smaller influence on loss (refer to Figure 90 for the Selective Weakening option) and thus the bias introduced with the fragility is reduced.

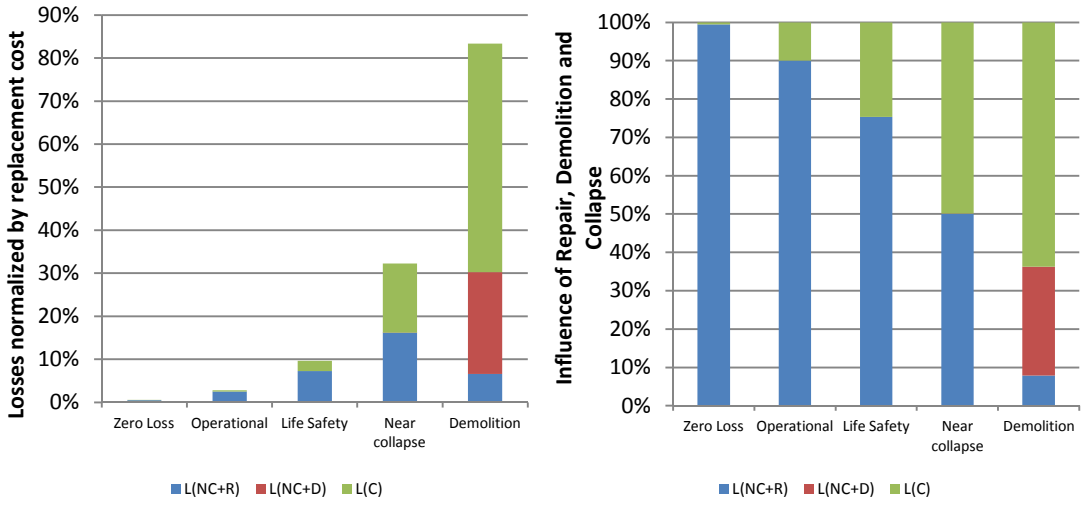

(a) (b)

Figure 90: (a) Losses normalized by the replacement cost; (b) Percentage of influence on the expected total losses at each performance level of repair costs, demolition and collapse losses - Frame retrofitted through Selective Weakening.

Effect of the methodology adopted to define the Collapse Fragility on the predicted EAL

As already anticipated, there are several approaches that could be adopted to define a collapse fragility. In particular, a judgment-based fragility based on a pushover performed "by-hand" was deemed suitable for the assessment being performed, due to the simplified nature of the methodology proposed. However, more refined methods could also be employed. In particular, using the results from the previous chapters, a comparison can be performed between the expected annual losses obtained introducing in the methodology fragilities obtained through different analysis methods.

Based on the results of Chapter 5, the collapse fragility could be defined from the pushover analysis performed on a structural model and computed by Ruaumoko. During the analysis, global and local parameters were monitored, and the simulation was stopped whenever the level of demand in one of the elements exceeded its capacity. Similarly to what was done for the previous simplified pushover curve, the structural response could then be represented in ADRS format, by means of a SDOF substitute structure transformation (refer to Figure 91). Then, the seismic action, reduced by an appropriate coefficient accounting for the effective damping of the structure reaching collapse, have been scaled to match the ultimate point of the capacity curve. This reduced spectrum represents the seismic action required to achieve/exceed the assessed limit state, which is in this case collapse. Once the action has

been identified, the spectrum was transformed back to the 5% conventional value of damping and the spectral acceleration at the fundamental period could be computed and adopted as the median value of the collapse fragility.

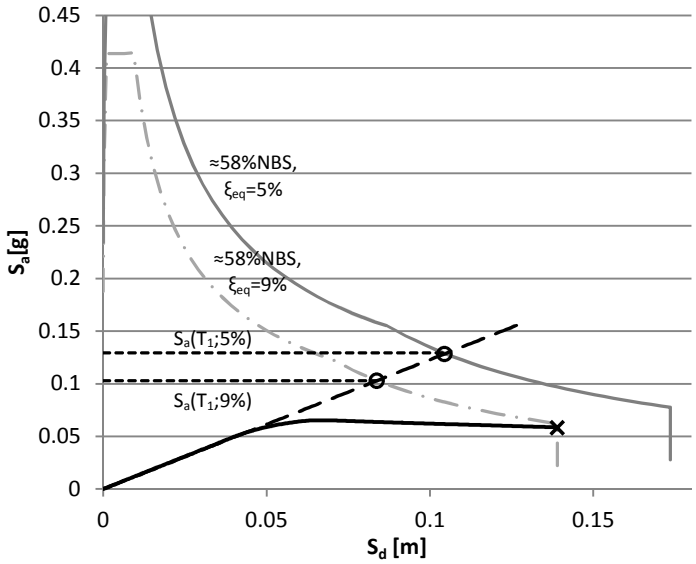

Figure 91: Identification of the seismic intensity leading to collapse.

The Pushover curves obtained "by hand" or through finite element modelling exhibit very similar trends, however the former analysis returns ultimate values of displacement around 90mm, which is much lower than the values obtained using Ruaumoko. This discrepancy effects the %NBS achieved at collapse (around 45% in the former case versus 58% in the latter). As a consequence, the spectral accelerations at the fundamental period are quite different, in fact the first calculation returned a median intensity measure of 0.117g while the second predicted a value of 0.129g. In both cases the dispersion must be selected using engineering judgement.

The IDA performed in Chapter 6 returned both median and logarithmic standard deviation describing collapse. It is worth noticing that the computed median value, 0.153g, is greater than the one obtained with the Pushover analysis using Ruaumoko.

The values of EAL obtained introducing in the simplified procedure these more accurate estimates of the collapse fragility are in line with those obtained using PACT, suggesting that the definition of collapse is the most delicate aspect of the proposed procedure.

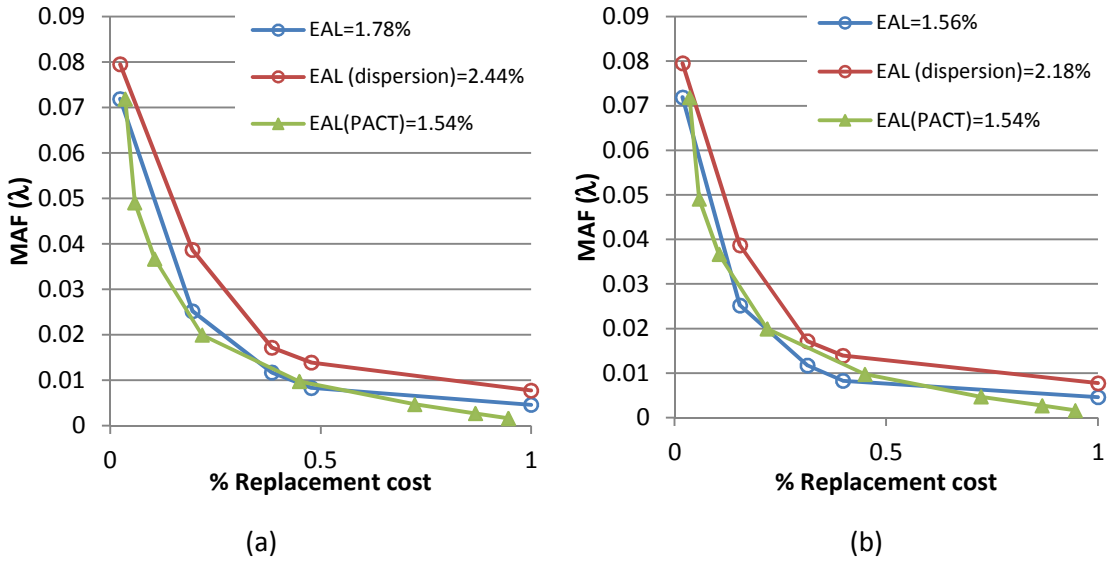

Figure 92: Comparison of loss curve obtained with PACT and the simplified method coupled with the collapse fragility evaluated through Pushover analysis on a non-linear model (a) or through Incremental Dynamic Analyses (b).

Limitations of the methodology

The proposed simplified displacement-based performance assessment methodology has numerous limitations that should be kept in mind. In particular:

- At this stage, only direct economic losses due to repair or replacement of the building are incorporated.
- The structural response is considered to be two-dimensional, decoupling the building response in the two predominant directions. Torsional response is not considered, therefore the methodology should not be employed for buildings with large strength or stiffness eccentricities without modifications. The application of the methodology to buildings with horizontal or vertical irregularities should be avoided.
- Both displacement-based assessment and displacement-based design are based on displaced shapes at the fundamental mode of vibration, therefore the proposed methodology will not capture building response due to higher mode effects. The methodology would not be considered applicable for buildings where a large degree of participation is expected from higher modes.
- Soil structure interaction and foundation failure mechanisms are not considered.

- Damage correlation between elements and between the two orthogonal directions of the buildings is not accounted for in this methodology.
- EDP-DV functions have currently been derived only for office buildings, hence the functions should be adapted before being employed for different occupancy types.
- Lastly, the definition of collapse should be addressed with great care, as it has been shown to have a strong influence on the performance evaluation, particularly in the case of existing buildings.

9. Conclusions

The common (mis)conception that the Percentage of New Building Standard (%NBS) to be achieved by a structure would be linearly correlated with both risk and cost of intervention often discourages building owners in undertaking seismic interventions beyond the minimum level required by the law. However, an increase of the targeted structural performance can result in a more than proportional reduction of risk, while the costs of the intervention required to reach this enhanced performance depends on the retrofit scheme adopted.

In this thesis, a framework to evaluate in a consistent manner the effects in terms of long-term costs, benefits and probabilities of collapse of alternative retrofit options have been developed, and the relationship between different metrics adopted to assess the seismic performance of existing buildings have been investigated.

For a case-study structure reflecting the typical deficiencies of a pre-1970 concrete frame building, four retrofit strategies have been considered. These possible interventions were identified according to the likely failure mechanism of the original structure, predicted through the hierarchy of strength assessment undertaken for each beam-column joint sub-assembly.

For each strategy, different %NBS were targeted, and the probabilities of reaching collapse as well as the annualized direct and indirect losses to be expected as a consequence of earthquake shaking have been estimated. Hence, valuable indications on the effectiveness of each retrofit option could be obtained for the structure selected as case study.

Moreover, some critical aspects related to the deterministic approach employed to evaluate the %NBS were disclosed. In fact, it was observed that in some cases the pushover analyses failed to predict the most probable failure mode and gave different performance ratings at two structures behaving substantially in the same way (as could be observed comparing the collapse fragilities), while possibly inducing excessive confidence on the reliability of the results when obtained through finite-element numerical models. On the other hand, the collapse fragilities were found to be valid indicators of the structural behaviour to be expected.

However, they are computationally onerous and getting a feel of the actual meaning of the probability of collapse can be quite a challenge.

Lastly, expected direct and indirect losses (monetary losses that an owner could have to face during a given time frame as a consequence of seismic activity, downtime but also the rate of people injured or killed by vulnerable elements within a building or due to its partial or total collapse) can provide some further, more tangible and understandable information on the expected performance that could be communicated to the client and non-technical audience. Yet, the probabilistic methodology adopted for its evaluation within this study is, again, computationally expensive and would hardly be used in common practice.

Furthermore, as the proposed framework aims at incorporating these performance metrics directly in the retrofit design process, the loss and risk assessment should be undertaken during the preliminary phases of the design in a recursive way in order to allow for the evaluation of earthquake-induced consequences for a variety of retrofit schemes and design choices. In this fashion, the designer could be enabled to identify the type of intervention that better suits his client priorities and needs.

For this reason, under cautelative assumptions, judgement-based fragility functions and simplified loss assessment approaches are currently being developed. In particular, the methodology adopted within this study relies on the principles of Direct Displacement Based Assessment, which makes it computationally efficient and suitable for multiple repetitions. The main drawback of this method, as expected, lies in the definition of the collapse fragility of the structure. In fact, economic losses were found particularly sensitive on the choice of the parameters describing this function, mainly because non-conforming structures are characterized by a relatively high chance of incurring in collapse at almost all the intensity levels describing the regional hazard. However, the discrepancy between losses evaluated using the simplified and probabilistic approach becomes less relevant when the performance of a retrofitted structure is assessed, reflecting in this case the lower incidence of collapse probability. This latter observation suggests that, particularly for comparative purposes, the information provided by the simplified method could be accurate enough to guide the choice of the intervention in the conceptual design phase, as long as only direct losses are of concern to the stakeholders.

Hence, by reducing the numerical burden associated with time history analyses, and aware of the limitations inevitably present in simplified procedures, collapse probabilities and expected direct losses could become widely applicable measures of structural performance to be accounted for in the design of retrofit interventions or even adopted to motivate building owners to undertake seismic retrofit interventions, providing evidences of the long-term benefits that could derive from an initial investment.

As already mentioned, in order to increase the reliability of the results of the simplified procedure, future advances should include improvements in the definition of the collapse fragility functions, especially in those cases where more than one failure mechanism could be expected to develop. Moreover, EDP-DV functions, relating structural response with the decision variable - usually the economic loss, should be defined for different occupancy types, as until now they have only been developed considering office buildings. Finally further research efforts could be devoted to the extension of the simplified approach to other performance metrics, such as downtime.

On top of this, as the current study has been limited to a single reinforced concrete frame building, further research will be required to investigate the influence of different geometries, design choices and material properties on the predicted values of loss. In particular, this development could possibly lead to the definition of charts relating the performance metrics of interest to the main characteristics of classes of buildings, assisting the designers in rapidly assessing the expected losses for a given building typology and also allowing to perform the assessment at a wider regional scale.

References

Abrahamson, N.A. and Silva, W.J. (2008). Summary of the Abrahamson & Silva NGA Ground-Motion Relations. *Earthquake Spectra*. **24**:**1**, 67-97.

ACI318-08 (2008). Building code requirements for structural concrete and commentary. Farmington Hills, MI, American Concrete Inst. (ACI).

ACI318-71 (1971). Building code requirements for reinforced concrete. Detroit, MI, American Concrete Inst. (ACI).

Akguzel, U. (2011). Seismic Performance of FRP Retrofitted Exterior RC Beam-Column Joints under Varying Axial and Bidirectional Loading, Department of Civil and Natural Resources Engineering, University of Canterbury.

Aki, K. and Richards, P.G. (1980). Quantitative Seismology: Theory and Methods. Vol. 1., W. H. Freeman and Co.

Alath, S. and Kunnath, S.K. (1995). Modeling inelastic shear deformation in RC beam-column joints. *Engineering Mechanics (1995)*. 822-825.

Andrino, T. and Park, R. (1986). Seismic design considerations of the properties of New Zealand manufactured steel reinforcing bars. *ulletin of the New Zealand Society of Earthquake Engineering Structures*. **19**:**3**, 213–246.

ASCE-SEI-41 (2007). Seismic Rehabilitation of existing buildings. *ASCE standard. American Society of Civil Engineering (ASCE)*.

ASCE (2006). ASCE-7: Minimum design loads for buildings and other structures, American Society of Civil Engineers, Reston, Virginia.

ATC (1985). ATC-13: Earthquake damage evaluation data for California, Report No. Report ATC-13, Applied Technology Council.

ATC (1996). ATC-40: Seismic evaluation and retrofit of concrete buildings, Report No.

ATC (2012). ATC-58: Seismic Performance Assessment of Buildings, Volume 1 and 2. *Applied Technology Council, Redwood City*.

Baker, J.W. (2014). Efficient analytical fragility function fitting using dynamic structural analysis. *Earthquake Spectra*.

Baker, J.W. and Cornell, C.A. (2005). A vector-valued ground motion intensity measure consisting of spectral acceleration and epsilon. *Earthquake Engineering & Structural Dynamics*. **34**:**10**, 1193 - 1217.

Baker, J.W. and Cornell, C.A. (2006). Spectral shape, epsilon and record selection. *Earthquake Engineering & Structural Dynamics*. **35**:**9**, 1077-1095.

Baker, J.W., Lin, T., Shahi, S.K. and Jayaram, N. (2011). New Ground Motion Selection Procedures and Selected Motions for the PEER Transportation Research Program, Report No. PEER 2011/03, Pacific Earthquake Engineering Research Center.

Bazant, Z.P., Pan, J. and Pijaudier-Cabot, G. (1987). Softening in reinforced concrete beams and frames. *ASCE Journal of Structural Engineering*. **113**:**12**, 2333-2347.

Bazzurro, P., Cornell, C.A., Shome, N. and Carballo, J.E. (1998). Three proposals for characterizing MDOF nonlinear seismic response. *Journal of Structural Engineering*. **124**:**11**, 1281-1289.

Beetham, T. (2013). Simplified Displacement Based Performance Assessment of Retrofit Alternatives for Decision Making. *Master Thesis, University of Pavia*.

Beres, A., White, R. and Gergely, P. (1992). Seismic behaviour of reinforced concrete frame structures with nonductile details: Part I - Summary of experimental findings of full scale beam-column joint tests., Report No. National Center for Earthquake Eng. Research.

Boore, D.M. and Atkinson, G.M. (2007). Boore-Atkinson NGA Ground Motion Relations for the Geometric Mean Horizontal Component of Peak and Spectral Ground Motion Parameters, Report No.

Bozorgnia, Y., Hachem, M.M. and Campbell, K.W. (2010). Ground Motion Prediction Equation ("Attenuation Relationship'') for Inelastic Response Spectra. *Earthquake Spectra*. **26**:**1**, 1-23.

Bradley, B.A. (2010). A generalized conditional intensity measure approach and holistic ground-motion selection. *Earthquake Engineering & Structural Dynamics*. **39**:**12**, 1321-1342.

Brunsdon, D.R. and Priestley, M.J.N. (1984). Seismic performance characteristics of buildings constructed between 1936 and 1975, Report No. Dept. of Civil Eng., University of Canterbury, Christchurch, NZ.

Building Act (2004). Department of Building and Housing–Te Tari Kaupapa Whare, Ministry of Economic Development, New Zealand Government, Wellington, New Zealand. **24**:

Buratti, N. (2009). Assessment of seismic safety: response surface approach and accelerogram selection issues, DISTART - Structural engineering, University of Bologna.

Buratti, N., Stafford, P.J. and Bommer, J.J. (2011). Earthquake Accelerogram Selection and Scaling Procedures for Estimating the Distribution of Drift Response. *Journal of Structural Engineering*. **137**:**3**, 345-357.

Calvi, G., Pinho, R., Magenes, G., Bommer, J., Restrepo-Vélez, L. and Crowley, H. (2006). Development of seismic vulnerability assessment methodologies over the past 30 years. *ISET journal of Earthquake Technology*. **43**:**3**, 75-104.

Calvi, G.M. (1999). A displacement-based approach for vulnerability evaluation of classes of buildings. *Journal of Earthquake Engineering*. **3**:**3**, 411-438.

Calvi, G.M., Magenes, G. and Pampanin, S. (2002). Relevance of beam-column joint damage and collapse in RC frame assessment. *Journal of Earthquake Engineering*. **06**:**spec01**, 75-100.

Campbell, K.W. and Bozorgnia, Y. (2007). Campbell-Bozorgnia NGA Ground Motion Relations for the Geometric Mean Horizontal Component of Peak and Spectral Ground Motion Parameters, Report No.

Carr, A. (2007). RUAUMOKO2D - The Maori God of Volcanoes and Earthquakes. *University of Canterbury*. Christchurch, New Zealand:

Chiou, S.J. and Youngs, R.R. (2008). An NGA Model for the Average Horizontal Component of Peak Ground Motion and Response Spectra. *Earthquake Spectra*. **24**:**1**, 173-216.

Christopoulos, C. and Pampanin, S. (2004). Towards performance-based design of MDOF structures with explicit consideration of residual deformations. *ISET Journal of Earthquake Technology*. **41(1)**:**1**, 53-73.

Coburm, A., Spence, R. and Pomonis, A. (1992). Factors determining human casualty levels in earthquakes: mortality prediction in building collapse. *Proceedings of the tenth world conference on earthquake engineering*. **10**:5989-5994.

Comerio, M.C. (2000). The economic benefits of a disaster resistant university: Earthquake loss estimation for UC Berkeley. *Institute of Urban & Regional Development*.

Comerio, M.C. (2006). Estimating downtime in loss modeling. *Earthquake Spectra*. **22**:**2**, 349-365.

Comerio, M.C. and Blecher, H.E. (2010). Estimating downtime from data on residential buildings after the Northridge and Loma Prieta Earthquakes. *Earthquake Spectra*. **26**:**4**, 951-965.

Cornell, C.A. (2005). On earthquake record selection for nonlinear dynamic analysis.

Cornell, C.A., Jalayer, F., Hamburger, R.O. and Foutch, D.A. (2002). Probabilistic basis for 2000 SAC federal emergency management agency steel moment frame guidelines. *Journal of Structural Engineering*. **128**:**4**, 526 - 533.

Crowley, H. and Pinho, R. (2004). Period-height relationship for existing European reinforced concrete buildings. *Journal of Earthquake Engineering*. **8**:**spec01**, 93-119.

El-Metwally, S. and Chen, W. (1988). Moment-rotation modeling of reinforced concrete beam-column connections. *ACI Structural Journal*. **85**:**4**,

Fajfar, P. and Dolšek, M. (2010). A practice-oriented approach for probabilistic seismic assessment of building structures. In *Advances in Performance-Based Earthquake Engineering*. Edited by Springer**:** 225-233.

Federal Emergency Management Agency (1997). FEMA 273: NEHRP Guidelines for the Seismic Rehabilitation of Buildings.

Federal Emergency Management Agency (1997). FEMA 274: NEHRP Commentary on the Guidelines for the Seismic Rehabilitation of Buildings.

Federal Emergency Management Agency (2000). FEMA-356: Prestandard and commentary for the seismic rehabilitation of buildings.

Federal Emergency Management Agency (2000). FEMA 350: Recommended seismic design criteria for new steel moment frame buildings.

Ferracuti, B., Pinho, R., Savoia, M. and Francia, R. (2009). Verification of displacement-based adaptive pushover through multi-ground motion incremental dynamic analyses. *Engineering Structures*. **31**:**8**, 1789-1799.

Ford, C.R. (1926). Earthquakes and building constructions, Whitcombe and Tombs Ltd, Auckland, NZ.

Giberson, M.F. (1967). The response of non linear multi-story structures subjected to earthquake excitation, California Institute of Technology, Pasadena, California.

Hakuto, S., Park, R. and Tanaka, H. (2000). Seismic load tests on interior and exterior beam-column joints with substandard reinforcing details. *ACI Structural Journal*. **97**:**1**, 11-25.

Hancock, J. (2006). The influence of duration and the selection and scaling of accelerograms in engineering design and assessment, Department of Civil and Environmental Engineering, Imperial College, University of London.

Hartzell, S.H. (1978). Earthquakes aftershocks as Green's Functions. *Geophysical Research Letters*. **5**:1-4.

Haselton, C.B. (2009). Evaluation of Ground Motion Selection and Modification Methods: Predicting Median Interstory Drift Response of Buildings, Report No. 2009/01, Pacific Earthquake Engineering Research Center.

Haselton, C.B., Liel, A.B., Taylor Lange, S. and Deierlein, G.G. (2008). Beam-Column Element Model Calibrated for Predictin Flexural Respose Leading to Global Collapse of RC Frame Buildings, Report No. Pacific Earthquake Engineering Research Center (PEER).

Idriss, I.M. (2008). An NGA Empirical Model for Estimating the Horizontal Spectral Values Generated By Shallow Crustal Earthquakes. *Earthquake Spectra*. **24**:**1**, 217-242.

Iervolino, I., Galasso, C. and Cosenza, E. (2010). REXEL: computer aided record selection for code-based seismic structural analysis. *Bulletin of Earthquake Engineering*. **8**:**2**, 339-362.

Irikura, K. (1983). Semi-empirical estimation of strong ground motions during large earthquakes. *Bullletin of the Disaster Prevention Research Institute (Kyoto University)*. **33**:63-104.

Jalayer, F. (2003). Direct probabilistic seismic analysis: implementing non-linear dynamic assessments, Department of Civil and Environmental Engineering, Stanford University.

Kam, W. and Pampanin, S. (2009). Experimental and numerical validation of selective weakening retrofit for existing non-ductile RC frames. *Proc. of ATC-SEI Conf on Improving the Seismic Performance of Existing Buildings and Other Structures*.

Kam, W.Y. (2010). Selective weakening and post-tensioning for the seismic retrofit of non-ductile RC frames, Department of Civil and Natural Resources Engineering, UNIVERSITY OF CANTERBURY.

Kam, W.Y., Pampanin, S., Palermo, A. and Carr, A.J. (2010). Self-centering structural systems with combination of hysteretic and viscous energy dissipations. *Earthquake Engineering & Structural Dynamics*. **39**:**10**, 1083–1108.

Katsanos, E.I., Sextos, A.G. and Manolis, G.D. (2010). Selection of earthquake ground motion records: A state-of-the-art review from a structural engineering perspective. *Soil Dynamics and Earthquake Engineering*. **30**:**4**, 157-169.

Lee, C.-L. and Filippou, F.C. (2009). Efficient beam-column element with variable inelastic end zones. *Journal of Structural Engineering*. **135**:**11**, 1310-1319.

Liel, A.B. and Deierlein, G.G. (2008). Assessing the collapse risk of California's existing reinforced concrete frame structures: Metrics for seismic safety decisions, Stanford University.

Liu, A. and Park, R. (2001). Seismic Behaviour and retrofit of pre-1970s as-built exterior beamcolumn joints reinforced by plain round bars. *Bull of New Zealand Soc of Earthquake Eng.* **34**:**1**, 68-81.

Lowes, L.N., Mitra, N. and Altoontash, A. (2003). A beam-column joint model for simulating the earthquake response of reinforced concrete frames, Pacific Earthquake Engineering Research Center, College of Engineering, University of California.

Megget, L.M. (2006). From brittle to ductile: 75 years of seismic design in New Zealand. *Proceedings of the Conference of the New Zealand society of earthquake engineering, NZSEE. New Zealand*.

Meletti, C. and Montaldo, V. (2007). Stime di pericolosità sismica per diverse probabilità di superamento in 50 anni: valori di a_g, Report No. Progetto DPC-INGV S1,

Mitrani-Reiser, J. (2007). An ounce of prevention: probabilistic loss estimation for performance-based earthquake engineering, California Institute of Technology.

Montejo, L.A. and Kowalsky, M.J. (2007). CUMBIA—Set of codes for the analysis of reinforced concrete members. *CFL Technical Rep. No. IS-07*.

Naeim, F. and Lew, M. (1995). On the Use of Design Spectrum Compatible Time Histories. *Earthquake Spectra*. **11**:**1**, 111-127.

New Zealand Society for Earthquake Engineering (2006). Assessment and Improvement of the Structural Performance of Buildings in Earthquakes. *Recommendations of a NZSEE Study Group on Earthquake Risk Buildings*.

NOAA (1972). A study of Earthquake losses in the San Francisco area: Data and Analysis, Report No. Department of Commerce.

NZS95:1935 (1935). New Zealand Standard model buildings by-laws. Wellington, NZ., New Zealand Standards Inst.

NZS95:1939 (1939). New Zealand Standard code of buildings by-laws. Wellington, NZ, New Zealand Standards Inst.

NZS95:1955 (1995). New Zealand Standard - Model Building By-Laws: Part IV and V. Wellington, NZ, New Zealand Standard Inst.

NZS1170.5 (2004). Structural Design Actions Part 5: Earthquake Actions. *New Zealand*.

NZS1900-64 (1964). NZS1900 - Model building bylaw. Wellington, NZ, New Zealand Standards Inst.

NZS3101:2006 (2006). Concrete structures standard. Wellington, NZ, Standards Association of New Zealand.

NZS4203:1976 (1976). Code of practice for general structural design and design loading for buildings. Wellington, NZ, Standards Assoc. of New Zealand.

Pampanin, S. (2006). Controversial aspects in seismic assessment and retrofit of structures in modern times: understanding and implementing lessons from ancient heritage. *Bulletin of the New Zealand Society of Earthquake Engineering*. **39**:**2**, 120-133.

Pampanin, S., Calvi, G.M. and Moratti, M. (2002). Seismic behavior of RC beam-column joints designed for gravity only. *12th European Conference on Earthquake Engineering.*

Pampanin, S., Christopoulos, C. and Priestley, M.J.N. (2002). Residual Deformations in Performance-Based Seismic Assessment of Frame Structures. *IUSS Press, Pavia, Italy*.

Pampanin, S., Magenes, G. and Carr, A. (2003). Modelling of shear hinge mechanism in poorly detailed RC beam-column joints. *Fib 2003 Symposium "Concrete Structures in Seismic Regions".*

Paulay, T. and Priestley, M.J.N. (1992). Seismic design of reinforced concrete and masonry buildings, John Wilet and Sons.

PEER/ATC-72-1 (2012). Modeling and Acceptance Criteria for Seismic Design and Analysis of Tall Buildings, Report No.

Pessiki, S., Conley, C., Gergely, P. and White, R. (1990). Seismic behaviour of lightly reinforced concrete column and beam-column joint details., Report No. National Center for Earthquake Eng. Research.

Porter, K.A. (2003). An Overview of PEER's Performance-Based Earthquake Engineering Methodology. *9th International Conference on Applications of Statistics and Probability in Civil Engineering.*

Porter, K.A., Beck, J.L. and Shaikhutdinov, R.V. (2004). Simplified Estimation of Economic Seismic Risk for Buildings. *Earthquake Spectra*. **20**:**4**, 1239-1263.

Power, M., Chiou, B., Abrahamson, N.A. and Roblee, C. (2006). The 'Next Generation of Ground Motion Attenuation Models' (NGA) project: an overview. *Proceedings of the 8th U.S. National Conference on Earthquake Engineering.* Paper No. 2022.

Press, W.H., Teukolsky, S.A., Vetterling, W.T. and P., F.B. (2002). Numerical recipes in C++: the art of scientific computing, Cambridge University Press.

Priestley, M.J.N. (1997). Displacement-based seismic assessment of reinforced concrete buildings. *Journal of Earthquake Engineering*. **1**:**1**, 157-192.

Priestley, M.J.N. and Calvi, G.M. (1991). Towards a Capacity-Design Assessment Procedure for Reinforced Concrete Frames. *Earthquake Spectra*. **7**:**3**, 413-437.

Priestley, M.J.N., Calvi, G.M. and Kowalsky, M.J. (2007). Displacement-based seismic design of structures, IUSS Press.

Priestley, M.J.N., Seible, F. and Calvi, G.M. (1996). Seismic Design and Retrofit of Bridges, John Wiley & Sons.

Ramirez, C.M. and Miranda, E. (2009). Building-specific loss estimation methods & tools for simplified performance-based earthquake engineering, Stanford University.

Ramirez, C.M. and Miranda, E. (2012). Significance of residual drifts in building earthquake loss estimation. *Earthquake Engineering & Structural Dynamics*. **41**:**11**, 1477-1493.

Rodriguez, M., Restrepo, J. and Carr, A. (2002). Earthquake-induced floor horizontal accelerations in buildings. *Earthquake Engineering & Structural Dynamics*. **31**:**3**, 693-718.

Ruiz-Garcia, J. and Miranda, E. (2004). Perfomance-based assessment of existing structures accounting for residual displacements, Stanford University Stanford, CA.

SEAOC (1995). Vision 2000 Report: Performance Based Seismic Engineering of Buildings.

Sewell, R.T., Toro, G.R. and McGuire, R.K. (1996). Impact of ground motion characterization on conservatism and variability in seismic risk estimates, Report No. Nuclear Regulatory Commission, Washington, DC (United States). Div. of Engineering Technology.

Sezen, H. and Moehle, J.P. (2004). Shear strength model for lightly reinforced concrete columns. *Journal of Structural Engineering*. **130**:**11**, 1692–1703.

Shome, N., Cornell, C.A., Bazzurro, P. and Carballo, J.E. (1998). Earthquakes, records, and nonlinear responses. *Earthquake Spectra*. **14**:**3**, 469 - 500.

Solberg, K.M., Dhakal, R.P., Mander, J.B. and Bradley, B.A. (2008). Computational and rapid expected annual loss estimation methodologies for structures. *Earthquake Engineering & Structural Dynamics*. **37**:**1**, 81-101.

Spence, R., Coburn, A., Pomonis, A. and Sakai, S. (1992). Correlation of ground motion with building damage: the definition of a new damage-based seismic intensity scale. *Proceedings of the Tenth World Conference on Earthquake Engineering, Madrid, Spain*. **1**:551-556.

Stirling, M., McVerry, G., Gerstenberger, M., Litchfield, N., Van Dissen, R., Berryman, K., Barnes, P., Wallace, L., Villamor, P. and Langridge, R. (2012). National seismic hazard model for New Zealand: 2010 update. *Bulletin of the Seismological Society of America*. **102**:**4**, 1514-1542.

Stoica, M., Medina, R.A. and McCuen, R.H. (2007). Improved probabilistic quantification of drift demands for seismic evaluation. *Structural Safety*. **29**:**2**, 132-145.

Sullivan, T. and Calvi, G.M. (2011). Considerations for the seismic assessment of buildings using the direct displacement-based assessment approach. *Proceedings of the 2011 ANIDIS conference, Bari, Italy*.

Sullivan, T.J., Priestley, M. and Calvi, G.M. (2012). A Model Code for the Displacement-based Seismic Design of Structures: DBD12, IUSS Press.

Taucer, F., Spacone, E. and Filippou, F.C. (1991). A fiber beam-column element for seismic response analysis of reinforced concrete structures, Earthquake Engineering Research Center, College of Engineering, University of California.

Vamvatsikos, D. and Cornell, C.A. (2002). Incremental dynamic analysis. *Earthquake Engineering & Structural Dynamics*. **31**:**3**, 491-514.

Watson-Lamprey, J.A. and Abrahamson, N.A. (2006). Selection of time series for analyses of response of buildings. *1st European Conference on Earthquake Engineering and Seismology (ECEES).*

Welch, D., Sullivan, T. and Calvi, G. (2014). Developing direct displacement-based procedures for simplified loss assessment in performance-based earthquake engineering. *Journal of Earthquake Engineering*. **18**:**2**, 290-322.

Welch, D.P., Sullivan, T.J. and Calvi, G.M. (2012). Developing Direct Displacement-based Design and Assessment Procedures for Performance-based Earthquake Engineering. *IUSS Press.*

Appendix A: Analysis of code-based ground-motion selection procedures in terms of inelastic interstorey drift demands

Introduction

Among the currently employed methods for the analysis and the design of structures potentially subjected to seismic actions, nonlinear dynamic analysis is the most accurate in describing the structural behaviour. Nonlinear time-history analyses allow to predict the response of every element of the structure, studying how they interact during the formation and propagation of damage. In this framework, the structural response for a given earthquake scenario is estimated by loading the structure with acceleration time-histories that are compatible with the scenario in question. So far, however, there are many open issues on selection procedures to obtain such sets of accelerograms.

Numerous approaches have been proposed for selecting recorded accelerograms in order to obtain robust estimates of the structural response. They can be divided in two main categories, depending on the target of the analysis to be performed (Cornell 2005; Baker and Cornell 2006; Hancock 2006; Watson-Lamprey and Abrahamson 2006; Bradley 2010; Iervolino, Galasso et al. 2010; Katsanos, Sextos et al. 2010; Baker, Lin et al. 2011; Buratti, Stafford et al. 2011): *i*) an analysis aimed at evaluating a central estimate, such as the mean or median, of the structural response (that may then be used for design purposes); ii) an analysis aimed at estimating the full distribution of the structural response. The latter type of analysis could be required in earthquake loss assessment procedures in which one must not only consider the potential damage associated with the expected response, but also the damage due to the full range of possible responses that may be experienced under a particular scenario. On the other hand, the first type of analysis is widely used by design codes. Seismic codes prescribe the use of suites of ground motions that are representative of the seismicity at the site under consideration and whose average pseudo-acceleration response spectrum is compatible with a given Uniform Hazard response Spectrum (UHS) in an appropriate range of periods. The so obtained suites of ground motions are used to estimate the structural response, typically the

interstorey drift, which is calculated considering the average of the results of the analyses performed using each ground motion. While this calculation of the response is correct for linear structures, it may lead to wrong estimates when dealing with non-linear systems. Furthermore in this latter case the results may become sensitive to some selection parameters like magnitude, source-to-site distance, epsilon, scaling, etc. Following this approach, many studies have been conducted investigating the influence of different selection criteria on the structural response (e.g. Haselton, 2009) but they are often limited in terms of number of structures considered and in terms of ground-motions used.

In this study, different selection procedures have been tested on various SDOF and MDOF structures with different nonlinear behaviours. In the first stage of the study, a reference ground motion data-set have been defined and used to derive ground-motion prediction equations for spectral accelerations and PGA. These attenuation relationships were then adopted to derive UHS, through the Probabilistic Seismic Hazard Analysis (PSHA), for a case study site. The so obtained UHS was employed to define a set of case study SDOF and MODF non-linear systems that were characterized by different periods and behaviour factors. Attenuation relationships were then derived for the interstorey drift of these systems and used to perform PSHA. This latter analysis allowed to define the interstorey drift values corresponding to different return periods. They were then used as the reference response for assessing different spectrum-based ground-motion selection procedures (refer to Figure 93).

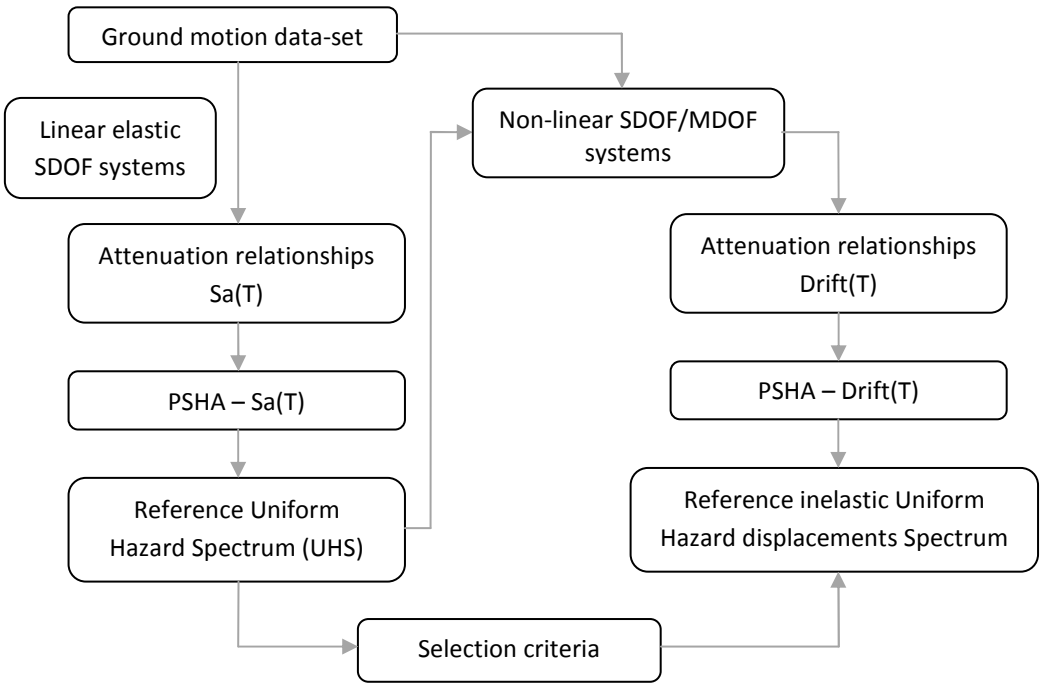

Figure 93: Flowchart of the procedure implemented.

The developed procedure allowed to investigate in a consistent and comprehensive way many issues related to code-based ground-motion selection procedures such as, for example, the effect of scaling the time histories, the influence of the range of magnitude and distance considered in the selection and the width of the interval of periods for which the compatibility is required.

Definition of reference UHS

In the first phase of the present work the reference UHS in terms of spectral acceleration was defined by performing PSHA for the case study site. In order to maintain consistency, the same ground motion data-set was used in all the different stages of the study.

Ground motion data-set

In this study, only a subset of the time–histories reported in the NGA-database (Power, Chiou et al. 2006) was adopted, in fact the ones with no information about the moment magnitude, the source-site distance, the shear wave velocity in the upper 30 m and the rupture mechanism were rejected. According to these criteria the accelerograms used in the analyses were 5523.

Attenuation models for spectral acceleration and peak ground acceleration

Attenuation models were developed for PGA and Sa at 75 different periods spanning from 0.05 s to 5 s using the dataset defined in the previous section. The number of accelerograms used to evaluate the spectral acceleration at different periods was not constant because recordings with too short Lowest Usable Periods were not considered. Ground motion prediction equations were then developed considering moment magnitude, M_w, Joyner–Boore distance, R_{JB}, and shear wave velocity in the upper 30 m, $V_{S,30}$, as independent variables. Inter–event, intra–event and inter–component error terms were considered in the non–linear regression model.

The functional form adopted was:

$$\log_{10}\mathrm{Sa(T)} = c_1 + c_2 \cdot M_w + c_3 \cdot (M_w - 6)^2 + (c_4 + c_5 \cdot M_w) \cdot \log_{10}\left(\sqrt{{R_{JB}}^2 + {c_6}^2}\right) + + c_7 \cdot \log_{10}(V_{S,30}) \quad \text{(A.1)}$$

The style of faulting was not included, as the regression analyses did not lead to statistically significant coefficients. A similar regression model was used by Buratti, Stafford et al. (2011).

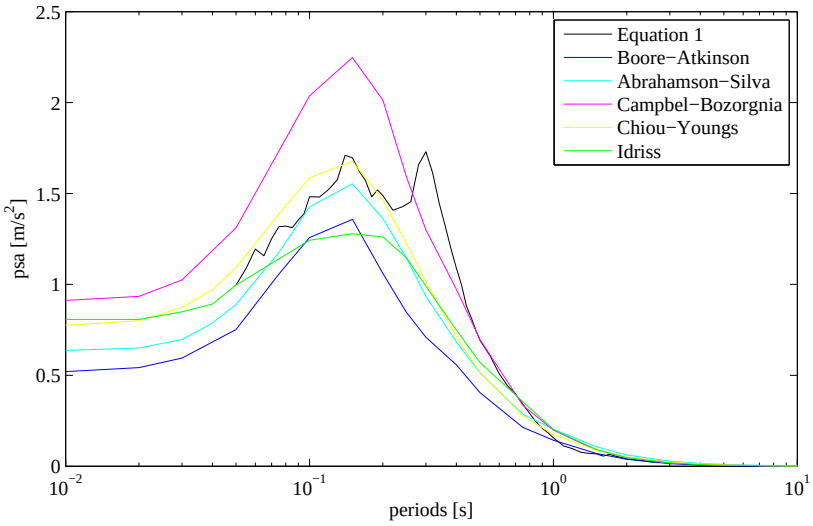

Figure 94: Comparison between different attenuation models (M_w = 5, R_{JB} = 10 km, $V_{S.30}$ = 1000 m/s^2)

The total standard deviation was obtained by combining the standard deviations of the error terms defined above as:

$$\sigma_T = \sqrt{\sigma_E^2 + \sigma_A^2 + \sigma_C^2} \quad \text{(A.2)}$$

where σ_E^2 is the variance of the inter–event term, σ_A^2 the variance of the intra–event term, and σ_C^2 the variance of the inter–component term. Moreover, the Sa and PGA values were assumed to be lognormally distributed. This assumption has already been used by many researchers (Bazzurro, Cornell et al. 1998; Shome, Cornell et al. 1998; Cornell, Jalayer et al. 2002; Baker and Cornell 2006; Stoica, Medina et al. 2007) and is well supported by the distributions of residuals obtained with the regression analyses.

Although many authors have already proposed attenuation models for the ground motion parameters considered, in the present work ground motion prediction equations have been independently derived in order to achieve the highest possible consistency with the results that will be discussed in the following Sections. In fact, the accelerograms that will be used for deriving attenuation relationships for interstorey drifts and that will be used to analyse UHS–based accelerogram selection criteria are the same used in this Section. Figure 94 shows a comparison among the attenuation model derived in the present study and the models derived by Boore-Atkinson(2007), Abrahamson-Silva (2008), Campbell-Bozorgnia (2007), Chiou-Youngs (2008) and Idriss (2008) NGA model. The curves in **Figure 94**correspond to the following scenario: M_w = 5.0, R_{JB} = 10.0 km, and $V_{S,30}$ = 1000 m/s^2.

Probabilistic Seismic Hazard Analysis

Using the attenuation models derived in the section above, a Probabilistic Seismic Hazard Analysis have been performed in order to obtain the UHS associated to the return period commonly used for life safety limit states (475 years).

The PSHA was carried out using CRISIS2007, a software developed by the Universidad Nacional Autonóma, México. The site considered for the analysis corresponds to Bologna, Italy. The source models defined by the INGV to derive the latest Italian Hazard maps were adopted; therefore no linear or punctual sources were considered. The seismicity of each zone was characterized by the Gutenberg-Richter recurrence relationships the parameters of which were calculated using the seismic catalogue CPTI04 and the completeness intervals CO-04.4 (Meletti and Montaldo 2007).

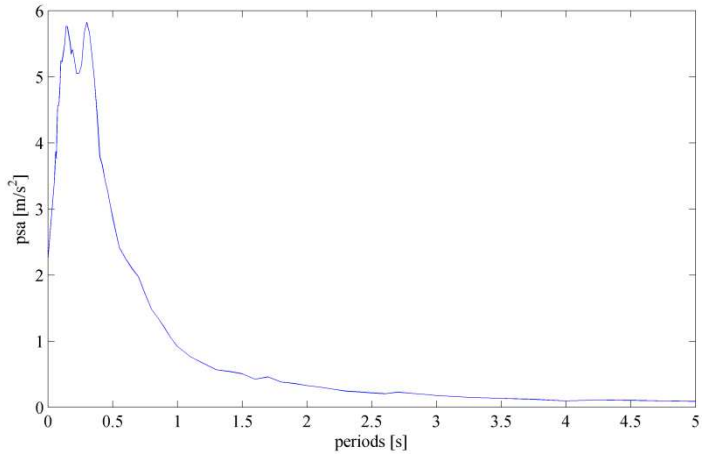

Figure 95: Uniform Hazard Spectrum (return period: 475 years)

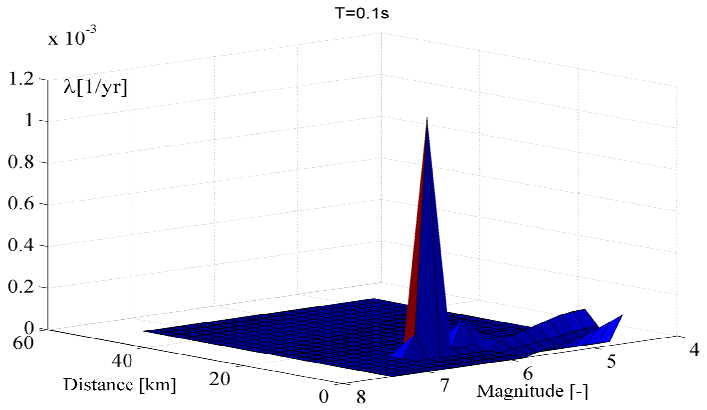

Figure 96: Disaggregation M_w-R_{JB} (fundamental period: 0.1s)

The PSHA gives, for each period, the level of the intensity measure considered (Sa in this case) associated to different mean annual frequencies of exceedance. Once the return period was

fixed (e.g. 475 years) the UHS depicted in Figure 95 was obtained by repeating the PSHA for every natural period considered. This spectrum will be used in the following as reference for ground motion selection procedures.

Another important result of the PSHA is the disaggregation. This latter allows to identify the seismic scenario (in terms of magnitude and distance) with the largest contribution to the hazard, in terms of one of the intensity measure considered, at the site under investigation. Figure 96 shows the disaggregation for the PSA at T = 0.1 s with a return period of 475 years. It can be pointed out that, if the fundamental period is smaller than 1 s, just one modal value could be identified, while for longer periods multimodal disaggregation were observed. Table 17 lists the couples of M and R_{JB} identified through the disaggregation for 5 of the 75 periods.

		M_w [-]	R_{JB} [km]			M_w [-]	R_{JB} [km]
T = 0.1 s	modal value 1	6.393	10.101	T = 1 s	modal value 1	5.812	5.051
T = 0.3 s	modal value 1	6.393	10.101	T = 2 s	modal value 1	5.086	0
T = 0.5 s	modal value 1	5.812	7.576		modal value 2	5.812	5.51

Table 17: M_w and R_{JB} associated to the modal values from the disaggregation (for T = 2 s we report the two most significant combinations of M_w/R_{JB})

Definition of reference nonlinear displacements

Structures considered

Once the UHS in terms of Sa was calculated, the structures to be subjected to the nonlinear dynamic analyses were defined. Both Single Degree of Freedom (SDOF) and Multi Degree of Freedom (MDOF) elastic–plastic systems were considered. These structures were defined from a simulated design procedure starting from the obtained UHS. In particular, the yielding force of the SDOF systems were calculated using behaviour factors, q, spanning from 1 to 5 and considering the natural periods 0.1 s, 0.3 s, 0.5 s, 1.0 s, and 2.0 s. A 5% hardening ratio was considered. Three MODF systems with 2, 4, and 10 degrees of freedom were considered. Their mechanical properties were defined using the same behaviour factor values adopted for the SDOF systems while the natural periods assumed were 0.3 s, 0.5 s and 2.0 s for the 2– and 4–degrees of freedom systems and 0.5 s, 1.0 s and 2.0 s for the 10–degrees of freedom system. Each structure was then analysed with the same subset of records from the Next Generation of Attenuation (NGA) database described before. Both interstorey and roof drifts were evaluated, as these parameters are the most widely used to characterize nonlinear structural response.

Attenuation models in terms of drift

Hence, a second regressions analysis was performed to evaluate a prediction model for the displacements. The same functional form used to define the spectral accelerations has been used also for the various measures of drift considered:

$$\log_{10} X_{max}(T) = c_1 + c_2 \cdot M_w + c_3 \cdot (M_w - 6)^2 + (c_4 + c_5 \cdot M_w) \cdot \log_{10}\left(\sqrt{R_{JB}{}^2 + c_6{}^2}\right) + + c_7 \cdot \log_{10}(V_{S,30}) \quad \text{(A.3)}$$

where X_{max} is the maximum value of interstorey or roof drift.

With reference to the SDOF structures, the empirical relationship obtained for q = 1 was compared with the attenuation model calculated for the linear elastic oscillators (refer to Figure 97). Since for a unitary behaviour factor the yielding strength of the elastoplastic systems coincides with the elastic force applied on the elastic ones, the expected excursions in the plastic range of the nonlinear structures are small.

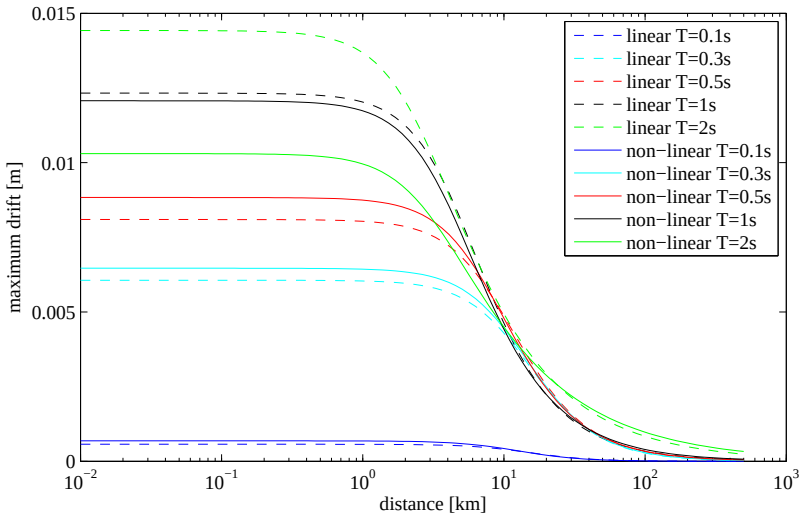

Figure 97: Comparison between elastic and elastoplastic attenuation relationships in terms of maximum displacement (q=1)

Figure 97 confirms that the elastic and elastoplastic attenuation relationships, both expressed in terms of maximum displacement, show a very similar trend with the exception of the oscillator characterized by a fundamental period of 2.0 s. It is believed that such a discrepancy between the displacements predicted by the two models is due to the fact that almost a half of the recordings applied induced non linear deformations on the elastoplastic structure and, therefore, a comparison between the behaviour of this oscillator and the elastic one is not significant. It is worth also noticing that the equal displacement rule was not verified in many cases, as already observed by other researchers (Bozorgnia, Hachem et al. 2010).

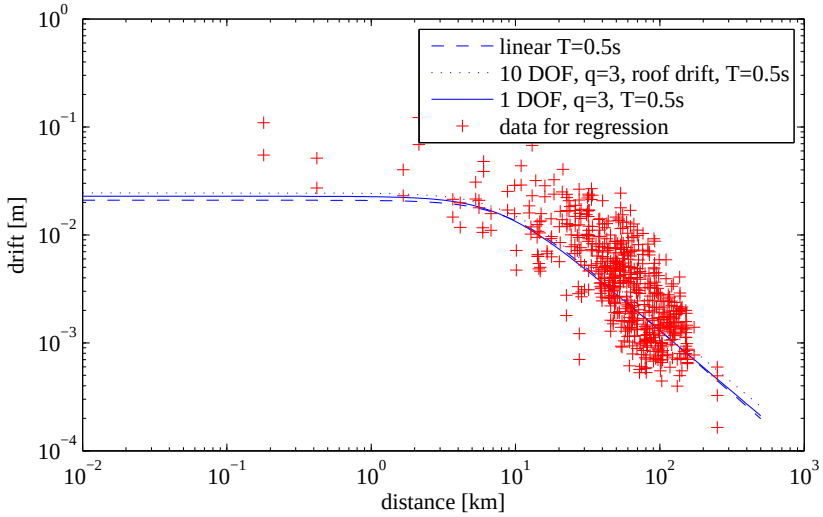

Figure 98: GMPE (M_w = 6.0, $V_{S,30}$ = 1000 m/s^2, T = 0.5 s) for the elastic case, the SDOF elastoplastic structure and the 10 degree of freedom system (q = 3) and the roof drift data used for the regression (M_w = 6.0 ± 0.5)

Figure 98 compares the Ground Motion Prediction Equations (for M_w = 6.0 and $V_{S,30}$ = 1000 m/s^2) obtained for the elastic and the SDOF elastoplastic structure characterized by a fundamental period of 0.5 s with the elastoplastic 10 degree of freedom system when the behaviour factor is equal to 3. In the latter case the structural response considered is the maximum roof drift. Figure 98 also shows, with red crosses, the data used for the regression (M_w = 6.0 ± 0.5). It should be pointed out that in order to compare the displacements (and the attenuation relations) associated to the MDOF oscillator with the two other types of displacements, the first ones had to be divided by its participation factor.

As for the elastic case, some tests were made to verify if the functional form adopted could be considered appropriate to represent the data. Particular attention was devoted to the quantiles of the residuals. It was observed that the distribution of logarithm of the standardized residuals of the displacements followed the Normal distribution in a closer way for longer vibration periods than for shorter ones, while the behaviour factor seemed to have no particular influence on the normality of the residuals. Although the hypothesis of lognormal distribution could still be considered valid, an improvement in the regression analyses could be reached by replacing the logarithmic transformation with an exponential one.

PSHA in terms of drift

The crucial point in evaluating the performance of accelerogram selection procedures is the definition of a reference structural response: in the present work the effectiveness of the

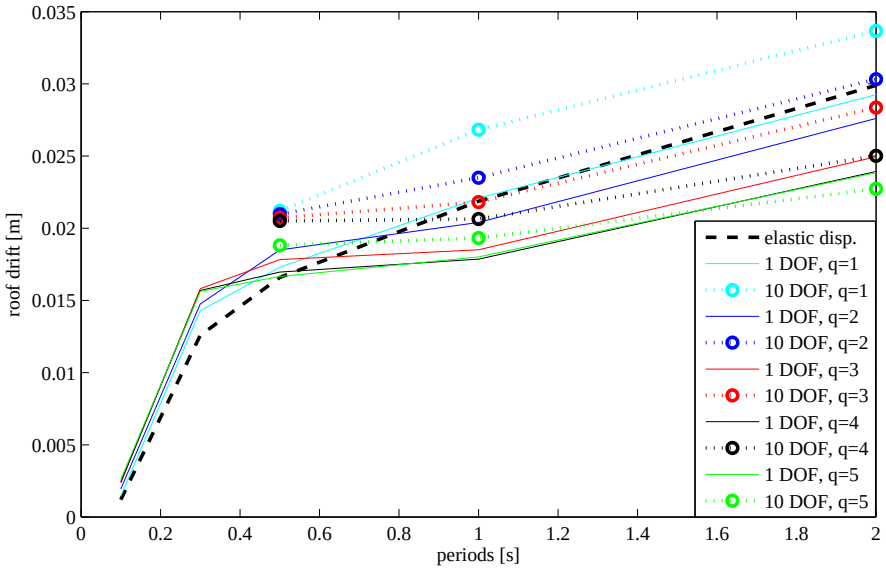

Figure 99: Uniform Hazard elastic displacement response Spectrum vs. Inelastic Uniform Hazard displacements/drifts Spectrum for SDOF systems and 10–degree of freedom systems (q = 1,2,3,4,5)

considered criteria was studied comparing the response estimated with sets of ground motions selected according to different criteria to the structural response levels associated to the return period of interest. These levels were defined by carrying out a second PSHA using the attenuation models in terms of drift. Through this process it could be possible to obtained the maximum displacements (for the SDOF oscillators) and the interstorey and roof drifts (for the MDOF oscillators) with a 475 years return period. Figure 99 shows the uniform hazard elastic displacement response spectrum and the inelastic uniform hazard displacements/drifts for SDOF systems and 10–degree of freedom systems. The behaviour factor spans from 1.0 to 5.0.

Analysis of the ground motion selection procedures

The aim of the present work was to assess the compatibility between the UHS and sets of accelerograms selected according to different criteria. The general idea was to make a preselection of the recordings contained in the database in order to obtain groups of time histories characterized by the same particular properties (e.g. the same interval of source-site distance), and then evaluate how the application of each of these criteria to the data-set affected the composition of the spectrum compatible suites of ground motions. In particular, the main objective was to check whether there were selection procedures allowing to identify the accelerograms that generated on the system a structural response comparable to the one expected.

The criteria taken under consideration were:

- maximum magnitude;
- maximum distance;
- preselection in terms of a combination of magnitude and source-site distance;
- preselection in terms of compatibility of the individual accelerograms;
- preselection in terms of width of the periods range for which the compatibility is required;
- preselection in terms of a combination of magnitude and source-site distance of scaled accelerograms.

Results

In this section an application of the method proposed on a 4-degree of freedom system is presented. 12 values of magnitude spanning from 5.8 to 7.41 have been considered as well as 10 values of distance from 5 to 105 km. These were the central values of the intervals used for the selection. For each combination of the aforementioned M_w and R_{JB}, the time histories characterized by a magnitude included in the interval $M_w \pm 0.2$ and by a distance belonging to the range $R_{JB} \pm 20$ km have been selected. Among the identified accelerograms, only those with an average pseudo-acceleration response spectrum compatible with the UHS in a range of periods including the fundamental one (in this case T = 0.5 s) were chosen. The so obtained suites of ground motions were used to estimate the mean structural response, which was calculated by averaging the results of the analyses performed using each ground motion. Figure 100 and Figure 102 show a comparison between this structural response and the reference displacement for both unscaled and scaled ground motions (considering q = 1). The error between the two displacements was calculated for every combination of M_w and R_{JB} using the general expression:

$$\Delta_{ij} = \left| \frac{\delta_{ij} - \delta_{ij,ref}}{\delta_{ij,ref}} \right| \quad \text{(A.4)}$$

where δ_{ij} is the roof drift associated to the i-th period and the j-th behaviour factor. If the root-mean-square difference between the average spectrum and the UHS in the range of periods of interest was larger than 0.2 the suite of accelerograms were rejected and a value equal to one was associated to Δ_{ij}. Two restrictions on the scaling factor were also imposed: it had to be smaller than 5 and larger than 1/5.

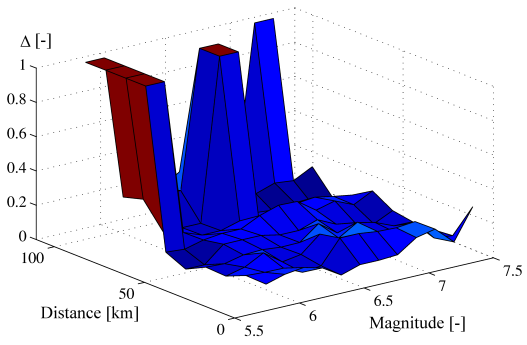

Figure 100: Drift error when considering unscaled accelerograms (period range 0.48 - 0.55, q = 1)

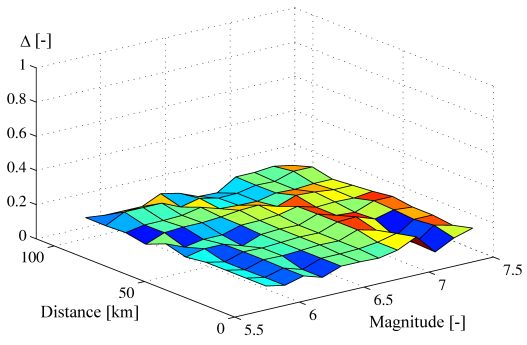

Figure 102: Drift error when considering scaled accelerograms (period range 0.48 - 0.55, q = 1)

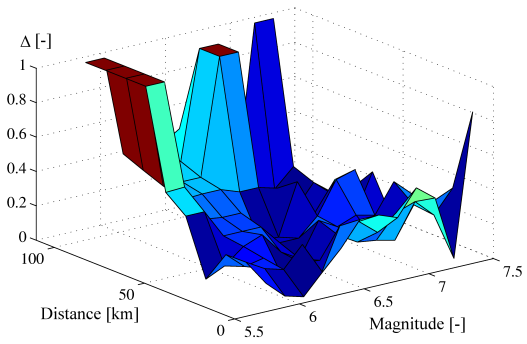

Figure 101: Drift error when considering unscaled accelerograms (period range 0.48 - 0.55, q = 5)

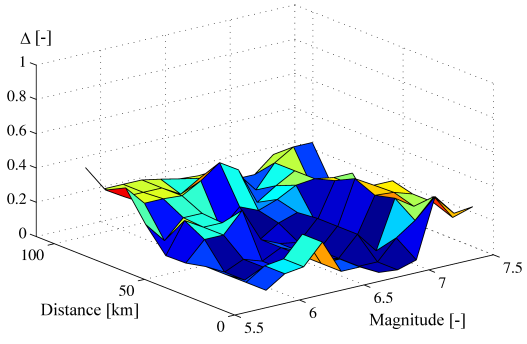

Figure 103: Drift error when considering scaled accelerograms (period range 0.48 - 0.55, q = 5)

Figure 101 and Figure 103 show the values of Δ when the behaviour factor considered was 5. It can be noticed that with the introduction of the scaling procedure, at least one suite of accelerograms with a root-mean-square difference smaller than 0.2 could be found and, in general, that the error between the displacements resulted less influenced by the range of magnitude and distance used for the selection. However, as it can be observed from the graphs, an increase of the behaviour factor results in an increment of the error term. Nevertheless, it could still possible to identify an area of the surfaces, corresponding to ranges of distance and magnitude including the values returned by the disaggregation, where Δ remained relatively small.

Conclusions

A reference structural response is needed for the study of the reliability of various selection criteria of the accelerograms used in nonlinear dynamic analyses. In the present study, a procedure to evaluate the reference displacement associated to a desired return period has been presented.

The return period considered is 475 years and 75 periods and 5523 time histories from the NGA-Database have been analyzed. This data was necessary to calibrate the empirical model that predicts the pseudo-acceleration once the magnitude, the source-site distance and the $V_{S,30}$ were known. A Uniform Hazard Spectrum associated to the chosen return period was identified using a Probabilistic Seismic Hazard Analysis. This UHS was then used to design SDOF and MDOF elastoplastic structures once the behaviour factor q was introduced. The next step was to define an attenuation model from the drifts induced on the oscillators by the time histories and to perform a second PSHA using this ground motion prediction equation. This procedure allowed to identify the displacements expected with a fixed return period.

Adopting this methodology, a comprehensive study of the reliability of different selection procedures is currently under development and will constitute the subject of future research.

Appendix B: Fragility Groups adopted in the loss assessment

Fragility Groups	
B: Shell	
B10: Super Structure	B104: Reinforced Concrete Elements
B20: Exterior Enclosure	B201: Exterior Non-structural Walls
	B202: Exterior Window Systems
C: Interiors	
C10: Interior Construction	C101: Partitions
C20: Stairs	C201: Stairs
C30: Interior Finishes	C301: Wall Finishes
	C303: Ceilings and Ceiling Lighting
D: Services	
D10: Conveying	D101: Elevators & Lifts
D20: Plumbing	D202: Domestic Water Distribution including hot water heaters
	D203: Sanitary Waste Piping System
	D205: Chilled Water Piping
	D206: Steam Piping
D30: HVAC	D303: Chillers, Cooling Towers and Compressors
	D304: Distribution Systems including Fans, Drops & Diffusers and VAV Boxes
	D305: Package Air Handling Units
D40: Fire Protection	D401: Sprinklers Horizontal Distribution including Risers and Drops
D50: Electrical	D501: Electrical Service & Distribution